Developing Radioactive Carbon Isotope Tagging for Monitoring, Verification and Accounting in Geological Carbon Storage

Yinghuang Ji

Submitted in partial fulfillment of the

requirements for the degree

of Doctor of Philosophy

in the Graduate School of Arts and Sciences

COLUMBIA UNIVERSITY

2016

ABSTRACT

Developing Radioactive Carbon Isotope Tagging for Monitoring, Verification and Accounting in Geological Carbon Storage

Yinghuang Ji

In the wake of concerns about the long-term integrity and containment of sub-surface CO_2 sequestration reservoirs, many efforts have been made to improve the monitoring, verification, and accounting methods for geo-sequestered CO_2. This Ph.D. project has been part of a larger U.S. Department of Energy (DOE) sponsored research project to demonstrate the feasibility of a system designed to tag CO_2 with radiocarbon at a concentration of one part per trillion, which is the ambient concentration of ^{14}C in the modern atmosphere.

Because carbon found at depth is naturally free of ^{14}C, this tag would easily differentiate pre-existing carbon in the underground from anthropogenic, injected carbon and provide an excellent handle for monitoring its whereabouts in the subsurface. It also creates an excellent handle for adding up anthropogenic carbon inventories. Future inventories in effect count ^{14}C atoms. Accordingly, we developed a ^{14}C tagging system suitable for use at the part-per-trillion level. This tagging system uses small containers of tracer fluid of ^{14}C enriched $_{CO2.}$ The content of these containers is transferred into a CO_2 stream readied for underground injection in a

controlled manner so as to tag it at the part-per-trillion level. These containers because of their shape are referred to in this document as tracer loops. The demonstration of the tracer injection involved three steps.

First, a tracer loop filling station was designed and constructed featuring a novel membrane based gas exchanger, which degassed the fluid in the first step and then equilibrated the fluid with CO_2 at fixed pressure and fixed temperature. It was demonstrated that this approach could achieve uniform solutions and prevent the formation of bubbles and degassing downstream. The difference between measured and expected results of the CO_2 content in the tracer loop was below 1%.

Second, a high-pressure flow loop was built for injecting, mixing, and sampling of the fast flowing stream of pressurized CO_2 tagged with our tracer. The laboratory scale evaluation demonstrated the accuracy and effectiveness of our tracer loops and injection system. The $^{14}C/^{12}C$ ratio we achieved in the high pressure flow loop was at the part per trillion level, and deviation between the experimental result and theoretical expectation was 6.1%.

Third, a field test in Iceland successfully demonstrated a similar performance whereby $^{14}CO_2$ tracer could be injected in a controlled manner into a CO_2 stream at the part per trillion level over extended periods of time. The deviation between the experimental result and theoretical expectation was 7.1%.

In addition the project considered a laser-based ^{14}C detection system. However, the laser-based ^{14}C detection system was shown to possess inadequate sensitivity for detecting ambient

levels of $^{14}CO_2$. Alternative methods for detecting ^{14}C, such as saturated cavity absorption ring down spectroscopy and scintillation counting may still be suitable.

In summary, the project has defined the foundation of carbon-14 tagging for the monitoring, verification, and accounting of geological carbon sequestration.

TABLE OF CONTENTS

LIST OF FIGURES

LIST OF TABLES

ACKNOWLEDGEMENTS

First and foremost I would like to thank my advisor, Professor Klaus Lackner, who has provided tremendous guidance, support, encouragement, and inspiration throughout my Ph.D. journey. I truly appreciate all the time and effort Professor Martin Stute and Professor Juerg Matter have invested in advising me on this research project and reviewing my dissertation. I am also grateful to the other members of my defense committee, Professor Paul Duby and Professor Robert Farrauto, for their insightful feedback.

A special thanks to Allen Wright. His generous help has been crucial to the success of all the experiments. I also thank Professor Ah-Hyung (Alissa) Park, Dr. Cantwell Carson, and Lisa Phillips for their support. Fellow students and researchers at the Lenfest Center for Sustainable Energy have provided a lot of joy and intellectual stimulation along my Ph.D. adventure.

Finally, I gratefully acknowledge the National Energy Technology Laboratory at the U.S. Department of Energy for the research funding (Award DE-FE0001535), which has made this work possible.

Dedicated to My Mom, Jiangli Qu

And My Grandparents, Xingzhi Qu and Chunying Song

For their unconditional love

Chapter 1 Introduction

1.1 Climate Change and Sustainable Development

Certain gases such as carbon dioxide, methane, and nitrous oxide, in the atmosphere contribute to the greenhouse effect, which is the trapping of radiant heat in the Earth's atmosphere. Greenhouse gases allow direct sunlight (short wavelength radiative energy) to reach the Earth's surface unimpeded. As the shortwave energy heats the surface, longwave infrared energy is reradiated to the atmosphere. Greenhouse gases absorb this energy, thereby allowing less heat to escape back to space, and 'trapping' the heat in the lower atmosphere. The greenhouse effect is a natural and important process in the Earth's atmosphere. One greenhouse gas of particular interest is CO_2, because it is one of the most prevalent greenhouse gases. Atmospheric CO_2 originates from both natural and manmade sources. Natural sources of CO_2 include volcanic outgassing, the combustion and decay of organic matter, and respiration. Man-made, or anthropogenic, sources of CO_2 are produced from the burning of various fossil fuels for power generation and transportation, as well as from industrial activities.

The combustion of fossil fuels for electricity generation plays an essential role in energy security and in the smooth functioning of the global economic system. At present, approximately one-third of the CO_2 emissions in the United States come from power plants and other industrial facilities contribute approximately one-third of the remaining emissions. Greenhouse gas levels have significantly increased above pre-industrial levels, from approximately 280 parts per million (ppm) to now 401 ppm. According to the U.S. Energy Information Administration,

annual global energy-related CO_2 emissions had reached approximately 32 billion metric tons in 2012. Global consumption of fossil fuels continues to increase, driving growth in worldwide CO_2 emissions.

Many scientists consider this increase in atmospheric greenhouse gases a major factor in global climate change (IPCC, 2005). Energy demand is a leading contributor and it is very difficult to eliminate these emissions. Even when assuming that current policy commitments and pledges by governments around the world to tackle climate change are all implemented, it is expected that fossil fuels will still account for 75% of global energy demand in 2035 (Van der Hoeven, 2013). Demand growth is expected to be particularly strong in developing countries. In its World Energy Outlook 2013, the International Energy Agency (IEA) estimated that based on their assumptions energy-related CO_2 emissions would rise by 20% between 2013 and 2035. This would leave the world on a trajectory consistent with a long-term average temperature increase of 3.6 degrees Celsius (°C), far above the internationally agreed 2°C target (Van der Hoeven, 2013). This 2°C target is generally viewed as the limit of what can safely be tolerated (IPCC, 2005).

It is clear that much more needs to be done to limit CO_2 emissions. Technological approaches that are effective in reducing atmospheric greenhouse gas concentrations, while, at the same time, allowing the economic growth and prosperity associated with energy use, are needed. Work has been under way through the United Nations Framework Convention on Climate Change (UNFCCC) to reach a new global climate change agreement, which recently took place in Paris at the end of 2015. This agreement is vital if greenhouse gas (GHG) concentrations in the

atmosphere are to be stabilized at a level that will avoid the worst impacts of climate change and ensure that sustainable development goals can indeed be reached.

1.2 Carbon Capture, Utilization, and Storage

In the “Climate Stabilization Wedges” carbon mitigation initiative produced by Princeton University researchers (Pacala and Socolow, 2004), it is claimed that global warming is a problem which can be attacked using today's commercially available technologies to reduce CO_2 emissions. In order to stabilize CO_2 concentrations below 500 ppm for the next fifty years, they proposed 15 carbon mitigation strategies which fell in 4 different categories.

Category I: Efficiency and Conservation: increased transport efficiency; reducing miles traveled; increased building efficiency; increased efficiency of electricity production.

Category II: Decarbonization of Electricity: fuel switching (coal to gas); fossil-based electricity with carbon capture & storage (CCS); coal synfuels with CCS; fossil-based hydrogen fuel with CCS.

Category III: Decarbonization of Fuels: nuclear electricity; wind-generated electricity; solar electricity; wind-generated hydrogen fuel; biofuels.

Category IV: Natural Sinks: forest storage; soil storage.

Among the multiple approaches to cut back on greenhouse gas emissions, carbon capture, utilization, and storage (CCUS) is a technology for achieving large emission reductions from fossil fuel use. It must play a significant role alongside renewables, energy efficiency, nuclear

energy and other mitigation options in the global action on climate change. No single approach is sufficient to stabilize the concentration of greenhouse gases in the atmosphere, especially when the growing global demand for energy and the associated potential increase in greenhouse gas emissions is considered.

CCUS promises to provide a significant reduction in greenhouse gas emissions. It especially could play a key role in curbing CO_2 emissions from fossil fuel-based power generation. According the International Energy Agency (IEA), in the 2 Degrees Celsius Scenario (2DS, global warming stays below 2 °C), CCS will contribute up to 20% of the total CO_2 emissions reduction by 2050, while end-use fuel and electricity efficiency contribute 31%, renewables contribute 29%, end-use fuel switching contributes 9%, nuclear contributes 8%, and power generation efficiency and fuel switching contributes 3% (IEA, 2012).

The total investment cost for CCS across power and industrial applications equates to approximately USD 31/tCO_2 avoided (115 GtCO_2 avoided through CCS) by 2050 (IEA, 2012). It's worth noting that power generation investment cost for CCS includes the total cost of the power plant, not just the incremental cost of capture; in 2012, the incremental cost of capture is about 50% of the total cost of a coal-fired power plant with CCS. However, investment cost for CCS in industrial applications do not include the cost of transport and storage, thus these analyses probably underestimate the true cost of CCS in this sector by 20%-30%. In 2DS, a 5% decrease in coal-fired electricity generation capacity and nearly 30% increases in gas-fired and nuclear capacity globally are required in 2050 without CCS. As a result, removing CCS from the list of options to reduce emissions in electricity generation increases the required capital

investment necessary to meet the same emissions constraint by 40% in the electricity sector (approximately USD 3.1 trillion).

Further, CCS is the only option available to significantly reduce direct emissions from many industrial processes at the large scale needed in the long term. In total, the IEA models projected CCS to contribute at least 22 percent of the necessary reductions from power and industrial sources (IEA, 2012).

CCUS consists of a suite of technologies that can benefit an array of industries, including power plants (fossil, biofuel, and geothermal), refineries, and other industrial sources of CO_2 that could be captured. The opportunity to apply CCUS to these facilities will have significant benefits for the environment, as well as add to economic activity, even if it raises the cost of energy. Its future role in an "all of the above" energy strategy will require that industry considers carbon management as a key issue that must be addressed.

CCUS involves a set of processes that consists of capturing CO_2 from major stationary sources, transporting CO_2 by pipelines to a point of use or disposal, and finally achieving long-term isolation from the atmosphere through either utilization or storage. By keeping CO_2 out of the atmosphere, CCUS enables industries to continue operations while emitting fewer greenhouse gases, making it a powerful tool to address climate change.

CCUS begins with the separation and capture of CO_2 from coal-based power plant flue gas or from syngas. These same capture technologies are also applicable to natural gas and oil-fired power plants, as well as for other industrial CO_2 sources. There are three major methods of CO_2 capture: 1) Pre-combustion CO_2 capture is mainly applicable to gasification plants, where fuel

(coal, biomass, or coal/biomass mixture) is converted into gaseous components by applying heat under pressure in the presence of steam and sub-stoichiometric oxygen. 2) Post-combustion CO_2 capture is primarily applicable to conventional coal-fired, oil-fired, or gas-fired power plants, but could also be applicable to Integrated Gasification Combined Cycle (IGCC) and Natural Gas Combined Cycle (NGCC) flue gas capture. 3) Oxy-combustion CO_2 capture is applicable to both new and existing coal-fired power plants (IPCC, 2005).

Once the CO_2 gas has been captured, the volume must be reduced to cost-effectively transport and store it. Either compression or a combination of refrigeration/pumping needs to be done to convert the CO_2 gas to a liquid or a supercritical fluid. Then it's transported from the power plant to a selected location for permanent, safe storage or beneficial reuse, such as enhanced oil recovery (IPCC, 2005).

CO_2 is a commodity that can be used for enhanced oil and gas recovery. In many situations there is a strong business case to be made. In the United States, there is a long history of oil production over the past 100 years, as well as more than 40 years of EOR utilizing CO_2. In 2010, approximately 50 million metric tons (MMt) of CO_2 per year from naturally occurring sources were used to recover additional oil (NETL, 2010). There is an opportunity to supplement and eventually replace the naturally occurring CO_2, derived from underground wells, and used for EOR with CO_2 from anthropogenic sources, reducing the carbon footprint of these fuels, as well as contributing to the energy independency. However, to put the scale in perspective, CO_2 used in enhanced oil recovery amounts to roughly one percent of the annual carbon dioxide emissions in the United States.

There are mainly three categories of CO_2 storage methods, i.e., geological storage, ocean storage, and mineral carbonation (IPCC, 2005). Among them, geological carbon storage appears to be the most promising and widely used approach due to its very large CO_2 storage capacity, the industrial analogues with existing technology developed by the oil and gas industry, and economical feasibility.

1.3 Geological Carbon Storage

Geological carbon storage is the containment of CO_2 in a subsurface formation, so that it will remain safely and permanently stored. Many different formations are suitable for geological storage, including depleted oil and gas reservoirs (estimated storage capacity 675-900 Gt CO_2), deep unused saline water-saturated reservoir rocks (estimated storage capacity 1,000-10,000 Gt CO_2), deep unmineable coal seams (estimated storage capacity 15-200 Gt CO_2), and other suggested options like caverns, basalts formations and organic-rich shales (IPCC, 2005). All types of geological carbon storage reservoirs are targets of the carbon-14 isotope tagging technology developed in this dissertation.

There have been natural accumulations of CO_2 in geological reservoirs for millions of years. Geological carbon storage involves site selection through screening and initial characterization followed by detailed site characterization through tools such as seismic surveys, core analysis, and modeling. Studies in the United States, Australia and Europe (Pearce et al., 1996; Allis et al., 2001; Stevens et al., 2002; Watson et al., 2004) indicate that, with appropriate selection and management of geological carbon storage reservoirs, it may be possible to achieve comparable performance of the fraction of the CO_2 retained (exceeding 99% over 1000 years).

Geological sequestration is even more attractive, because, the technologies involved in the injection of CO_2 in deep geological formations, such as well-drilling, injection technology, computer simulation of storage reservoir dynamics and monitoring methods, are the same as the ones developed and employed in the oil and gas exploration and production industry, and they only require relatively little additional development and optimization for the operation of geological carbon storage systems.

The effectiveness of geological carbon storage depends on a combination of physical and geochemical trapping mechanisms (IPCC, 2005). There are four types of trapping mechanisms that control the acceptable storage density and the leakage potential of the CO_2 injected into geological sinks (Figure 1).

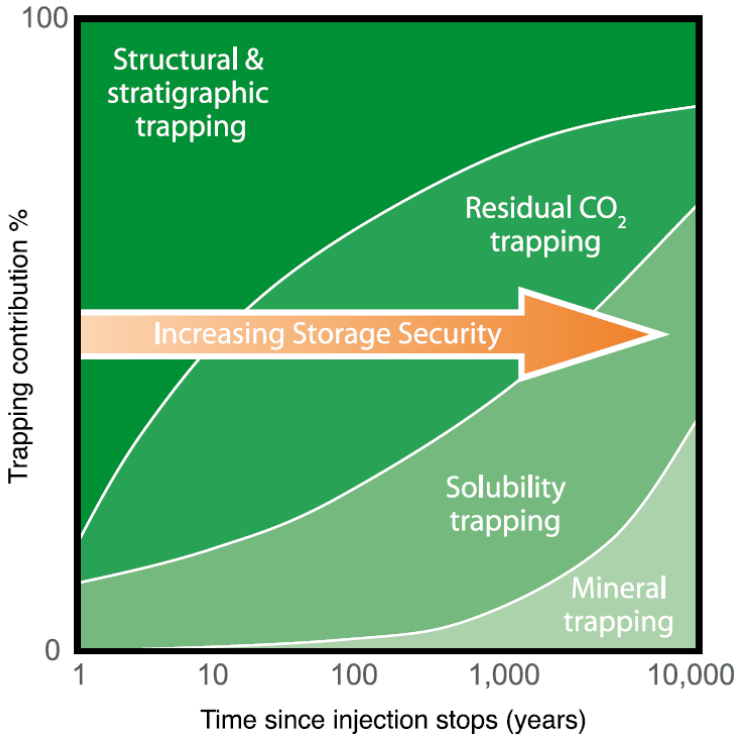

Figure 1: CO_2 storage mechanisms in geological formations (IPCC, 2005).

Initially, physical trapping of CO_2 below low-permeability seals is the principal means to store CO_2 in geological formations. Shale or salt beds with very low permeability are the most common types of caprocks. Faults can act as permeability barriers in some circumstances and as preferential pathways for fluid flow in other circumstances (Salvi et al., 2000). Therefore, care must be taken not to exceed the allowable overpressure to avoid fracturing the caprocks or re-activating faults (Streit et al., 2005). Hydrodynamic trapping can occur in saline formations that do not have a closed trap, but where fluids migrate very slowly over long distances. In the longer term, significant quantities of CO_2 dissolve in the formation water and then migrate with the groundwater. Where the distance from the deep injection site to the end of the overlying impermeable formation is hundreds of kilometers, the time scale for fluid to reach the surface from the deep basin can be millions of years (Bachu et al., 1994).

Carbon dioxide in the subsurface can undergo a sequence of geochemical interactions with the rock and formation water that will further increase storage capacity and effectiveness. In the process of solubility trapping, once CO_2 is dissolved, it no longer exists as a separate phase, thereby eliminating the buoyant forces that drive it upwards. It will form ionic species as the rock dissolves, accompanied by a rise in the pH. Dissolution of CO_2 in formation waters can be represented by the chemical reaction:

$$CO_2\,(g) + H_2O \leftrightarrow H_2CO_3 \leftrightarrow HCO_3^- + H^+ \leftrightarrow CO_3^{2-} + 2H^+$$

Mineral trapping is believed to be comparatively slow, potentially taking a thousand years or longer. CO_2 dissolved in water produces a weak acid, which reacts with the sodium and potassium basic silicate or calcium, magnesium and iron carbonate or silicate minerals in the reservoir or formation to form bicarbonate ions. Formation of carbonate minerals occurs from

continued reaction of the bicarbonate ions with calcium, magnesium and iron from silicate minerals such as clays, micas, chlorites and feldspars present in the rock matrix (Gunter et al., 1993, 1997). Mineral trapping results in the most stable and permanent form of geological carbon storage.

1.4 Monitoring, Verification, and Accounting

Through its core research and development program administered by the National Energy Technology Laboratory (NETL), the U.S. Department of Energy (DOE) emphasizes monitoring, verification, and accounting (MVA), as well as computer simulation and risk assessment, of possible carbon dioxide leakage at CO_2 geological storage sites. MVA efforts focus on the development and deployment of technologies that can provide an accurate accounting of stored CO_2, with a high level of confidence that the CO_2 will remain stored underground permanently. Effective application of these MVA technologies will ensure the safety of geological storage projects with respect to both human health and the environment, and can provide the basis for establishing carbon credit trading markets for geologically storing CO_2. Computer simulation can be used to estimate CO_2 plume and pressure movement within the storage formation as well as aid in determining safe operational parameters; results from computer simulations can be used to refine and update a given site's MVA plan.

Before, during, and after the injection process, monitoring, verification, and accounting (MVA) efforts focus on the development and deployment of technologies that can provide accurate accounting of stored CO_2 and a high level of confidence that the CO_2 will remain safely and permanently stored. Throughout the CCUS process, risk assessment identifies and quantifies

potential health and environmental risks associated with CCUS, and helps to identify appropriate measures to ensure that these risks remain low.

MVA capabilities are critical to ensuring the long-term viability of CCUS in satisfying both technical and regulatory requirements. MVA efforts aim to track the amount of CO_2 stored at a specific sequestration site, monitor the site for leaks or other deterioration of storage integrity over time, and verify that the CO_2 is retained at expected levels of permanence.

As a very important part of the overall risk management strategy for geological storage projects, MVA is needed for a wide variety of purposes (IPCC, 2005):

1) Ensure effective control of the conditions (e.g., injection rate, pressure, temperature) in injection wells, which have to remain within a predetermined safety envelope;
2) Verify the quantity of injected CO_2 and monitor the ongoing processes associated with the various storage mechanisms;
3) Demonstrate that CO_2 remains contained in the intended storage formations and does not escape from these formations;
4) Optimize the efficiency of the storage project;
5) Detect leakage and provide early warnings if storage systems fail.

At a geological carbon sequestration site, MVA can be used for mineral carbonation study, i.e., identifying the phase of CO_2 trapping mechanisms in the geological reservoirs; as well as used for any potential leakage detection near some faults in the geological formations.

MVA techniques include atmospheric and remote sensing techniques, near-surface monitoring techniques, wellbore monitoring techniques, deep surface monitoring techniques, and

accounting protocols (NETL, 2010). Some surface-based techniques like CO_2 sensors with alarms and the sampling of groundwater and the soil between the surface and water table might be useful for directly detecting CO_2 leakage. However, high-quality baseline data are essential for the reliability, resolution and sensitivity in the context of geological storage.

Geophysical methods for detecting CO_2 in situ are very powerful, but they are qualitative to semi-quantitative. 4D seismic, cross well seismic, vertical seismic profiling (VSP), and wire line logging are excellent tools for tracking the migration of CO_2 within the reservoir and providing certain information on CO_2 concentration and saturation in case of VSP (e.g., Benson et al., 2004; Metz et al., 2005; Hovorka et al., 2006). These tools are excellent in showing that CO_2 moved into a particular location.

However, most geophysical detection methods require that CO_2 is present as a separate phase, e.g., as supercritical gas. Once CO_2 is fully dissolved in water, standard geophysical monitoring techniques, such as seismic surveys or VSP cannot be applied. Thus, dissolved carbon (solubility trapping) and chemically transformed carbon (mineral trapping) avoid detection (Gasperikova et al., 2006). Also, pressure changes in the reservoir even without CO_2 migration can change 4D seismic images and create false positive signals of leakage (Hoversten et al., 2006). A lack of a signal does not prove the absence of leakage, nor is the presence of a signal sufficient to prove leakage. Carbon already resident in the formation prior to injection further confounds a quantitative accounting. Whether the CO_2 that moved is actually anthropogenic CO_2 and not carbon that has already been in the reservoir prior to the injection remains a great challenge in carbon storage accounting.

In conclusion, geophysical detection methods are far from ideal in serving as a surveying tool that would allow a self-contained set of measurements to unambiguously determine the amount of carbon stored. As stated by Benson (2006), currently the only practical way of establishing an inventory of stored CO_2 is to add up all injections and subtract any leakage to the surface that has been detected. This can be a satisfactory proof for scientific inquiry, but it would not hold up in a court of law, if for example, the veracity of the initial injection records were challenged, or if it turns out that the party in charge of monitoring leaks had an economic interest in the integrity of the storage site.

The most direct method for a quantitative accounting is to tag the injected CO_2. Geochemical monitoring techniques using non-reactive and reactive tracers are useful for directly monitoring the dynamics and reactivity of the injected CO_2 and mobile formation fluids (Matter et al., 2008, 2014). The varieties of tracers are transported differently, and measurement of their concentrations and changes in their ratios can be used to quantitatively characterize physical and geochemical processes at field scale.

We developed a technology for tagging the CO_2 with $^{14}CO_2$. The rationale behind using ^{14}C is threefold. First, all natural carbon in the deep aquifers is generally free of ^{14}C because of the long residence time of the groundwater and the relatively short half-life time of ^{14}C (5,730 years, Godwin, 1962). Second, the behavior of the ^{14}C in the transport processes in the underground is very similar to that of other carbon isotopes and therefore this tag it is not separated from the injected CO_2 as the gas undergoes fluid transport, phase changes, and chemical transformations. In this regard it is very different from, for example, SF_6 (sulfur hexafluoride), which will not follow chemical or phase transitions the CO_2 may go through. If CO_2 undergoes mineralization

^{14}C will follow. Third, even though ^{14}C is very similar in its behavior to that of other carbon isotopes, it is nevertheless a reactive tracer with slightly different reaction kinetics. This means that the ratio of carbon-13 to carbon-12 in the groundwater will slightly change as a result of dissolution and precipitation of carbonate minerals. Thus, if mineral carbonation occurs after the injection of CO_2, it can be monitored and verified by measuring the isotopic composition of reservoir fluid and rock samples with mass spectrometry or other detection techniques as long as it is not masked by mixing from pre-existing carbon in the surrounding environment.

Our goal was to develop an inventory technology that makes it possible for the public to gain trust in the reality, safety and permanence of CO_2 storage. Our approach provides a surveying tool for not only injected CO_2, but also dissolved and chemically transformed CO_2. Tagging also creates a means of providing ground-truthing of these geophysical observations and thus can in the future increase the reliability and efficiency in carbon accounting. This radioactive tagging ability together with sample collection of some conservative geochemical tracers (e.g., SF_5CF_3 and SF_6) can augment other geophysical monitoring methods and establish a detailed picture of anthropogenic CO_2 distribution below ground.

The advantages of ^{14}C as a radioactive tracer for geological carbon sequestration, incremental risks mitigation, underlying challenges identification, and potential optimizations are further discussed in the subsequent chapters.

Chapter 2: Tagging CO_2 to Enable Quantitative Inventories of Geological Carbon Storage

In October 2009, The Earth Institute at Columbia University in the City of New York began work on a U.S. Department of Energy (DOE) funded project titled, *Tagging CO_2 to Enable Quantitative Inventories of Geological Carbon Storage*, which will be referred as the C14 project subsequently. The objective of the C14 project was to develop and demonstrate a system for adding a rare carbon isotope (^{14}C) as a geochemical tracer to geo-sequestered CO_2. ^{14}C is naturally produced in the atmosphere. Near the surface of the Earth approximately one in a trillion carbon atoms is ^{14}C. Because ^{14}C has a half-life of only 5730 years and is produced from cosmic rays interacting with nitrogen in the air, it is essentially non-existent in the sub-surface where CO_2 would be stored. CO_2 produced from fossil fuels also does not contain ^{14}C and, thus, would be perfectly camouflaged among pre-existing carbon in the subsurface. In order to identify the anthropogenic CO_2 clearly, the goal is to tag it with an amount of ^{14}C that makes it look like normal surface carbon. With such a tag, anthropogenic carbon injected into the underground can be clearly differentiated from natural carbon deposits in the ground and its whereabouts can be tracked.

2.1 Problem Statement

The latest IPCC special report (Stocker et al., 2013) stated that stabilizing the carbon dioxide concentrations at safe levels will require prolonged periods of negative emissions. Creating negative emissions is only possible if technologies to store excess carbon safely and permanently can be implemented. Therefore, in the view of the IPCC, some form of CCS is a necessity. The IPCC already in 2005, in its special report on carbon dioxide capture and storage (Metz et al., 2005) provided a detailed analysis of CCUS options.

The idea of CCUS offers an appealing solution to the greenhouse gas emissions from fossil fuels that are warming the planet. However, public doubts over safety and accountability of carbon storage have caused political uncertainties, which hamper the implementation of CCUS. For example, in 2006, the United Nations Framework Convention on Climate Change in Nairobi failed to sanction geological storage due to political uncertainties (De Figueiredo, 2007). Since then many carbon sequestration projects failed to move forward because of public concerns over safety and permanence. Planned underground storage on land in the Netherlands was stopped because of local opposition (Chazan, 2009). German policy makers declared that terrestrial geological sequestration is not an option for Germany (Slavin and Alok, 2009). Positive proof will be required to demonstrate that CO_2 is successfully stored in geological reservoirs. Thus, to gain the trust of the public at large, CCUS research will need to show the safety and efficacy of carbon storage technologies. This calls for a focus on monitoring, verification and accounting.

Ideally, MVA methods should provide a complete inventory of geological carbon storage without having to rely on past measurements. This requires tools for accurate inventory

accounting and verification of the amounts of CO_2 stored in a reservoir. These tools need to ensure that the amount of CO_2 injected is equal to the amount claimed, and that losses during the injection stage and subsequent losses from storage are accurately determined.

2.2 Importance of Research

In recognition of the importance of MVA, the Department of Energy has set ambitious goals for CO_2 retention, demanding strict accounting standards for storage inventories, and engaged in an extensive research program to develop, test, and deploy innovative technologies (Figueroa et al., 2008). The C14 project has been performed under a call to develop innovative ways of monitoring carbon in the ground and to accurately account for the amounts of carbon stored.

The overall objective of the U.S. Department of Energy's (DOE) Carbon Storage program is to develop and advance CCS technologies will significantly improve the effectiveness of the technology, reduce the cost of implementation, and be ready for widespread commercial deployment in the 2025–2035 timeframe. To accomplish widespread deployment, technical and economic barriers must be addressed. The data and information generated must be communicated to inform regulators and industry on the safety and permanence of CCS. Four program goals have been established that support the scale-up and development of CCS leading to widespread deployment. 1) Develop and validate technologies to measure and account for 99 percent of injected CO_2 in the injection zones. 2) Develop technologies to improve reservoir storage efficiency while ensuring containment effectiveness. 3) Support industry's ability to predict CO_2 storage capacity in geological formations to within ± 30 percent. 4) Develop best practice manuals for monitoring, verification, accounting (MVA), and assessment; site screening,

selection, and initial characterization; public outreach; well management activities; and risk analysis and simulation (Figueroa et al., 2008).

An inventory tool that will allow the independent and accurate accounting of the injected carbon is critical to ensure the large-scale adoption of CCUS as an approach towards climate change mitigation. Measurements of flows during the injection process are far easier than accurate inventories of the CO_2 stored in the reservoir. Methods that can create such an inventory without having to rely on a historic record of injections and a continuous observation of potential leak paths would be highly preferable. With the measures in place so far, it is impossible to verify that records about injection are indeed correct. Independent inventory assessments become important when the veracity of injection data is challenged in court.

There are a number of dynamic effects that make accurate accounting of CO_2 in an underground geological reservoir difficult. For example, it is possible for CO_2 to migrate out of the storage reservoir. Whether or not this leads to actual leakage to the surface is difficult to determine. However, carbon dioxide that escaped from the location it was supposed to stay in should be considered lost. The converse assumption would mean that one has to explain to the public that a mistake was made; the CO_2 did not stay where it was supposed to stay, but that one is still in an excellent position to assure that it will not migrate any further. Such a line of reasoning would usually strain the credulity of an unbiased observer.

This is exacerbated by the fact that observing leaks is not easy. The relatively high background of CO_2 in the atmosphere and soil, coupled with seasonal fluctuations in CO_2 fluxes, make accurate detection of slow or highly distributed leaks very difficult. Chemical conversion, dissolution, and precipitation of CO_2 further complicate a full accounting. Not all of the CO_2 can

be expected to remain in gas form, but it could show up as dissolved inorganic carbon in pore waters, or as solid carbonates that precipitate out in the pore space.

Our work started from the concern that CCUS might fail, not because the procedure is unsafe or unreliable, but because it is not yet possible to determine the inventory of CO_2 stored independently and objectively. Unless accounting schemes can be developed that are able to measure the total amount of injected carbon from first principles without having to trust prior observations, the public will, quite rightly, remain skeptical. There are enormous financial stakes involved in reservoir construction and maintenance. As a result it necessary to develop an inventory tool that will allow an independent and accurate accounting of the injected carbon.

Our belief that current MVA technologies are insufficient might be controversial. We do not disagree as to the efficacy of other technologies, but we consider it necessary to strive for a higher standard. It would be necessary to improve existing monitoring technologies, develop novel systems, and protocols to satisfy regulations to track the fate of subsurface CO_2 and quantify any emissions from reservoirs. If necessary, the tool will support project developers to help quantify emissions from CCUS projects in the unlikely event that CO_2 migrates out of the injection zone.

The research, summarized in this dissertation, was laying the groundwork for an ambitious technology that can provide quantitative inventories of carbon stored underground and demonstrate its location. The basis for the technology is radiocarbon (^{14}C) tagging of CO_2 before it is put in storage. By making CO_2 stored deep underground look like surface carbon by adding tiny amounts of ^{14}C, the injected carbon is clearly identifiable as anthropogenic. It can then be tracked, its whereabouts can be established and inventories can be built that verify that the

amount injected is still equal to the amount initially stored. ^{14}C tagging makes it possible to follow the CO_2 that is moving underground and may be undergoing chemical reactions, thus it can help to win the public's faith that CO_2 is safely and permanently stored in geological reservoirs.

The technique involves the active tagging of the injected CO_2 with low levels of radiocarbon (^{14}C) as a reactive tracer in combination with the injection of non-reactive tracers such as sulfur hexafluoride (SF_6) and trifluoromethylsulphur pentafluoride (SF_5CF_3). The $^{14}C/^{12}C$ ratio, the total dissolved or precipitated carbon, SF_6 and SF_5CF_3 analyses of the fluid and rock samples are needed to estimate a carbon mass balance which can quantify carbonation and estimate in situ reaction rates for the geological carbon storage sites. One major challenge of this technology is to get access to reservoir samples via boreholes. At the CarbFix carbon sequestration site in Iceland, a 600 meter deep borehole was drilled near the injection zone to retrieve core and samples to verify mineral carbonation (Matter et al., 2008).

The proposed development of a quantitative inventory tool using ^{14}C for geological carbon storage would enable for the first time a true inventory of the stored anthropogenic CO_2 in geological reservoirs. A successful implementation of carbon tagging can unambiguously determine the amount of carbon stored and validate that the carbon dioxide has been effectively stored in the geological formation. In combination with conventional geophysical monitoring technologies and complex hydrological modeling, it would significantly improve the overall resolution of the monitoring and will contribute to injection optimization subsequently. Finally, coupled with our improved measurements of the solubility trapping and mineral trapping rates

and reservoir models, MVA tools will make more accurate prediction of CO_2 storage capacity in geological formations.

2.3 Advantages of ^{14}C Tagging

^{14}C is a radioactive isotope of carbon. It has a half-life time of 5730 years, and is produced naturally by cosmic radiation or it can be made artificially by neutron capture (Clark and Fritz, 1997). ^{14}C is a widely used dating tool for materials that contain carbon compounds derived from atmospheric CO_2 either by simple mixing processes or by carbon exchange.

In the atmosphere, ^{14}C produced from ^{14}N is incorporated into $^{14}CO_2$ and takes part in the global carbon cycle. It is assimilated by plants. Except for a slight isotope fractionation, ^{14}C in living organic matter is the same as that in atmospheric CO_2. After organic matter dies, the ^{14}C concentration decreases due to radioactive decay. If there is no isotope exchange, radioactive decay is the only ^{14}C sink and if the initial ^{14}C activity is known, an age can be calculated from the measured ^{14}C activity of a sample (Clark and Fritz, 1997).

In groundwater applications, dissolved inorganic carbon (DIC = $CO_{2(aqueous)} + HCO_3^- + CO_3^{2-}$) is typically extracted from the water and its measured ^{14}C activity is compared to the initial ^{14}C activity. Determination of the initial ^{14}C activity can be challenging and typically requires correction models that account for the carbon chemistry in the unsaturated and saturated soil zones (e.g., Fontes and Garnier, 1979; Stute and Deák, 1989).

Isotope tracers are well suited to tagging, because they are chemically identical to the tagged material and therefore do not get separated from the bulk injection even if the injected material

undergoes chemical transformations. Since the main interests of geological carbon storage study lay in the fate of the carbon injected, ^{18}O is not a good candidate for this purpose. During certain geochemical reactions with groundwater, O in the CO_2 molecule will exchange with the O in the water molecule and therefore lose its tracking ability (Stute and Deák, 1989). Another option is ^{13}C, a stable isotope of carbon. The ambient $^{13}C/^{12}C$ ratio is about 1%. There are cases where the injected and the ambient ^{13}C content are sufficiently different so that it is possible to separate them out. However, if we would like to track Gigatons of CO_2 per year with ^{13}C at the ambient concentration, the amount of ^{13}C needed makes it not economically feasible.

Compared to ^{18}O and ^{13}C, ^{14}C has some clear advantages to serve as an extremely sensitive tracer for tagging massive anthropogenic carbon underground. ^{14}C decays with a half-life of 5730 years. Because of long residence times, the carbon in deep reservoirs and in fossil fuels contains less than 0.5% of modern carbon (the remainder is due to in situ production by other radioactive decay processes). As a result, fossil fuel produced CO_2, which is practically ^{14}C free, can be tagged with ^{14}C up to ambient levels (or higher), prior to geo-sequestration. While it is beneficial from the scientific point of view to tag the CO_2 to unique $^{14}C/^{12}C$ ratios, i.e., above atmospheric levels, staying near natural atmosphere or surface levels helps to reduce concerns over the use of radio-isotopes. The activity of the injected CO_2 is no higher than that of CO_2 released in human breath. Even though ^{14}C tagging does not help in seeing sequestered carbon come out the ground at the surface, the presence of ^{14}C at depth would be a clear indication of the presence of anthropogenic carbon in any subsurface location. The movement of anthropogenic carbon well below the surface can be tracked with ^{14}C. For example, a rising plume could be monitored long before it reaches the surface.

The ambient concentration of $^{14}C/^{12}C$ is roughly one part per trillion (ppt) (Wigley and Schimel, 2005). Because of the low level of tagging, the total amounts of ^{14}C involved in geological carbon storage tagging would always be small. A Gigaton of CO_2 would require 320 g of pure ^{14}C. A disposal site accepting 1000 kg of CO_2 per second would require a daily dose of 0.29 g of $^{14}CO_2$ with an activity of 123 mCi, comparable to the activity of a typical medical source. A typical iodine dose for outpatient thyroid cancer, which is ingested by the patient, is of the order of 100 mCi (Grigsby et al., 2000).

The tagged CO_2 stream can be safely stored and handled without posing any safety or environmental issues, since tagged CO_2 is indistinguishable from natural surface carbon. On the other hand, the ^{14}C to be injected is radioactive and its production, transport and handling must be carefully planned and monitored. The annual production of ^{14}C in nuclear power plants and DOE facilities in the United States is around 600 Ci/year (Peterson et al., 2007). The amount of ^{14}C required for this project or even a large single injection site is readily available. Production of ^{14}C in a high flux reactor like those at Oak Ridge or at Chalk River in Canada could easily cope with any CCUS induced demand in the future. The world emissions of fossil CO_2 would require about 10 kg of ^{14}C. A single fuel rod in a nuclear reactor could be modified to convert the equivalent amount of magnesium nitrate and water into magnesium bicarbonate. (The neutron cross section of nitrogen to form ^{14}C is much larger than the absorption cross sections of Mg and O, limiting the neutron production to that of ^{14}C).

The proposed work focuses on the development of an injection system for accurately tagging large streams of CO_2 with ^{14}C at the part per trillion level and the simultaneous injection of other tracers, such as SF_6. Counting ^{14}C atoms in the reservoir can establish a mass balance and

determine the anthropogenic carbon content. It does not matter whether carbon is present as supercritical CO_2, dissolved carbonate or bicarbonate, organic carbon, etc. Relative to its precision of measurement, the isotopic fractionation of ^{14}C and ^{12}C is only minimal, i.e., ~4% maximum fractionation during the precipitation of minerals (Clark and Fritz, 1997; Mook and Rozanski, 2000). Therefore, total ^{14}C count is directly proportional to the anthropogenic carbon in the reservoir.

In summary, carbon-14 isotope is the best option for tagging to trace the carbon in the CO_2 molecule itself. This technology will serve as an accurate and effective approach to monitoring, verification and accounting in geological carbon storage. It is worth noting that even though the concept of underground carbon-14 accounting is conceptually very similar to other techniques used in exploration and mining engineering, the details of these techniques are still to be worked out. The first step in this direction, which is central to this thesis project, is the successful demonstration that large carbon dioxide streams can indeed be tagged reliably with one part per trillion of $^{14}CO_2$. If this first demonstration of a core part of the technology can be demonstrated, more work is required to move this MVA technology to technical maturity.

2.4 Research Objectives and Dissertation Structure

The specific aim of this research project was to lay the foundation of a future inventory technology for geological CO_2 storage systems based on tagging carbon dioxide for sequestration with ^{14}C so at to make it look like natural carbon on the surface. It was felt that adding the ^{14}C content beyond that of modern surface carbon would cause environmental and safety concerns which would make its introduction unlikely. Moreover, at least conceptually there is little to be

gained by higher tagging levels. Mixing with preexisting carbon would make it impossible to assure that tagged carbon flows always show ^{14}C levels in excess of the natural level. On the other hand, while ^{14}C undoubtedly undergoes a radioactive decay, there should be little safety concern if the ^{14}C content in the mixture is no higher than it is in carbon on the surface, including the carbon that is incorporated into the human physiology.

Project objectives were to construct and test a system for tagging a high flow stream of fossil CO_2 with ^{14}C to a level that does not exceed atmospheric CO_2. Such tagging is in itself a challenging endeavor, because it requires the accurate dosage of miniscule amounts of material into a large stream, ideally without creating any waste streams of unused ^{14}C. While the tagged CO_2 is certainly safe, the high concentration of ^{14}C in the tagging fluid raises safety issues during handling and disposal of waste materials. This risk is managed by minimizing the amount of waste left after filling the tagging cartridges and after injection of their content into the CO_2 stream and by making the tagging cartridges so small that the accidental release of the content of an individual cartridge would still only pose a minor risk.

At roughly one part per trillion, the concentration of ^{14}C in modern carbon is extremely small. There are several technical challenges in tagging a carbon dioxide stream for geo-sequestration.

1) Tagging has to be reliable and accurate and operate on an extremely large mass flow. Pipelines could deliver large flows, as large as 1 ton/second.
2) The ratio of the tagging flow to the tag flow is on the order of 10^{12}:1. This means for every ton of CO_2 flowing by, one needs to add one microgram of $^{14}CO_2$.

3) The ^{14}C content of the CO_2 stream could vary over time and the tag will need to be adjusted to such changes. For example, the CO_2 could derive from capture at a coal fired power plant that at some time also co-fires a certain amount of biomass.
4) The tagging operation must be safe, and the risk of accidental release of concentrated $^{14}CO_2$ must be minimal. It must be lower than the risks of mishaps in medical applications of radioisotopes.
5) The success of the tagging process must be verifiable and ideally can be monitored in real time.

The research, presented in this thesis, involved the development of a filling station to fill a cartridge with tagging material, i.e., tiny volumes of highly concentrated $^{14}CO_2$ for injection; the development of an injection (or tagging) station where the tag is added to a large CO_2 stream; the demonstration of the filling and tagging processes in the laboratory; and the demonstration of tagging in the field.

As will be discussed below, the cartridges developed for holding the concentrated $^{14}CO_2$ tracer have been shaped in the form of long thin tubes wound into lose spiral shape. Therefore these cartridges will be referred to in the following section of this document as tracer loops.

In addition, we worked on the development of new techniques for measuring in real time the ^{14}C concentration in a CO_2 sample. The concept of online ^{14}C monitoring provides a real time control of CO_2 injection and monitoring during the geological sequestration process (Figure 2). The development of the $^{14}CO_2$ monitor is largely outside of the scope of this thesis.

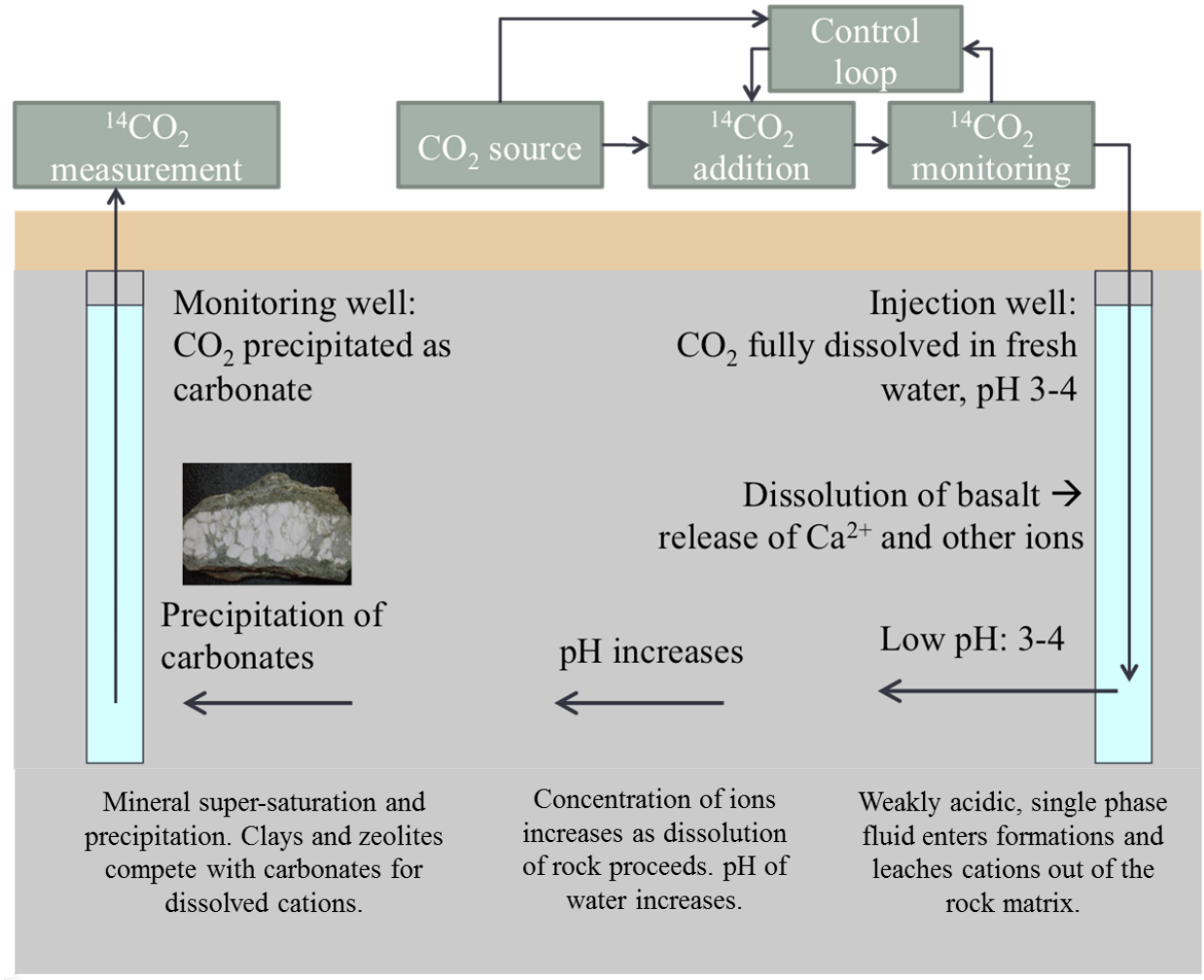

Figure 2: Diagram of online ^{14}C monitoring for a carbon mineralization storage site, as used in the Icelandic Carbfix program (modified from Aradóttir et al., 2011).

Beyond the management task, the project was structured into five major technical tasks to accomplish these goals and objectives:

Task 1: Design of the ^{14}C tagging tracer loop injection system and filling station for the tracer making process. A tracer loop is a very thin short tube in the form of a small loop that holds in its small interior volume a fluid rich in $^{14}CO_2$ for tagging. This effort included designing and fabricating a filling station to generate tracer loops that can hold dissolved tracer gas (SF_6 and

$^{14}CO_2$). These tracer loops would be designed to inject tracer gases at the one part per trillion (ppt) levels.

Task 2: Laboratory-scale evaluation of the injection system. This part included designing and constructing a high-pressure flow loop for injecting, mixing and sampling purposes. This loop contained a finite volume of water or liquid CO_2 that was recirculated in order to simulate a large flow in the pipe. Tracer injection would therefore be accumulating making the detection of successful tagging easier. Together with $^{14}CO_2$, SF_6 was also used as a secondary tag and a non-radioactive, inert substitute during the early testing of the filling and tagging equipment. Current atmospheric concentration of SF_6 is about 5 parts per trillion (ppt) (Busenberg and Plummer, 2000). SF_6 can be measured fairly easily in gas or aqueous samples in the sub-ppt concentration range with a gas chromatograph with electron capture detector (e.g., Ho and Schlosser, 2000). On the high-pressure flow loop, injections first with SF_6 and later with $^{14}CO_2$, were performed to demonstrate the controlled tracer injection into water, or liquid CO_2 or supercritical CO_2.

Task 3: Field test of developed $^{14}CO_2$ tagging system. The CarbFix demonstration project in Iceland offered an excellent opportunity to test the proposed technology under realistic conditions, with measurements to be verified by conventional ^{14}C detection methods. Even though the level of sophistication of our design exceeds what is necessary at the CarbFix test site, the location offers the entire necessary injection infrastructure to try out this system. The site has a CO_2 capture plant, CO_2 pipelines, injection and observation wells and most importantly all the required licenses and authorization for using ^{14}C (Matter et al., 2009; Gislason et al., 2010).

The CarbFix project was established by Icelandic, French and American scientists and was launched in 2007. One of the main tasks of the project is to conduct a field-scale CO_2 injection

into a permeable basalt formation in 600 m depth (Alfredsson et al., 2008; Gislason et al., 2010). The CarbFix test site is unique among all the on-going CO_2 pilot injection projects because it uses ^{14}C among other tracers (SF_6, SF_5CF_3 and amidorhodamine-G) for monitoring and verification of CO_2 storage.

Task 4: Development of $^{14}CO_2$ Detection System. Current monitoring equipment for ^{14}C activity was designed for other applications, and needed to be streamlined and improved for online monitoring and accounting in geological carbon storage.

Task 5: Hazard and environmental analysis. Although the quantity of ^{14}C involved in the proposed work is quite minimal compared to existing sources (i.e., nuclear power plants, hospitals, etc.), a full life cycle analysis of the ^{14}C cycle from the production to discharge is performed in order to minimize the safety and environmental issues and ensure the safety of the proposed MVA protocol.

These basic steps were organized into the set of tasks listed above. I took the lead in Tasks 1, 2, and 3, i.e., developed the membrane system as the filling station for making the ^{14}C tagging tracer loops; designed the high-pressure flow loop system for laboratory-scale evaluation, and conducted the field test in Iceland. In this dissertation, I used chapters 3, 4, and 5 to describe the activities and results associated with Tasks 1, 2, and 3, respectively. My former colleague, Dr. Cantwell Carson was mainly responsible for Task 4. As for Task 5, the safety analysis, I contributed to this part, while it was not a major component of my responsibilities. Therefore, in Chapter 6, I briefly summarized the high-level findings and results of Task 4 and 5, and made recommendations on future work accordingly. In Chapter 7, I provided a conclusion section for the entire work.

Chapter 3: Filling Station for the ^{14}C Tag Production

Designing and building a filling station for tracer fluid cartridges was the first task of this project. The objective was to design and fabricate micro-cartridge systems at two different scales that can hold either compressed tracer gas (SF_6 and $^{14}CO_2$) or the same tracer gases dissolved in water. The micro cartridges holding the tracer were designed to accurately inject tracer gases into the CO_2 stream at the one part per trillion (ppt) level. A device, i.e., the filling station, to fill the micro cartridges (tracer loops) with tracer gas was designed and built. The development of the filling station became a central part of the thesis research.

Two distinct ways for injecting CO_2 into the flow of a large pipe were considered. In one case, a small cartridge filled with $^{14}CO_2$ gas would release the tag into the main pipe through a small port. In the second design, the $^{14}CO_2$ gas cartridge was replaced with a somewhat larger cartridge (the tracer loop) in which $^{14}CO_2$ was dissolved in an aqueous solution. Even though the latter approach would invariably introduce water into the CO_2 flow, the total amounts would be too small to raise any concerns about humidification of the CO_2 flow. As we aimed to add only one part per trillion of ^{14}C, the water vapor added was just one part per billion of the CO_2 flow, and therefore negligible in a stream of industrial CO_2 that would certainly have not been dried to such exacting standards that one additional part per billion would represent a significant change.

We developed both approaches, i.e., the gas cartridge and the aqueous solution tracer loop, to the point we could decide which one was better. We settled on the latter one, because it greatly

simplified the control of the injection and it made it possible to create very accurately filled cartridges. My former colleague, Ed Chen conducted the design of the pure gas micro cartridge approach; while Dr. Cantwell Carson constructed a mercury pump system for the aqueous solution tracer loop approach. We thought those efforts are worth mentioning here, not only because the lessons learned led us to the final design of the membrane system, but also in comparison to them, the membrane system stands out for its neatness, effectiveness and accuracy. A brief description of the early attempts follows.

For the pure gas micro cartridge design, we assumed that our micro cartridge would need to withstand pressures exceeding 100 atmospheres (1,470 psi) and for safety should be rated to withstand a full order of magnitude higher pressure (Figure 3). The mounting of the micro cartridge to the filling station presented a design challenge within our system because of the high pressures involved, as well as the need to precisely calibrate the volume and pressures inside the dispensing units. The mounting piece was to be designed with a seal so that it was capable of withstanding the pressures that may cause a failure of contact between the cartridge and the filling station.

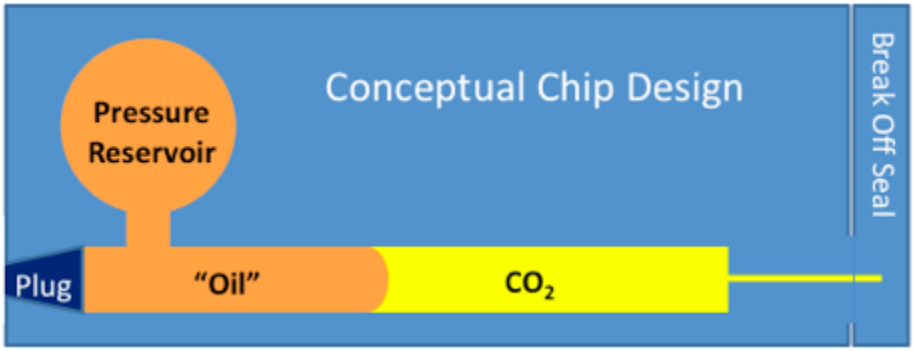

Figure 3: Conceptual drawing of pure gas micro cartridge design.

The $^{14}CO_2$ reservoir was to be inside Poly-Ether-Ether Ketone (PEEK) tubing. An existing Tee fitting was to be used as the structural support for the micro cartridge (Figure 4). The tube actuator was to be made of Gallium Alloy, a liquid metal which could both serve as the sealing material and pressurize the gas inside PEEK tubing. The nozzle, which was the tracer injection port, was another component to be designed. Laser ablation might be used to precisely create a nozzle hole through the sealing plug on site. This seemed to be the most economic means of producing and using the pure gas micro cartridge. Otherwise, the attachment of the nozzle to the cartridge proved to be prohibitively expensive.

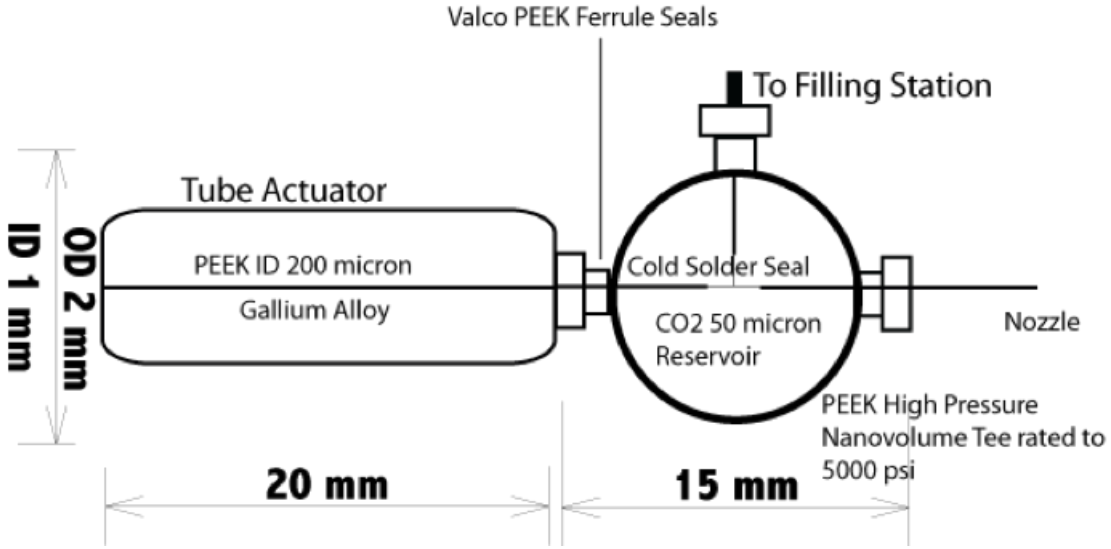

Figure 4: Schematic diagram of the pure gas micro cartridge with PEEK tubing inside a Tee fitting, which connect the filling station, the tube actuator, and the nozzle.

We considered the construction and the performance of the pure gas micro cartridge system as a major uncertainty. Since mechanical failure of the cartridge systems would lead to a sudden release of the entire ^{14}C content into the ambient environment, we decided to abandon the pure gas micro cartridge approach and focus on the aqueous solution tracer loop approach.

We then explored a modified mercury pump system as the filling station (Figure 5). It used four three-way ball valves and three two-way valves. The system was designed to be evacuated by a mechanical pump and then backfilled with $^{14}CO_2$. Deionized (DI) water was then injected into the chamber with the $^{14}CO_2$. Mercury was introduced from a reservoir to return ambient pressure to the system. The concentration of CO_2 in water was then allowed to equilibrate over the course of a few hours. To start filling attached tracer loops, the valve to the chamber with the solution was opened and the mercury reservoir was raised until it could provide the pressure needed to push the solution into sample loops. A small length of transparent tubing was used to gauge the level of the mercury.

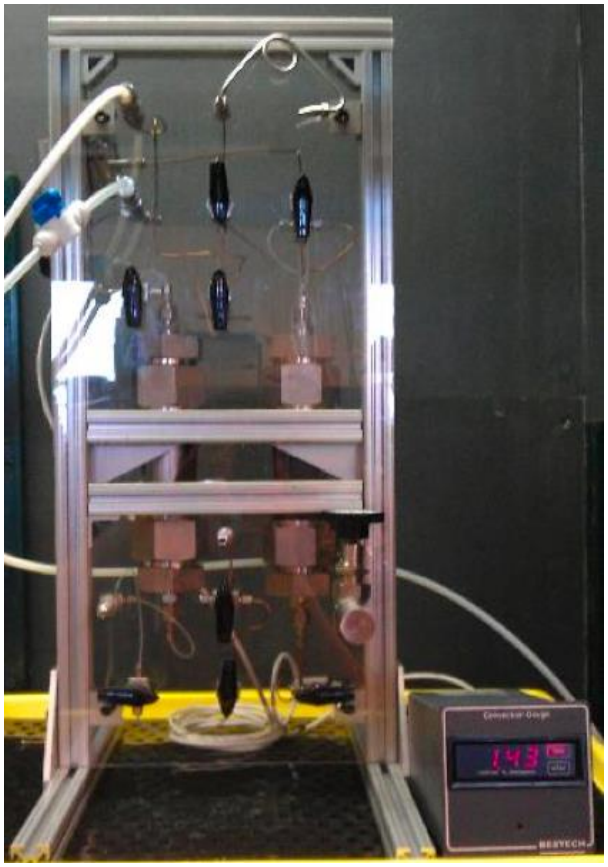

Figure 5: An early attempt of a modified mercury pump system as the filling station.

This approach did enable us to get CO_2-water tracer solutions. However, it still resulted in some technical issues that remained unresolved, like being time-consuming during the tracer making process, allowing for the introduction of bubbles into the solutions and therefore causing not uniform tracer concentration. Moreover, mercury itself is a hazardous material, which introduces additional risks and complexities in to the filling station design and into the practical filling process.

Based on the lessons learned from the first two unfavorable designs, we were able to develop a novel membrane based gas exchange system as the tracer loop filling station. The design is described in details in the following sections.

3.1 Background of Dissolving CO_2 into Water with Microporous Hydrophobic Hollow Fibers

Hollow fiber membrane contactors have been used to achieve gas/liquid transfer both in industrial processes and for research purposes (Gabelman and Hwang, 1999). They have been shown to be effective in the absorption of CO_2 into aqueous solutions (Rangwala, 1996; Zhang et al., 2006). These fibers are widely used, for example, in the beverage industry to carbonate soft drinks. Therefore, microporous hydrophobic hollow fibers were used to make the membrane CO_2/H_2O exchanger.

Specifically, the characteristics of the X30-240 Microporous Hollow Fibers (Liqui-Cel, Charlotte, NC) used in our gas exchange system are listed as below:

- Internal Diameter (nominal): 240 μm;
- Wall Thickness (nominal): 30 μm;

- Outer Diameter (nominal): 300 μm;
- Effective Pore Size: 0.04 μm;
- Porosity (nominal): 40%.

3.2. Membrane Exchanger – Plastic Prototype and Proof of Concept

A plastic membrane CO_2/H_2O exchange station was built as the membrane exchanger prototype. We used DI water in equilibrium with air as the water inlet. Water flowed through the hollow fibers. In the first stage, we degassed water by connecting the outside of the fibers to a vacuum pump; then in the second stage, the outside of the fibers was connected to a CO_2 containing syringe (Figure 6).

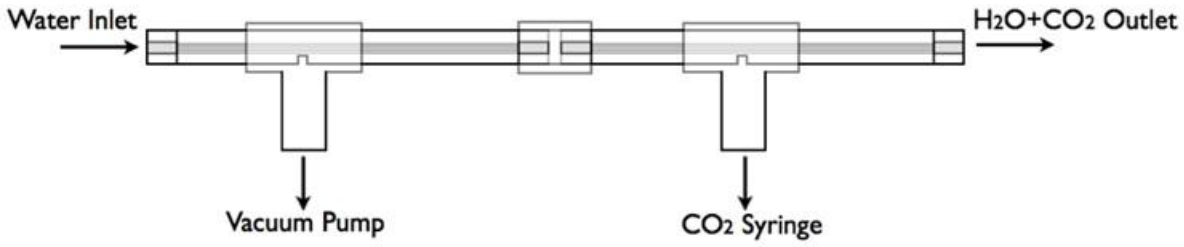

Figure 6: A diagram of the membrane CO_2/H_2O exchange station.

The two-stage design could remove the atmospheric air in the first stage so that the total dissolved gas pressure would be dominated by CO_2 in the second stage. If air was left in there, it would dilute the CO_2 in the second stage which would make the CO_2 concentration of the gas side of the second stage undefined. We also controlled the temperature and/or partial pressure of CO_2 in the second stage to achieve a concentration lower than the equilibrium concentration of CO_2 in water under 101.3 kPa of CO_2 at ambient temperature, which prevented the formation of

bubbles and degassing as the cartridges are stored or moved. The product of the two stages was a water solution with a fixed concentration of CO_2 dissolved in it uniformly.

We used Hardman 4001-BG10 Epoxy to glue the end of a bundle of fibers together and also to the inner hole of a plastic plug. The outside of the plastic plug was then glued to the inside of a plastic tube at one end; the other end of the bundle of fibers was sealed in the same manner to the other end of the plastic tube. The only path for liquid to flow through the tubes was through the hollow fibers. A cross sectional view of the Liqui-Cel hydrophobic fibers at the tips shows the openings that water flowed through (Figure 7).

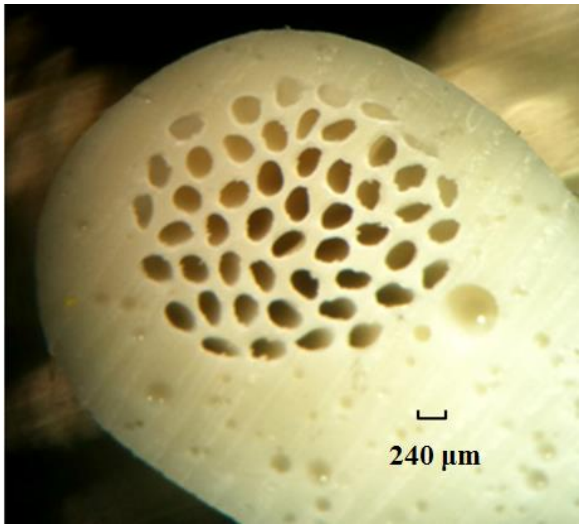

Figure 7: A micrograph of the ends of a bundle of Liqui-Cel fibers showing the openings that the water flowed through (the nominal Internal Diameter of each fiber is 240 µm).

In order to prove the viability of this gas exchange approach, we first built a simple setup with the two-stage membrane exchanger (Figure 8). We connected a water aspirator-type vacuum pump and a syringe filled with pure CO_2 to the two stages of the membrane exchanger, respectively. A syringe pump was used to pump de-ionized water (in equilibrium with air)

through the membrane exchanger. A pH meter was used to measure pH value of the outlet solution.

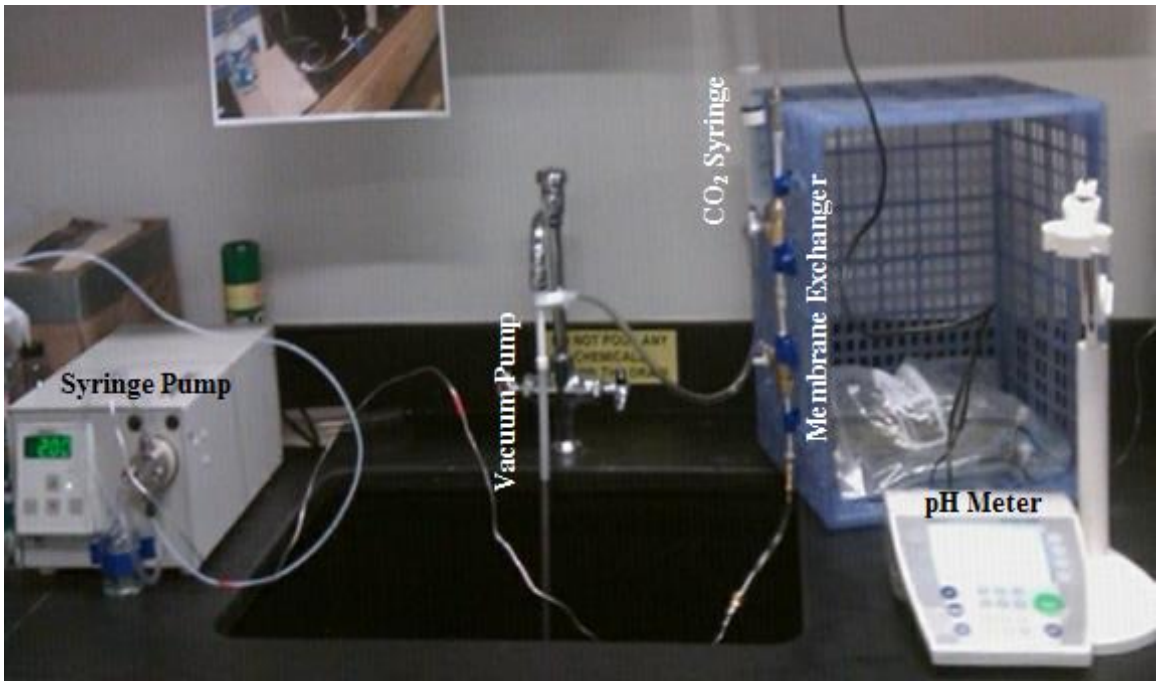

Figure 8: A picture of the initial testing setup with a vacuum pump and a CO_2 syringe connected to the membrane exchanger, a syringe pump for water inlet injection, and a pH Meter for outlet solution pH value measurement.

At the beginning of the test, we opened the valve connecting the first stage of the membrane contactor with the vacuum pump, during this stage the valve connecting the second stage with the CO_2 syringe remained closed. We pumped de-ionized water at 2 mL/min with the syringe pump. When we opened the valve of the CO_2 syringe, the pH value of the outlet solution started dropping and stabilized at 4.34 (Figure 9). This test result indicated that the membrane contactor was able to dissolve CO_2 into water and achieve a certain CO_2 concentration in the outlet solution, therefore this experiment served as the initial proof of concept.

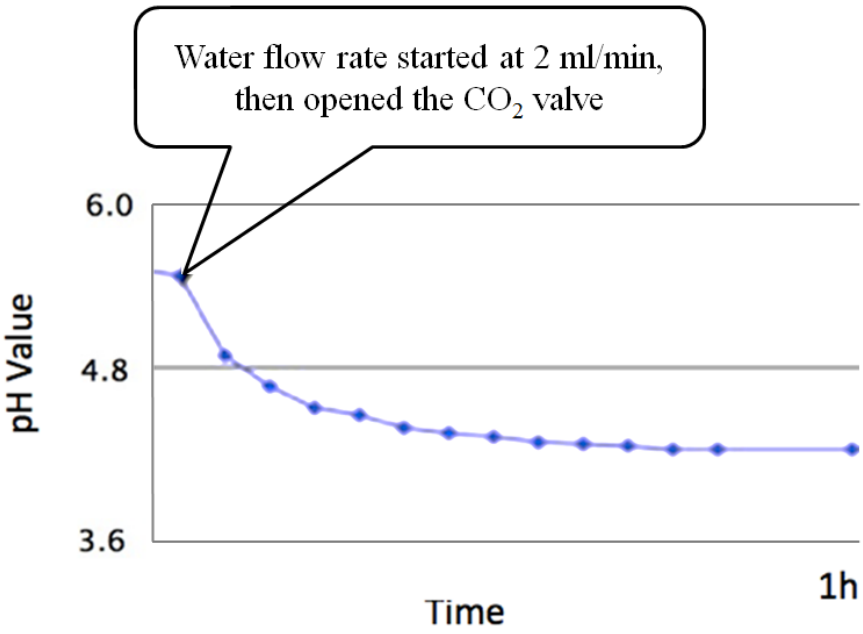

Figure 9: pH value corresponding to the CO_2 concentration in the outlet solution shown in an initial proof of concept test.

3.3 IRGA flow loop – Characterization of the Filling Station

The filling station would ultimately be designed for making $^{14}CO_2$-water tracer loops for the field tests in Iceland. However, since $^{14}CO_2$ is radioactive and hazardous, we planned to use the filling station first to make $^{12}CO_2$-water tracer loops and SF_6-water tracer loops, characterize the filling station with these gases, optimize it for the $^{14}CO_2$-water tracer making process, and then use it to make the $^{14}CO_2$-water tracers for the field tests in Iceland.

A flow loop with an infrared gas analyzer (IRGA) was designed to continuously analyze the CO_2 concentrations achieved in $^{12}CO_2$-water tracer solution (Figure 10).

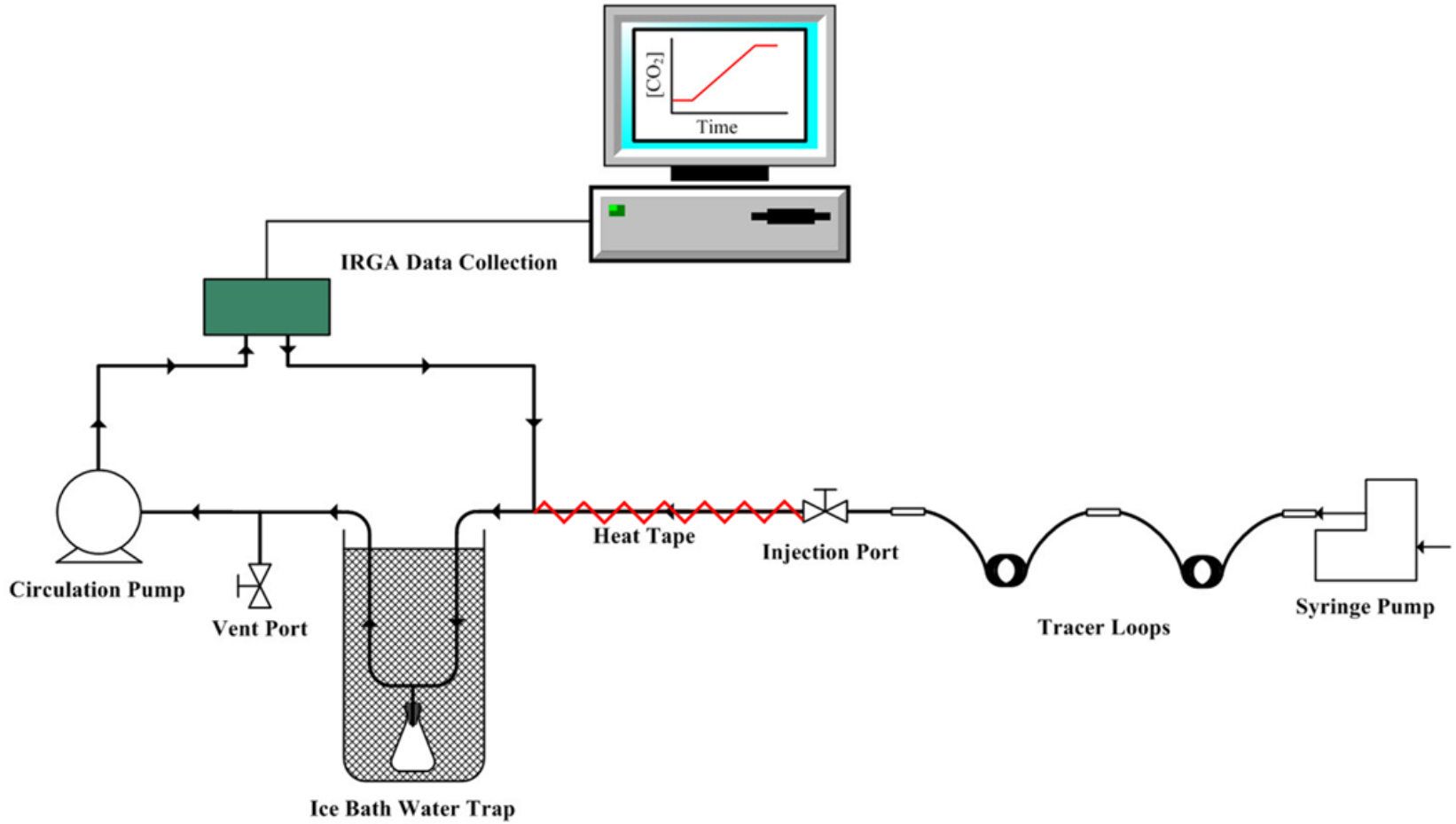

Figure 10: Schematic diagram of the experimental setup to test the performance of tracer loops, with the dark green rectangular block indicating the IRGA, the tracer solution injected flowing through a heating path and an ice trap to get the CO_2 gas separated from water and diffused in the internal volume of the IRGA flow loop.

The tracer loops, were prefilled with the outlet solution from the membrane exchanger, then injected into the IRGA flow loop. The internal volume of the IRGA flow loop was prefilled with ambient air. The circulation pump circulated the gas mixture into the IRGA for real time analyzing and data logging of the CO_2 concentration in the gas mixture.

The IRGA used, was an LI-840A CO_2/H_2O analyzer (LI-COR, Lincoln, NE). The measurement ranges for CO_2 and H_2O are 0-20,000 ppm and 0-60 mmol/mol, respectively. For the tracer loops, off-the-shelf Valco-Vici sample loops were used. There are different models with different internal volume of these sample loops. The selection criteria will be discussed later.

The principle of the tracer loop performance evaluation, i.e., filling station characterization, with the IRGA flow loop is straightforward. The IRGA records the CO_2 concentration increase during the injection of the tracer solution; therefore, the slope of the CO_2 concentration curve vs. the volume of tracer solution injected can serve as an indicator of the CO_2 concentration in the tracer solution. It also measures our ability for constant delivery of tracer solution from the tracer loop during the injection process.

Pure CO_2 gas was used as a reference to calibrate the slope of the CO_2 concentration curve. The CO_2 injected was at room temperature and pressure (about 22 °C and 101.3 kPa). The internal temperature and pressure of the gas mixture in the IRGA flow loop were around the similar level. Those conditions were within reasonable tolerances where both air and CO_2 could be treated as ideal gases. Under the ideal gas law, we can derive the rate of CO_2 concentration increase, $r_{[co_2]_{pure\ co_2}}$, expressed as ppm per mL CO_2 injected (Eq. 1). Δn_{co_2} is the molar amount of CO_2 injected, $\Delta V_{co_2}(RTP)$ is the volume of CO_2 injected at room pressure (P_r) and room

temperature (T_r). n_{in} is the molar amount of gas mixture (mainly air and small fraction of CO_2 injected) inside the IRGA flow loop, while P_{in}, T_{in}, and V_{in} are the internal pressure, temperature, and volume, respectively.

$$r_{[co_2]_{pure\ co_2}}(ppm/mL) = \frac{\frac{\Delta n_{co_2}}{n_{in}}}{\Delta V_{co_2}(RTP)} = \frac{\frac{\Delta n_{co_2}}{\Delta V_{co_2}(RTP)}}{n_{in}} = \frac{\frac{P_r}{T_r}}{\frac{P_{in}V_{in}}{T_{in}}} = \frac{P_r T_{in}}{P_{in}V_{in}T_r} \quad (1)$$

We could use the same setup to record the slope of the CO_2 concentration curve during the injection of any CO_2-water tracer solution. In this case the CO_2 concentration increase rate, $r_{[co_2]_{co_2-water}}$, is expressed as ppm per mL solution injected (Eq. 2). $\Delta V_{solution}$ is the volume of CO_2-water tracer solution injected, Δn_{co_2} is the molar amount of CO_2 dissolved in the tracer solution injected, $\Delta V_{co_2}(RTP)$ is the volume of the CO_2 injected expressed at room pressure (P_r) and room temperature (T_r), while other terms are the same as described previously. It's also worth noting that since the water injected was captured in the cold trap, the volume added in the IRGA flow loop was the CO_2 gas rather than the water.

$$r_{[co_2]_{co_2-water}}(ppm/mL) = \frac{\frac{\Delta n_{co_2}}{n_{in}}}{\Delta V_{solution}} = \frac{\frac{\Delta V_{co_2}(RTP)P_r}{T_r}}{\frac{\Delta V_{solution}P_{in}V_{in}}{T_{in}}} = \frac{\Delta V_{co_2}(RTP)}{\Delta V_{solution}}\frac{P_r T_{in}}{P_{in}V_{in}T_r} \quad (2)$$

Since the same setup was used for all tracer injection tests, we could assume the internal pressure, temperature, and volume to be the same as well. Then we could calculate the CO_2 concentration in the tracer solution, expressed as cc STP CO_2 per mL solution (Eq. 3). P_s and T_s are the standard pressure (101.3 kPa) and temperature (0 °C), respectively.

$$[CO_2]\ in\ solution(cc\ STP/mL) = \frac{\Delta V_{co_2}(STP)}{\Delta V_{solution}} = \frac{\Delta V_{co_2}(RTP)}{\Delta V_{solution}}\frac{P_r T_s}{P_s T_r} = \frac{r_{[co_2]co_2-water}}{r_{[co_2]pure\ co_2}}\frac{P_r T_s}{P_s T_r} \quad (3)$$

Therefore, the amount of CO_2 delivered in the tracer loop by the filling station is described as a function of the $\frac{r_{[co_2]co_2-water}}{r_{[co_2]pure\ co_2}}$ ratio.

Further, since the microporous hollow fiber membrane is very effective in dissolving CO_2 into water, and the water was pumped at very slow flow rates (0.15-0.25 mL/min), we assumed that the tracer solution was pure DI water saturated with CO_2 and had no alkalinity at the outlet of the membrane contactor. Then the only uncertainty left was the tracer solution temperature at the outlet of the membrane contactor.

By comparing the CO_2 concentration calculated from the above equation with theoretical CO_2 solubility data (Span and Wagner, 1996), our measurements resulted in an equivalent outlet temperature of the membrane contactor. This number can be used for estimating the performance of the membrane system when processing other solutes and solvents.

With the IRGA flow loop, we further examined the effectiveness of the membrane contactor prototype in dissolving CO_2 into water by making CO_2-water solutions at three different water flow rates, 0.15 mL/min, 0.2 mL/min, and 0.25 mL/min, respectively. During this set of experiments, there was no heating mechanism on the membrane contactor. The solutions were collected and then injected into the IRGA flow loop to compare their CO_2 concentrations.

The curves of CO_2 concentration in the IRGA flow loop are plotted as a function of the volume of tracer solution injected (Figure 11). The first order linear trend lines are presented as well.

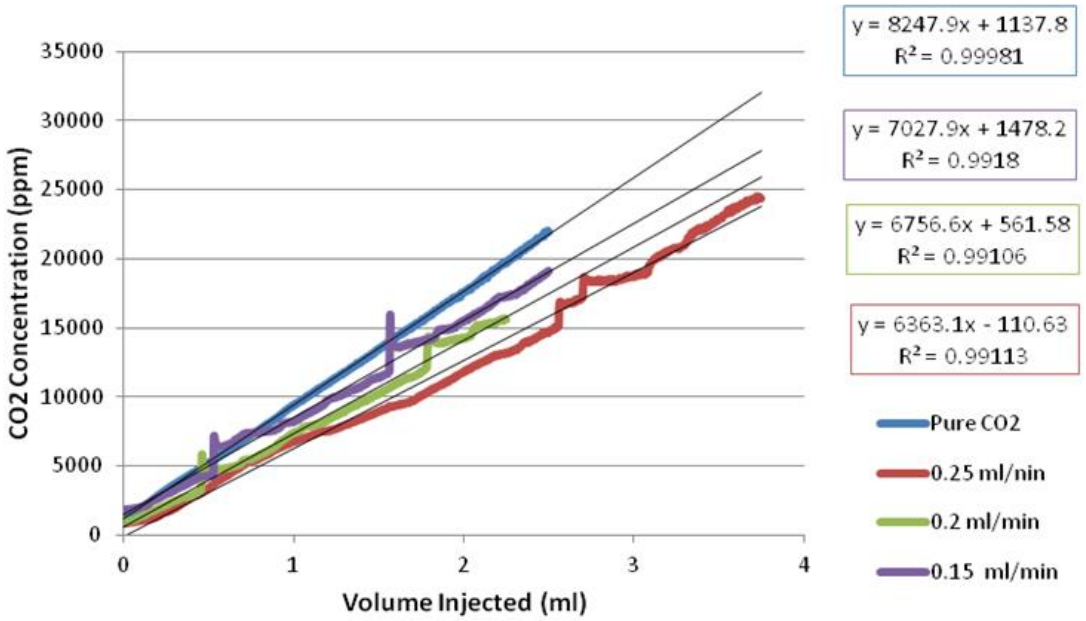

Figure 11: The concentration of CO_2 inside the IRGA flow loop as a function of volume injected, for pure CO_2 and CO_2-water tracer solutions made at three different water flow rates.

In the first stage of the membrane contactor, where the outside space of the hollow fiber membrane was connected to vacuum, the water flow was degassed. At the same time, a small portion of the water flow also evaporated since Liqui-Cel hydrophobic fibers are somewhat permeable for water vapor, and this evaporation lowered the water temperature. Then in the second stage of the membrane contactor, where the outside space of the hollow fiber membrane was connected to CO_2 at 101.3 kPa and ambient temperature, the water flow dissolved CO_2, and became fully saturated at the outlet of the membrane contactor. Therefore, lower water flow rate, i.e., longer residence time in the membrane contactor, resulted in lower water temperature, i.e., higher equilibrium CO_2 concentration. The larger CO_2 concentration slope during the injection of CO_2-water solution made at lower water flow rates validated our analysis, and thus demonstrated the feasibility of the membrane contactor.

It's also worth noting that because of the Ice Bath Water Trap structure in the IRGA flow loop (Figure 10), when we were injecting the tracer solution, some tiny water droplets would start to accumulate inside the tube connected to the erlenmeyer flask, and after a while they would turn into a bigger droplet and fall in the erlenmeyer flask. This process introduced a sudden volume decrease of the IRGA flow loop, thus resulting in the spikes in the CO_2 concentration curves of the CO_2-water tracer solutions (Figure 11). The spikes have nothing to do with the CO_2 concentration in the tracer loops, since inside one tracer loop, the CO_2-water solution should have one uniform concentration. The pure CO_2 gas tracer injection didn't involve any water phase change, therefore it resulted in a straight line.

At this point, the experiment only aimed for the proof of concept, the performance of the membrane exchanger (e.g., the difference between expected and measured CO_2 concentration) was evaluated quantitatively once we constructed the complete filling station.

3.4 Design and Construction of the Filling Station

After we demonstrated that the plastic version of membrane contactor prototype could degas water and equilibrate CO_2 efficiently, the next step was to make a membrane contactor with stainless steel tubing. Also, we needed to design and construct the whole filling station with the consideration of safety and waste management issues in order to be able to deal in later experiments with radioactive $^{14}CO_2$. The initial design of the membrane system, i.e., the filling station, is shown in a schematic diagram (Figure 12). The details on the design and the purposes of all the tubing and valves are described in the following.

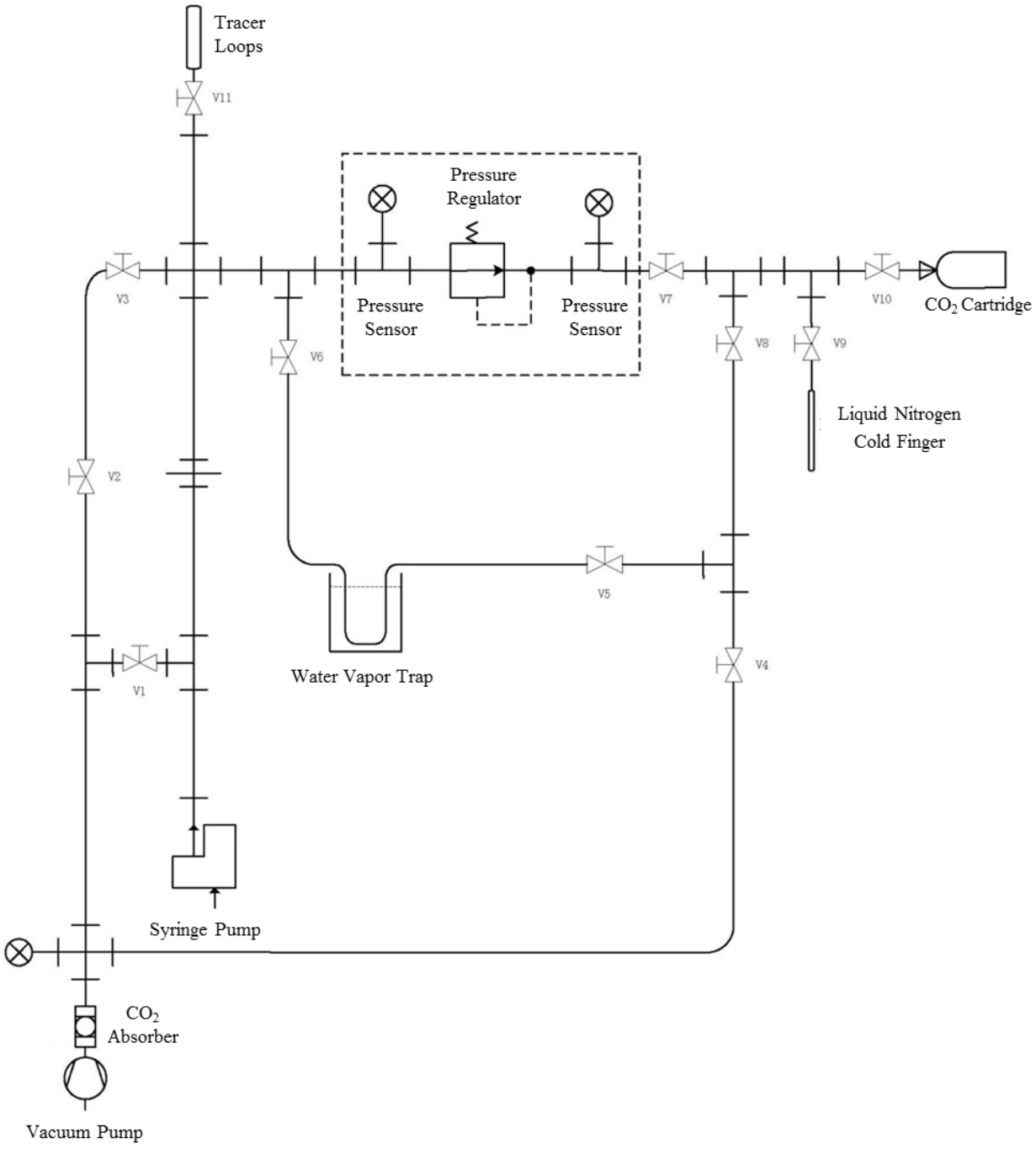

Figure 12: Schematic diagram of membrane system initial design, which contains pressure control mechanism for tracer gas supply during the tracer making process and structures for waste management and safety purposes in dealing with $^{14}CO_2$.

The most important part of the membrane system is the membrane contactor, consisting of two tubes with a hollow fiber membrane inside, one stage for water degassing, the other for CO_2 dissolving, as discussed previously. It's shown as the line between the syringe pump and V11 (Figure 12).

We added some lines to make the connection between the tubes and the vacuum pump. Also, one pressure regulator and two pressure sensors transducer were installed on the CO_2 side to control the pressure. The other structures in the membrane system, such as pipelines and valves, the $^{14}CO_2$ cartridge, the liquid nitrogen cold finger, the water vapor trap and the CO_2 absorber are constructed for dilution, recycle, and safety purposes in dealing with $^{14}CO_2$.

Most of the lines were made of 1/4" stainless steel tubing. The exception was the horizontal lines connecting from the cross (on the second stage of the membrane exchanger) to the CO_2 cartridge, and the Liquid Nitrogen Cold Finger. These lines were made of 1/8" stainless steel tubing in order to reduce the dead volume on the tracer gas source side. Minimizing the dead volume is of importance when handling the $^{14}CO_2$ cartridge as the gas source.

This membrane system in its initial design aimed to generate a CO_2-water solution at a certain CO_2 partial pressure and water flow rate. Further optimizations were introduced later.

The operation steps of the membrane system for tracer making process are described as follows.

Evacuating:

1) All valves are closed at the beginning;
2) Open V1, V2, V3, V7, V9, and V10;

3) Turn on the vacuum pump to evacuate the system;

CO_2 loading:

1) Close V2, V3, open the valve to the full CO_2 cartridge;
2) Use the liquid nitrogen cold finger to trap all CO_2 from the cartridge;
3) Close V10, heat up the cold finger to release the CO_2 into the system;
4) Open V11, start the syringe pump to inject water;
5) The CO_2 syringe, i.e., tracer loops, will be filled up with CO_2-water solution;

Waste collecting:

1) Stop the syringe pump, close V1 and V11;
2) Open V4, V5 to evacuate the water trapping pipeline;
3) Close V4, stop the vacuum pump;
4) Open V6 and V8, use the liquid nitrogen cold finger to trap waste CO_2 from the system;
5) Close V5, V6 V7, and V8, heat up the cold finger to get CO_2 back into the cartridge, close the valve of the cartridge for future use.
6) Open V4 and V8, turn on the vacuum pump again;
7) The CO_2 left in the system gets adsorbed by the CO_2 absorber.

According to the alignment of components in the 2D schematic diagram, a Solid Works 3D drawing of the membrane system was produced as part of the pre-construction preparations (Figure 13). The pressure control parts (one pressure regulator and two pressure sensors) are presented as enclosed in the dark gray box.

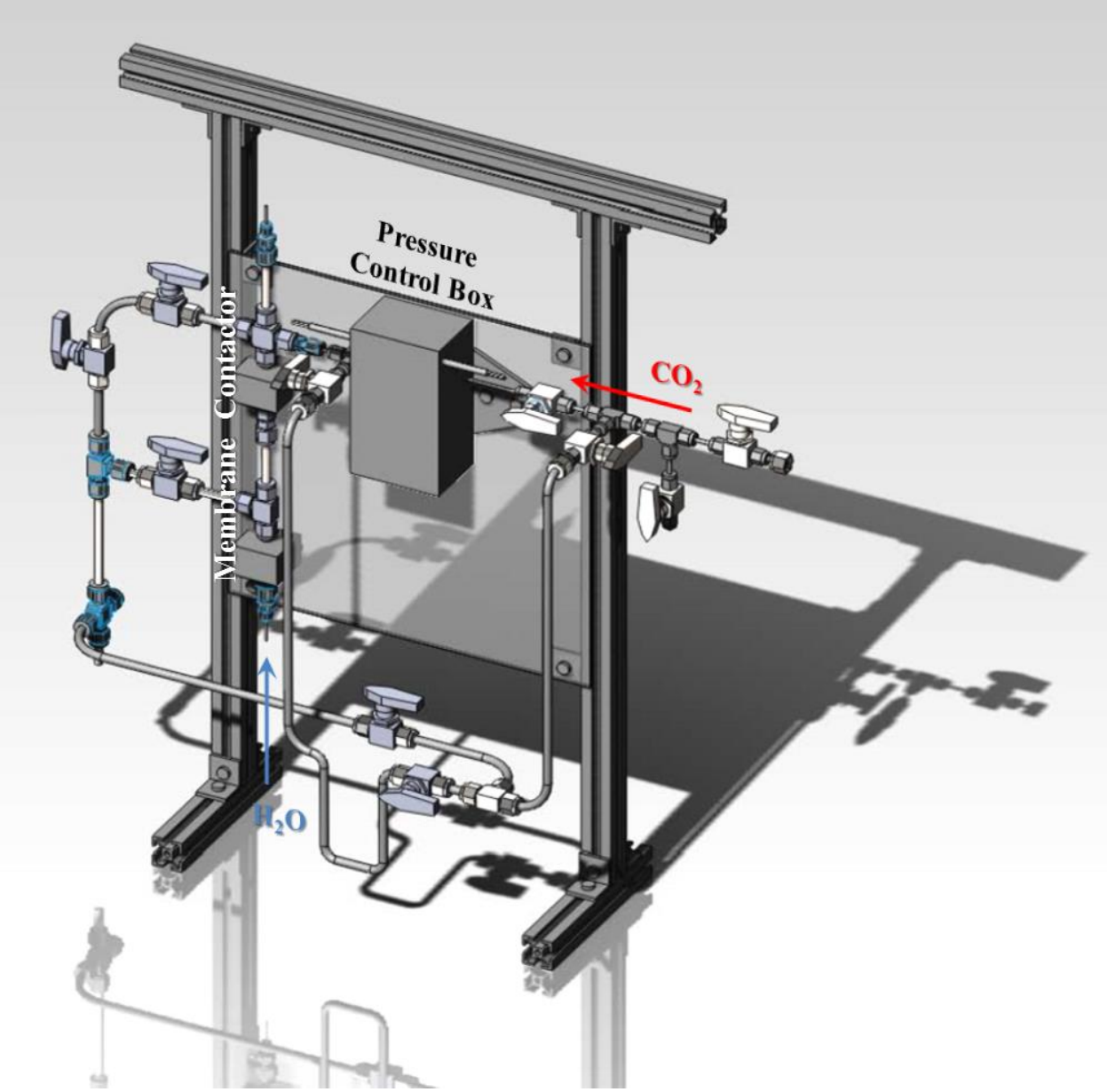

Figure 13: Solid Works 3D drawing of membrane system, showing the membrane contactor, pressure control box, CO_2 and H_2O flows.

The membrane contactor was made from 1/4" stainless steel tubing, with a bundle of 45 X30-240 microporous hollow fibers in both stages. The bundle of fibers was glued (Hardman 4001-BG10 Epoxy, light amber color, relatively softer to make a clean cut of the fiber bundle) to the

center of aluminum plugs, which were then glued (Hardman 4002-BG10 Epoxy, aluminum color, higher viscosity to make the seal more durable) to both tips of the tubes at both stages (Figure 14).

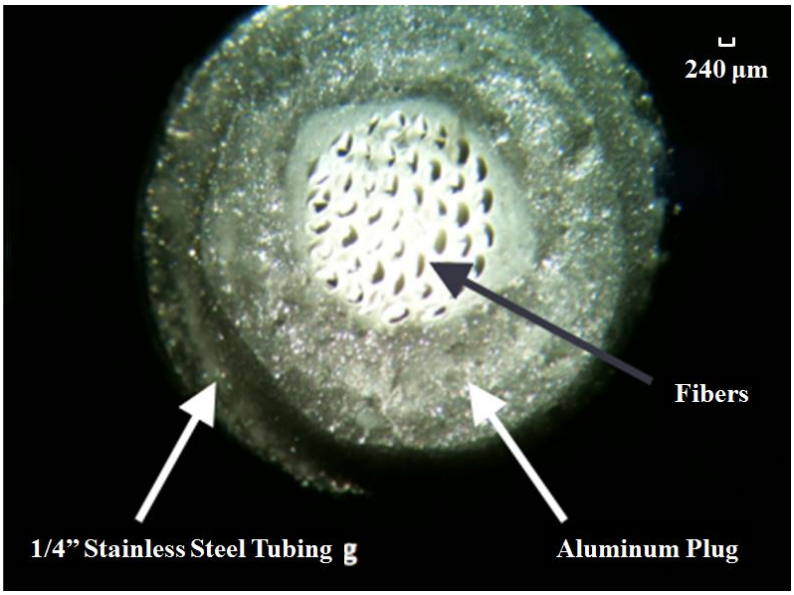

Figure 14: A micrograph of the tubing tips of the stainless steel membrane contactor.

Using the 3D drawing as reference, we constructed the membrane system (Figure 15). We conducted leak test on the membrane system by capping all the outlets (e.g., the tips of the membrane exchanger, the connection from V10 to the CO_2 cartridge) and evacuating the entire system. It was able to hold -97 kPa of vacuum for days.

The initial design had a 0-689.5 kPa (0-100 psi) gage pressure sensor (Omega PX71-100GV) on the upstream of the tracer gas supply, and a 0-103.4 kPa (0-15 psi) absolute pressure sensor (Omega PX71-015AV) on the downstream of the tracer gas supply, which was connected to the second stage of the membrane contactor. There is a pressure transducer between the two pressure regulators. The purpose of this design was to create a partial pressure of the tracer gas less than

the ambient pressure to prevent the formation of bubbles and degassing from the tracer solution when it is in use. However, after the system was constructed, the pressure regulator (Beswick Engineering, PRDB-18MM-A-B-C) did not give a stable performance in controlling the downstream of the tracer gas supply at a certain pressure below ambient.

Figure 15: Initial construction of membrane system, showing the membrane contactor, pressure control box, liquid nitrogen cold finger, CO_2 and H_2O flows.

Due to the restrictions in time and budget, we decided to not pursue the pressure control approach, but rather, revise to temperature control at the second stage of the membrane contactor in our final design (Figure 16).

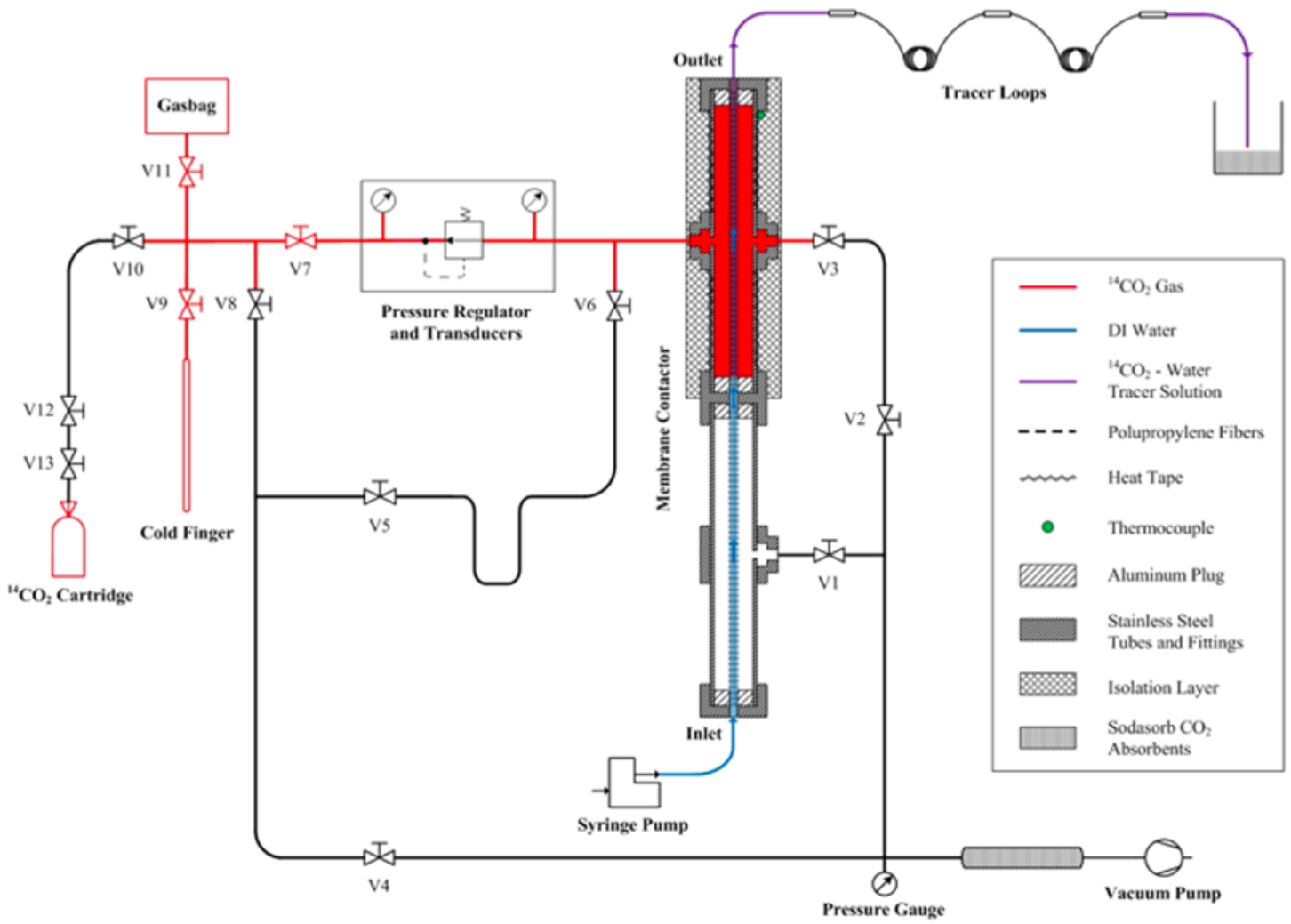

Figure 16: Schematic diagram of membrane system final design, showing the $^{14}CO_2$ cartridge, cold finger and gasbag for mixing, pressure control parts; the red and blues lines indicate $^{14}CO_2$ and H_2O flows in the membrane contactor, respectively.

This design served as the final version of our membrane system, i.e., filling station. It represents the status of the $^{14}CO_2$-water tracer loop making process. The lines filled with $^{14}CO_2$ are marked in red; blue lines indicate deionized (DI) water; black lines indicate vacuum. On the tracer gas supply side, we first used the liquid nitrogen cold finger to trap radioactive gas mixture out of the cartridge, and then used the gasbag at the upstream end as a buffer to maintain the pressure at 1 atm in the membrane contactor on the downstream side. The tubing between V10 and the $^{14}CO_2$ cartridge was in contact with $^{14}CO_2$ when transferring the gas source from the cartridge to the cold finger. However, once we opened the cartridge and introduced $^{14}CO_2$ to the cold finger side, we closed the valve on the cartridge. We then used the liquid nitrogen cold finger to trap all CO_2 in the lines and closed V10. Therefore, the line between V10 and the cartridge was supposed to be no longer filled with $^{14}CO_2$ during the tracer making process and shown in black color.

The main component, i.e., the two-stage membrane contactor, is exaggerated in relative size in the schematic diagram. The syringe pump injects DI water in equilibrium with air from the inlet. In the first stage, water is degassed by connecting the outside of the fibers in this section to a vacuum. In the second stage, the outside of the stainless steel tubing is wrapped with a heating tape, with a thermocouple placed near the outlet of the membrane contactor. The thermocouple is connected with a PID controller, which is used for controlling the heating tape and maintaining the outlet temperature at a set value. We also kept the pressure regulator and transducers, and used the downstream pressure transducer to monitor the pressure in the second stage of the membrane contactor to make sure it was at ambient level. Finally, with DI water degassing in the first stage and dissolving tracer gas in the second stage, the outlet will be our target tracer solution. Also, we added CO_2 absorber in a beaker to trap any droplets that might come out from

the tip of the tracer loops and CO_2 absorber in a chamber between the membrane system and vacuum pump to clean any radioactive residues inside the system after we finished the tracer making process.

By controlling the set temperature of the membrane contactor outlet and the composition of the gas source outside the fibers in the second stage, we can use the membrane system to generate solutions with different tracer gases at target concentrations (no more than equilibrium levels). We would use this system to make tracer loops filled up with SF_6-water solution or $^{14}CO_2$-water solution, and test them in our injection systems accordingly.

3.5 Parameter Setting of the Filling Station

As explained previously in section 3.3, the CO_2 concentration in the CO_2-water tracer solutions generated from the membrane system was described as a function of $\frac{r_{[co_2]co_2-water}}{r_{[co_2]pure\ co_2}}$, which could be obtained from the IRGA flow loop measurements. In order to set the parameters of the membrane system (e.g., water flow rate, outlet set temperature, etc.) for different tracer solution making processes, we needed to first obtain $r_{[co_2]_{pure\ co_2}}$, i.e., the rate of CO_2 concentration increase in the IRGA flow loop per volume of pure CO_2 injection; then test the performance of CO_2-water tracer solutions made at different conditions. All these tests were performed with $^{12}CO_2$ for safety and simplicity. $^{14}CO_2$ was only introduced after the parameter settings of the filling station were fully established. Once we determined the parameters of the membrane system from the $^{12}CO_2$ tests, its performance with SF_6, $^{14}CO_2$, or any other gas, could be predicted based on this calibration.

3.5.1 Pure CO_2 gas injection

Pure CO_2 gas at room temperature and pressure (about 22 °C and 101.3 kPa) was injected into the IRGA flow loop. Since the volume of the IRGA loop is fixed, the slope of CO_2 concentration (ppm increase per mL CO_2 injected) should be quite constant, regardless of the pure CO_2 gas injection rate. We first conducted a series of tests to verify that. By changing the injection rate of pure CO_2, we achieved a series of CO_2 concentration slopes. They show a systematic trend that needs explaining (Figure 17).

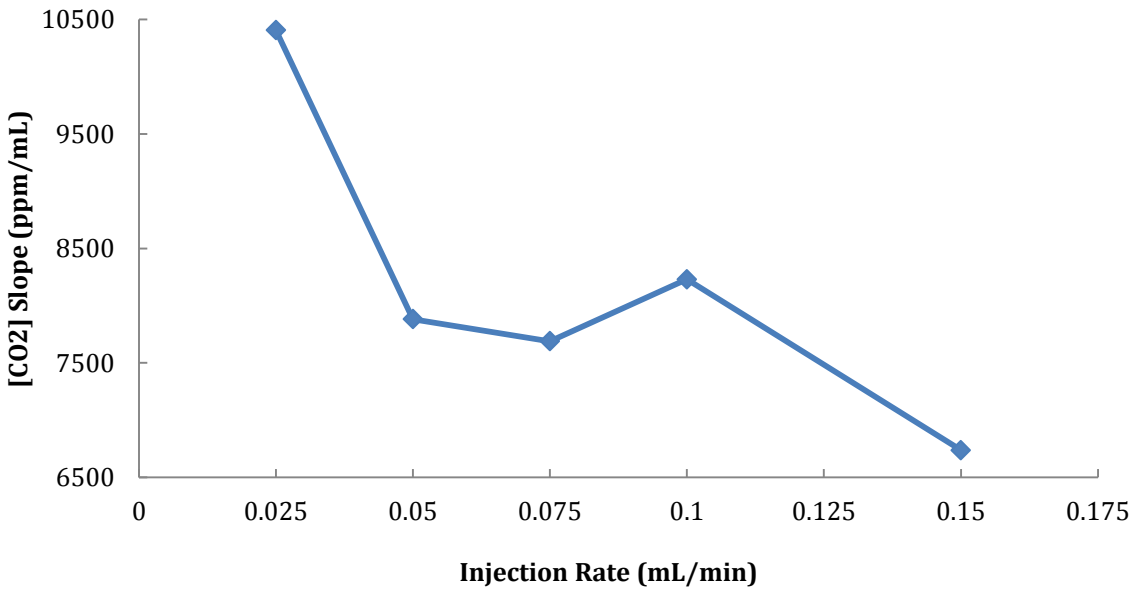

Figure 17: CO_2 concentration slopes at different injection rates of pure CO_2 gas.

In each test, 4 mL of CO_2 were injected, and the IRGA had an initial condition of [CO_2] = 470 ppm, [H_2O] = 6~7 ppt, T = 51.1 °C, P = 100.9~101.2 kPa; and an end condition of [CO_2] = 20700~31000 ppm, [H_2O] = 6~7 ppt, T = 51.1 °C, P = 103.3~104.1 kPa. It's worth noting that, unlike other parameters, the T here only represents the temperature inside the IRGA detection

chamber, rather than the average temperature inside the IRGA flow loop. Because the optical bench of the IRGA is at an elevated temperature relative to the rest of the gas volume, the volume established by this analysis is an effective volume that accounts for the gas density difference between different parts of the system.

From the plot, we can see that the slope decreases with injection rate of pure CO_2 in general. The injection rate was measured by the rate at which the syringe advanced excess pressure and diffusion could lead to a different effective rate of CO_2 delivery. We used a 60 mL syringe filled with pure CO_2 gas as the gas source in the injection tests above. In the inlet path of our apparatus, the syringe and the two-way valve were connected with Poly-Ether-Ether Ketone (PEEK) tubing (Figure 18).

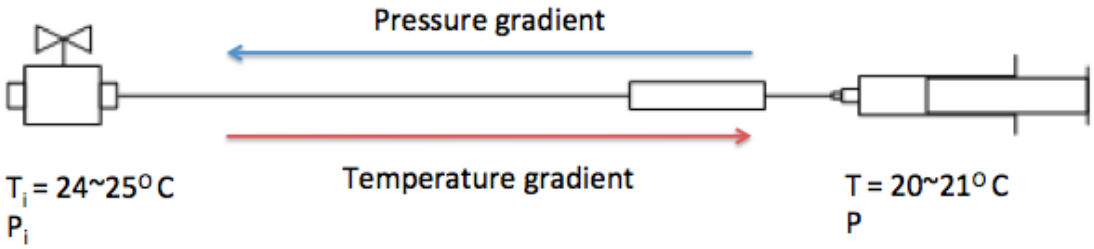

Figure 18: Schematic diagram of IRGA flow loop inlet path.

The bore size of the PEEK tubing used was very small (~0.007”). Therefore, when the injection rate was relatively high, the small bore diameter would produce a large pressure gradient from the syringe to the valve, which was the entrance of pure CO_2 gas into the IRGA flow loop. Since gas is compressible, the syringe pump was pressurizing the gas inside the syringe rather than pushing it into the IRGA system. Thus, the real pure CO_2 gas injection rate was smaller than the value set on the syringe pump. When the injection rate was relatively slow,

gas diffusion rate was comparable to the injection rate. That resulted in more gas entering the IRGA system than the nominal injection rate. Those effects caused our tests results of CO_2 concentration slopes to be inaccurate and not constant at various injection rates of pure CO_2 gas.

In order to effectively deliver the pure CO_2 gas from the syringe into the IRGA system, we decided to use the same method in which we made our CO_2-water solution tracer loops to make the pure CO_2 sample loops, then use a 60 mL syringe filled with water at the back to push the pure CO_2 gas into the IRGA flow loop. Since water is incompressible and the internal volume of the pure CO_2 sample loops was small (~3 mL), even though the pressure gradient still existed, the pure CO_2 gas would get injected at an injection rate very close to the set number on the syringe pump.

During the pure CO_2 sample loop making process, we push pure CO_2 gas through the sample loops. We also attached another piece of PEEK tubing at the end of the sample loops to eliminate the diffusion effect of pure CO_2 gas into the atmosphere, thus ensure the purity of the CO_2 gas inside the sample loop when we cap and seal it (Figure 19). The Valco-Vici sample loop could be capped on both ends with the screw-on caps that came with it.

The trick of attaching an extra piece of PEEK tubing was also used in our CO_2-water solution tracer loop making process, to get rid of tracer gas diffusion into the atmosphere via the open end of the tracer loops (Figure 19). These loops could be capped, stored and transported after they were made. At the time of use, one just needs to open both ends and connect the loops back into the inlet path. Capillary forces also help to hold the fluid in the tracer loops. However, small droplet losses can still occur during the tracer closing and reopening processes. Weight

measurements before and after the tracer loop filling process will somewhat help to reduce that impact. More on the tracer making process is discussed in subsequent sections.

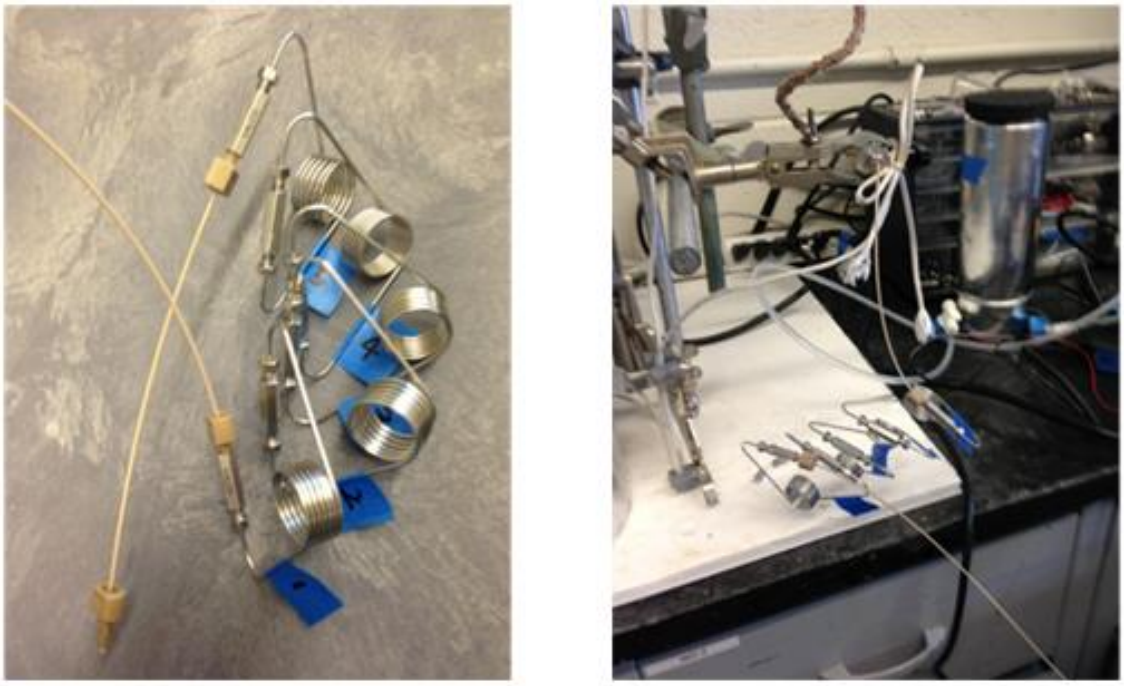

Figure 19: Pure CO_2 sample loop making (left) and injection (right) processes.

After we made these adjustments, we tested two different injection rates: 0.10 mL/min and 0.15 mL/min. The resulting slopes were 9,482.5 ppm/mL and 9,910.3 ppm/mL, respectively. Not only was the difference between those two slopes much smaller, but they were also considerably higher than the previous slopes from the same injection rates (8,230.3 ppm/ cc STP for 0.10 mL/min, and 6,737.6 ppm/ cc STP for 0.15 mL/min). This observation is explained by water being incompressible and the only volume getting compressed in the new structure was the pure CO_2 gas inside the sample loops, which was only 3 mL, while the syringe filled with water was 60 mL.

Table 1: Test result of pure CO_2 injection into IRGA flow loop, showing the different slopes as a function of injection rate.

Injection Method	$r_{[co_2]_{pure\ co_2}}$ (ppm/mL)
0.15 mL/min continuous injection	9,910.3
0.10 mL/min continuous injection	9,482.5
1mL point injection	9,702.0
1mL point injection	9,741.5
1mL point injection	9,887.0

In order to measure the CO_2 concentration in the tracer solution and characterize the membrane system, an accurate calibration of $r_{[co_2]_{pure\ co_2}}$ was needed. Two different methods of pure CO_2 gas injection into the IRGA flow loop were performed. One was the continuous injection described above, and the other was the point injection. We immediately injected 1 mL pure CO_2 into the IRGA loop and recorded the jump of CO_2 concentration inside the circuit. The point injections were repeated three times to ensure accuracy. The test results are listed in Table 1 above.

As indicated by the two injection methods, using water as the working fluid to inject pure CO_2 in the sample loops could delivery pure CO_2 precisely as expected, the compressibility issue

was negligible. The average CO_2 concentration increase rate, i.e., $r_{[co_2]_{pure\ co_2}}$ was calculated to be 9,744.7 ppm/mL, with a standard deviation of 171.9 ppm/mL (2% uncertainty).

3.5.2 Tracer solutions made at different temperatures

Knowing the internal volume of the IRGA flow loop, we stepped forward to test CO_2-water tracer solutions made by the membrane system. We varied the set temperature of the heating tape outside the second stage of the membrane exchanger to generate different CO_2-water tracer solutions. Those tracer solutions were kept in tracer loops, and then transferred to the IRGA flow loop injection tests.

The operating conditions of the tracer making processes in the membrane system were as follows: the water flow rate was kept constant at 0.15 mL/min, the CO_2 partial pressure in the second stage of the membrane contactor was 1 atm, the set temperature of the heating tape PID controller were 25 °C, 30 °C, and 35 °C. The curves of CO_2 concentration increase in the IRGA flow loop in responding to the tracer solution injections are plotted (Figure 20).

With the formula derived previously (Eq. 3), we were able to calculate the CO_2 concentration in the CO_2-water tracer solutions generated from the membrane system. Based on the assumption of full equilibrium at the outlet of the CO_2 dissolving fibers, the equivalent outlet temperatures are calculated to be 25.5 °C, 28.4 °C, and 31.7 °C for each the three set temperatures 25 °C, 30 °C, and 35 °C, respectively. Obviously, a higher set temperature resulted in a bigger difference between the equivalent outlet temperature and the set temperature. These differences were likely caused by the evaporative cooling phenomenon in the first stage of the membrane

contactor. Based on the weight measurement of the outlet solutions, the evaporation was approximate 3-5% of the total mass.

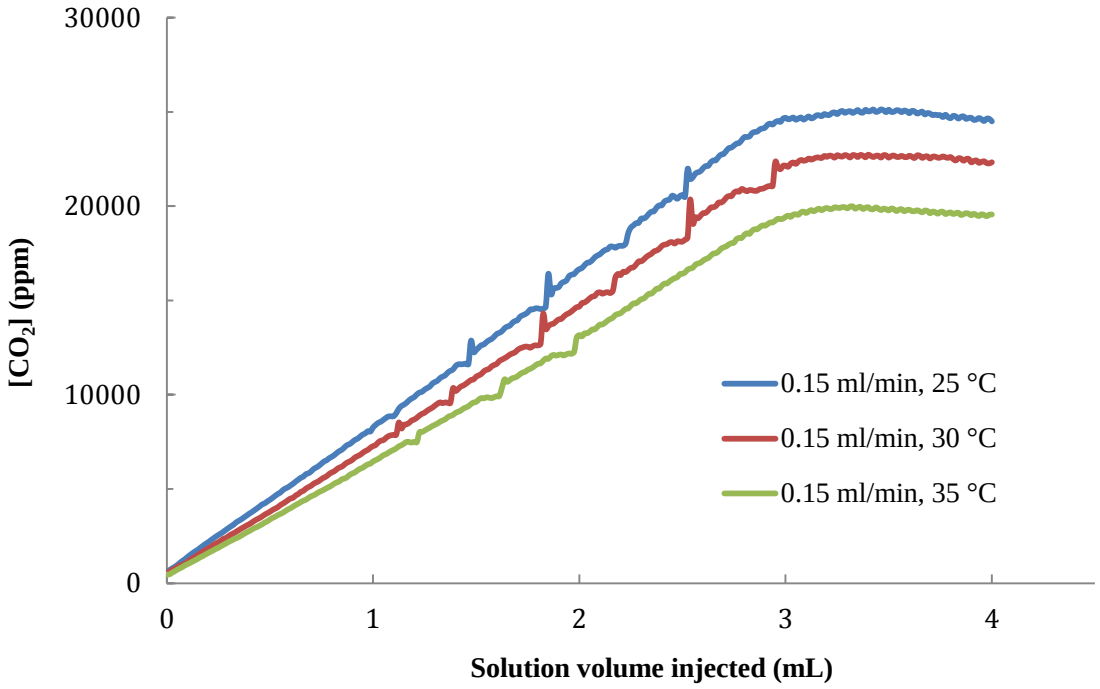

Figure 20: CO_2 concentration in IRGA flow loop vs. volume of tracer solution injected; solutions were made at different set temperatures, but constant water flow rate in the membrane system.

Operating the membrane contactor at an elevated temperature would result in a low CO_2 concentration in the solution. This in turn would assure that during use of the tracer loop under lower temperatures there would be no degassing of CO_2, which could lead to CO_2 bubbles in the tracer loop which would result in uneven delivery of the CO_2 into the flow stream. On the other hand, higher temperatures would lead to larger temperature drops and thus introduce more opportunity for variability in the result. Taking both effects into consideration, we decided to proceed with 30 °C as the set temperature for further investigations.

3.5.3 Tracer solutions made at different water flow rates

Once the set temperature at the second stage of the membrane contactor had been fixed at 30 °C, we used different water flow rates to make more CO_2-water tracer solutions in the membrane system. A series of IRGA flow loop injection test results are listed in Table 2.

Table 2: Test Results of tracer solutions (CO_2 concentration in cc STP/ mL) made at different water flow rates.

Experiment #	Tracer making water flow rate (mL/min)	$r_{[co_2]_{co_2-water}}$ (ppm/mL)	[CO_2] in tracer solution (cc STP/mL)
1	0.15	7,043.9	0.65
2	0.15	7,141.1	0.66
3	0.15	7,312.3	0.64
4	0.15	7,467.8	0.69
5	0.05	7,378.7	0.69
6	0.10	6,969.1	0.64
7	0.20	6,877.9	0.64

For experiments #1 to #4, all the tracer solutions were made in the membrane system at exactly the same conditions, i.e., set temperature of 30 °C, water flow rate of 0.15 mL/min. The CO_2 concentration in tracer solutions had an average of 0.66 cc STP/mL, with a standard deviation of 0.03 cc STP/mL (5% uncertainty). Based on that, the average equivalent outlet temperature was calculated to be 29.8 °C, with a standard deviation of 1.3 °C (4% uncertainty). Since the set temperature of the membrane exchanger outlet was 30 °C, the difference between measured and expected results was 0.2 °C (0.7% difference).

For experiments #4 to #7, the tracer solutions were made at the same set temperature 30 °C using different water flow rate in the membrane system. The CO_2 concentration in tracer solutions had an average of 0.66 cc STP/mL, with a standard deviation of 0.03 cc STP/mL (5% uncertainty). Based on that, the average equivalent outlet temperature was calculated to be 29.7 °C, with a standard deviation of 1.6 °C (5% uncertainty). Since the set temperature of the membrane exchanger outlet was 30 °C, the difference between measured and expected results was 0.3 °C (1.0% difference).

If we take experiments #1 to #7 all into comparison, the CO_2 concentration in tracer solutions had an average of 0.66 cc STP/mL, a standard deviation of 0.03 cc STP/mL (5% uncertainty). Based on that, the average equivalent outlet temperature was calculated to be 30.0 °C, with a standard deviation of 1.3 °C (4% uncertainty). Since the set temperature of the membrane exchanger outlet was 30 °C, the difference between measured and expected results was 0.0 °C (0.0% difference).

The statistical analysis showed us that standard deviation of injection tests of tracer solutions made at different water flow rates was on the same level as that of repeated injection tests of

tracer solutions made at an identical water flow rate. This result verified our assumption of full equilibrium at the outlet of the membrane contactor. We, therefore, are confident that at least a water flow rate of 0.15 mL/min is slow enough for CO_2-water saturation in the second stage of the membrane contactor. Another factor to take into consideration was the diffusion coefficients. CO_2-water and SF_6-water have different diffusion coefficients, specifically $D_{CO_2}/D_{SF_6} \approx 1.7$ at 25 °C. Thus, the SF_6-water saturation needs a slower water flow rate during the tracer making process.

At the end of the parameter setting of the filling station, we decided to use 0.05 mL/min, 30 °C as SF_6-water tracer making condition; 0.15 mL/min, 30 °C as $^{14}CO_2$-water tracer making condition. And our expectation of the tracer gas concentration in those solutions would be the gas solubility in water at 30 °C, with a 4% standard deviation.

3.6 Parameter Setting of the Tracer Loops

After the characterization of the filling station and definition of the parameters for the tracer making processes, the next step was to make the tracer loops based on these parameter settings. For our tagging purposes in the Iceland field test, one tracer loop was designed to be one daily dose. Because of the long time it would take to discharge the tracer loop we needed to consider the effects of dispersion on the interface between the pushing liquid and the sample fluid. This effect is known as Taylor-Aris dispersion and axial diffusion. It must be addressed in order to pick the most appropriate parameters (e.g., internal volume, inside diameter, etc.) of the tracer loops.

Taylor-Aris dispersion is an effect in fluid mechanics in which a shear flow can increase the effective diffusivity of a species, enhancing its spreading rate in the flow direction. Under the condition $L \gg \frac{a^2 U}{D}$, where L is the length, a is the radius, D is the coefficient of diffusion and U is the average axial velocity, the Taylor-Aris dispersion coefficient that accounts for both the axial and radial molecular diffusion mechanisms is expressed as $D_{eff} = D + \frac{a^2 U^2}{48D}$.

Fick's Second Law, expressed as $\frac{\partial C}{\partial t} = D_{eff} \frac{\partial^2 C}{\partial^2 x}$, predicts how diffusion causes the concentration to change with time. During the injection, $x = 0$ is the interface, C_1 is the $^{14}CO_2$ concentration in our tracer solution, and C_2 is the $^{14}CO_2$ concentration in the working fluid, i.e., DI water in our case (Figure 21). We want to calculate the axial diffusion length over the course of a single, daylong injection.

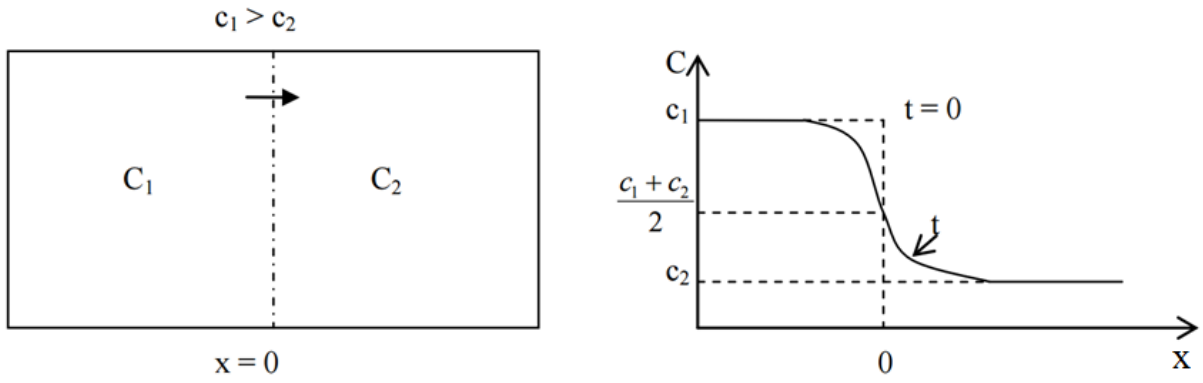

Figure 21: Schematic diagram of axial diffusion effect on the interface of tracer solution and water (Treybal, 1968).

In this case, we consider the working fluid ^{14}C free, use initial conditions of $(t = 0)$: $x < 0, C = C_1;\ x > 0, C = C_2 = 0$ and boundary condition $(t > 0)$: $x = -\infty, C = C_1;\ x = +\infty, C =$

$C_2 = 0$ to solve $\frac{\partial C}{\partial t} = D_{eff}\frac{\partial^2 C}{\partial^2 x}$, and derive the concentration distribution as a function of position and time (Eq. 4).

$$C(x,t) = \frac{C_1}{2}\left[1 - \mathrm{erf}\left(\frac{x}{2\sqrt{D_{eff}t}}\right)\right] \quad (4)$$

The characteristic length of the axial diffusion length can be calculated by setting Gauss error function $\mathrm{erf}(\beta) = 0.9995930$, when $\beta = 2.5$. For one day time period ($t = 8.64 \times 10^4$s), we get $x = 2.5 \times 2\sqrt{D_{eff}t} = 9.5$ cm. The inner diameter of our tracer loop tubing is 0.040" ± 0.001". If we use a 0.5 mL tracer loop, the axial diffusion length on the tracer loop side is 10.7% of the total loop length; while if we use a 2 mL tracer loop, then only 3.9% of the total length will be affected. After reviewing the predicted diffusion lengths involved, we decided to use the 2 mL Valco-Vici sample loops, which have same inner diameter but longer axial length than the 0.5 mL Valco-Vici sample loops, to make tracers for Iceland field test.

As for laboratory demonstrations, we also needed to make SF_6-water or $^{14}CO_2$-water tracer loops for injections in the high-pressure flow loop (HPFL), i.e., the injection system to simulate the field test in Iceland, which is elaborated in the next chapter. Unlike injecting tracer into continuous $^{12}CO_2$ flow at Iceland field test, the laboratory demonstrations were conducted by injecting the tracer into a fixed amount of $^{12}CO_2$ in a high-pressure flow loop. Therefore, it is not necessary to inject the tracer loop in one-day time period, the internal volume of the HPFL tracer loop doesn't need to be larger to minimize the axial diffusion effect. The internal volume of HPFL tracer loops remained as 0.5 mL.

Since the high-pressure flow loop has a fixed internal volume, the laboratory demonstration results were sensitive to the total amount of tracer gas inside each loop. The inner diameter of the tracer loop tubing was 0.040" ± 0.001". The tolerance could have a significant effect on this small volume, ± 5% of the total volume. Therefore, weight measurements were necessary before and after the tracer loops were filled with tracer solution during the tracer making process. This enabled us to get a better estimation of the tracer gas amount inside each particular tracer loop.

In summary, the tracer loop filling station we designed and constructed featured a novel membrane based gas exchanger, which degassed the fluid in the first step and then equilibrated the fluid with CO_2 at a fixed pressure and at a fixed temperature. It was demonstrated that this approach could achieve uniform solutions and prevent the formation of bubbles and degassing downstream.

The device was developed based on the following principle. First, commercially available $^{14}CO_2$ is expanded into an evacuated space in the filling station. Second, DI water was then loaded with known quantities of $^{14}CO_2$ by equilibration through a membrane. Thirdly, the infused liquid are then loaded into metal tubes (tracer loops). Finally, the tracer loops were sealed, containing precisely measured quantities of tracer solution with enough ^{14}C for daily or weekly use at MMt/year geological carbon sequestration sites. The detailed procedures of the carbon-14 tracer making experiments are described in Chapter 5, Iceland field test.

Chapter 4: Laboratory Evaluation of the $^{14}CO_2$ Tagging System

The laboratory evaluation of the tracer loops discussed in the previous chapter was another major component of this research project. The objective of this task was to design and construct a high-pressure flow loop circulating water and/or carbon dioxide for testing the tagging system at realistic injection conditions. We tested the injection systems first with SF_6 and later with $^{14}CO_2$ to demonstrate controlled tracer injection into supercritical CO_2.We had to demonstrate that 1) we were able to inject our tracer solutions into the target flow in a controlled manner, 2) the tagging concentrations stayed within the tolerance of our expectations, 3) the tracer loops could be handled safely throughout the entire processes. The efforts to achieve these goals are elaborated subsequently.

4.1 Design of Injection System – High-Pressure Flow Loop

Homogenous mixing of the tracer gases into the main high-pressure CO_2 transport line is critical for our proposed technology. The objective of this task was to design and construct an injection system to mimic the CO_2 injection conditions at a geological sequestration site, and also the specific situation for the Iceland field test. This injection test system should be equipped with pressure transducers and thermocouples to monitor and control the operating pressure and temperature during the experimental runs. The liquid/supercritical CO_2 flow rate and the pressure within the injection system should be able to achieve 1 kg/s and 100 atm respectively to match

the target CO_2 injection rate for geological sequestration supported by a daily dose $^{14}CO_2$-water tracer loop.

Based on the requirements and experimental design, a high-pressure flow loop was built to circulate water, liquid CO_2, supercritical CO_2, and water/CO_2 mixtures. The system was used to evaluate the performance of tracer injecting, mixing and tagging in pipeline flows. Our goal was to use the high-pressure flow loop to demonstrate controlled injections of both SF_6-water tracer loops and $^{14}CO_2$-water tracer loops.

To replicate the field test CO_2 flow condition in the high-pressure flow loop, we first performed theoretical calculation of the fluid flow, estimating the Reynolds number, a dimensionless ratio that indicates flow characteristics. Our goal had been to create turbulent flows similar to those one might expect in a much larger pipeline for CO_2 transport. This calculation helped us to select the inner diameter of the tubing in the high-pressure flow loop.

Second, we checked the boundary layer effects to determine if any significant boundary layer stagnation might occur during the tracer injection. In fluid dynamics, there are three types of boundary regimes, smooth region, transition region, and rough region, measured by the Reynolds numbers. With high Reynolds numbers, our turbulent flow fell in the rough region in all the possible scenarios. Thus, the boundary layer effects were negligible, and nearly all areas in the flow would demonstrate turbulent features. The calculations implied that the flow conditions in the high-pressure flow loop would be similar enough to simulate the tracer mixing performance for geological carbon storage in the Iceland field test and for even bigger pipelines that would be used in industrial scale carbon dioxide injection.

Third, for fully turbulent flow to develop in a pipe, there is an entrance length required. For turbulence flow, the entrance length is usually considered to be 30~60 times the tube's inner diameter. In the structure of the high-pressure flow loop, we designed several straight sections connected by four-way junction ports with adequate lengths in between. This construction provided flexibility in the configuration of the development regime. The four-way junction ports served as the access points to the inside flow for temperature and pressure measurements, as well as for injection and sampling ports. The tracer could be injected in both axial and radial directions into the flow.

Finally, we designed the system to handle temperatures from room temperature up to 60 °C, and pressures from 101.3 kPa up to 20,785 kPa (0-3,000 psig). These ranges enabled us to maintain CO_2 in either a liquid phase or supercritical phase inside the high-pressure flow loop. A carbon dioxide compression pump was selected to compress CO_2 gas to the high-pressure range. The pressure drop within the flow loop was also calculated to determine the desired features of the circulation pump. The whole system was wrapped with electrical heater/insulation jackets to maintain any set temperature.

The design of the high-pressure flow loop is shown in a schematic diagram (Figure 22).

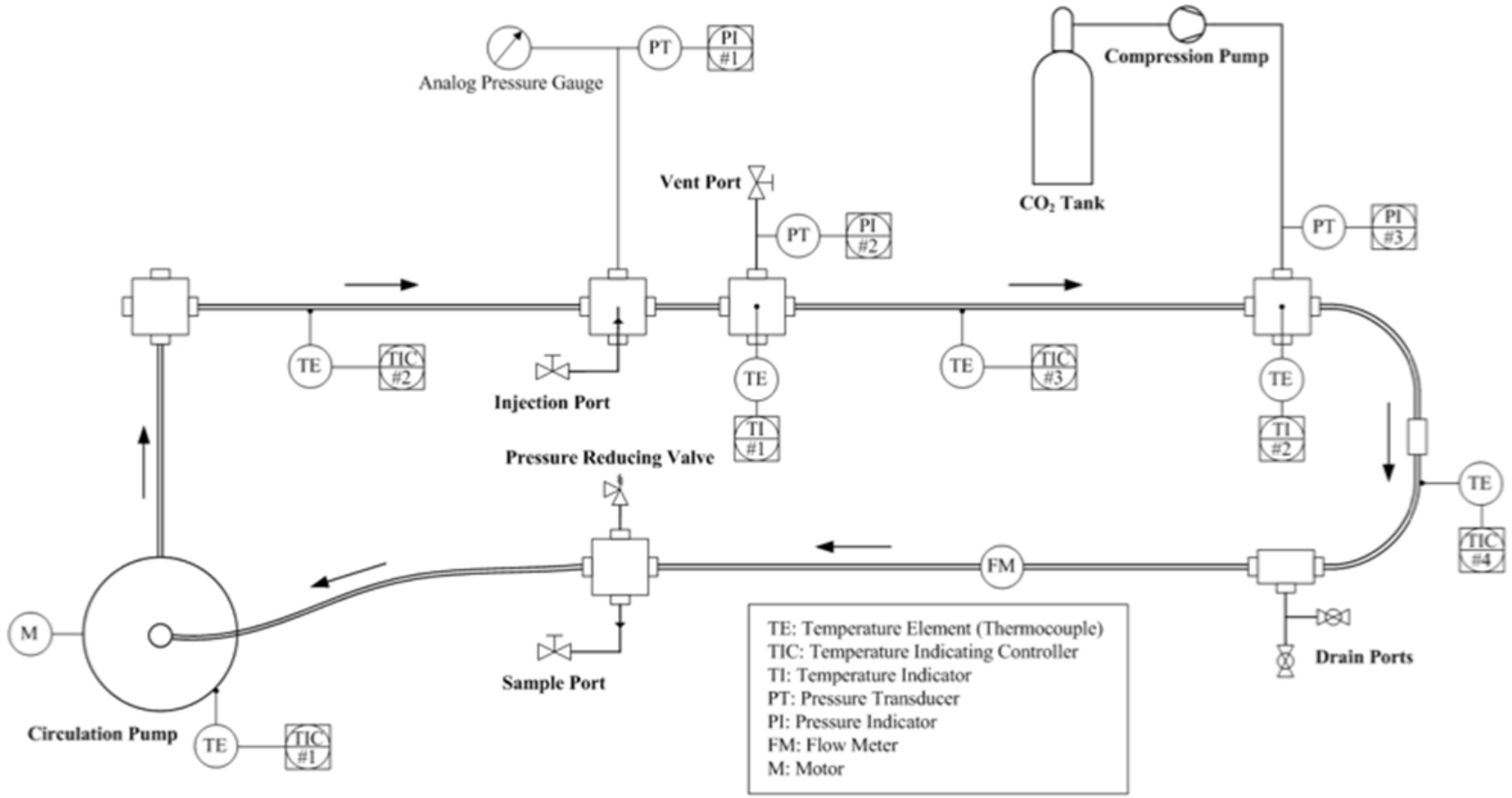

Figure 22: Schematic diagram of the high-pressure flow loop (custom design from Progressive Equipment Corporation).

Aside from the features mentioned previously, the system also included overpressure protection as well as vent and drain valves. A flow meter was installed to obtain real-time reading of the flow rate. The speed of the circulation pump can be adjusted from 0 to 100% of the nominal capacity. Operating with supercritical CO_2 at 40% of full speed, the flow rate was about 20 L/min.

In general, for cylindrical pipes, turbulent flow is present at Reynolds number greater than 2000. Under the temperature and pressure ranges of the high-pressure flow loop, the Reynolds numbers were 2-4 orders of magnitude greater, which put the flow condition in the high turbulence regime. The turbulent flow regime insured the injected tracer solution get well mixed with the target CO_2 flow, thus eliminating the necessity of adding baffles.

An electronic control package was included to control the heating elements, and monitor the pressures and temperature. The control system maintained process information in a data log file, which could be accessed via Ethernet or USB memory device.

A third party company (Progressive Equipment Corporation, Doylestown, PA) constructed the high-pressure flow loop bases on our design. The system was transported to and reassembled at Columbia University (Figure 23). We performed leak testing to confirm its ability to hold internal pressure up to 20,785 kPa (3,000 psig).

The list of major components is shown in Table 3.

Table 3: Major Components Listing of high-pressure flow loop.

<table>
<tr>
<td>Loop Tubing and Fittings (Maxpro Technologies, Model 15N16M-6-316 & 21X16M)
• 1” Outer Diameter and 0.688” Inner Diameter
• 316 Stainless Steel
• Six segments, long enough for development regime</td>
<td>Circulation Pump (Autoclave Engineers, Model MP2365-02-55-60)
• 1.5 HP and Variable speed AC drive
• Max Operating Speed: 3,450 RPM
• Max allowable working pressure: 2,500 psig
• 316 Stainless Steel</td>
</tr>
<tr>
<td>Carbon Dioxide Pump (Supercritical Fluid Technologies, Model SFT10)
• Flow range: 0.01 to 24.0 mL/min
• Pressure: Up to 10,000 psig
• Pump head thermoelectrically cooled</td>
<td>ISCO Pump (Teledyne, Model 500D Syringe Pump)
• Flow range: 0. 001 - 204 mL/min
• Flow Accuracy: 0.5% of setpoint
• Pressure Range: 10 - 3,750 psig
• Capacity: 507 mL</td>
</tr>
<tr>
<td rowspan="2">Control System
• PLC based
• 10” color touchscreen
• Ethernet port
• Data log to USB thumb drive</td>
<td>Heating/Insulation (Glascol custom)
• Fabric style blanket for flexibility in development regime configuration</td>
</tr>
<tr>
<td>Thermocouples (Qty 6, Type T)
• Stainless Steel Sheath</td>
</tr>
<tr>
<td>Overpressure protection (Maxpro Technologies, Model 21SH16M & MT-10RV)
• Rupture disk and relief valve</td>
<td>Pressure Transducers (Qty 3, Setra, Model 206)
• 0-3,000 psig
• 4-20 mA output</td>
</tr>
</table>

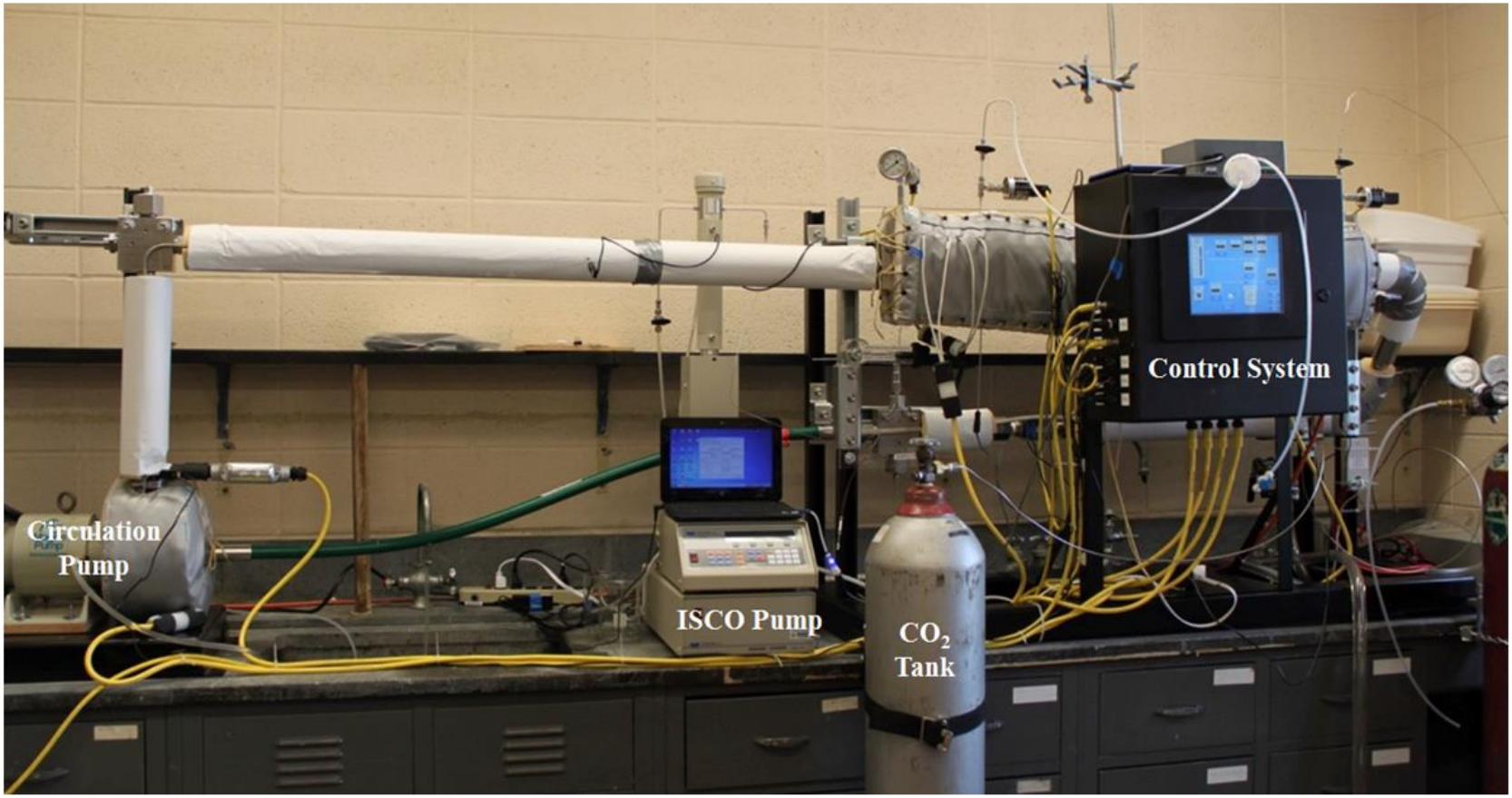

Figure 23: Picture of the high-pressure flow loop after the completion of installation, showing the circulation pump, ISCO pump, CO_2 tank and control system.

4.2 Electrical Conductivity Measurement Experiments

Before we proceeded to SF_6-water and $^{14}CO_2$-water tracer injection testing, we needed to verify the turbulence flow condition and homogenous mixing in the high-pressure flow loop. We decided to inject an ionic solution (NaOH or NaCl dissolved in water) into water flow in the high-pressure flow loop. In this mode of operation, water was circulating in the flow loop at near ambient pressure. There was no need to operate at any elevated pressure because water is nearly incompressible. Electrical conductivity measurement of the cross-section profile would get us a better understanding of the mixing properties in the high-pressure flow loop.

The idea behind the measurement concept was to inject a salt brine into the water flow and measure the electrical conductivity to detect the local concentration of salt. By measuring the electrical conductivity of the solution along a radial line inside the flow channel some distance downstream from the injecting point we were able to verify the mixing characteristics of the system. The simultaneous measurement of conductivities along a line was accomplished by creating a small flat panel, in effect a circuit board with a number of electrodes that could measure electric conductivities at various locations along the length of the board. The measurement of the flow electrical conductivity profile was achieved by laying exposed metal pads on the surface of the circuit board that would act as electrodes to detect the voltage drop across the gap between them when placed in an ionic solution. The 0.688” inner diameter of high-pressure flow loop tubing allowed us to accommodate 8 of such exposed pads. This setup would provide eight channels of measurements to detect any changes in the solution concentration profile in the flow cross-section.

The principle of the electrical conductivity measurements is illustrated in a circuit diagram (Figure 24).

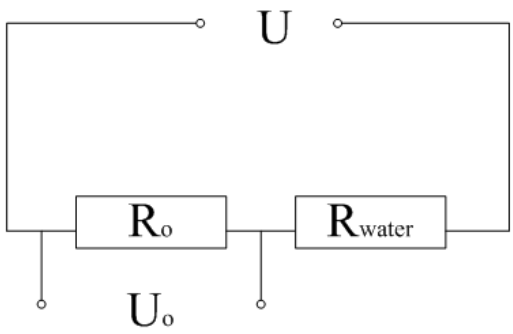

Figure 24: Schematic diagram of electrical conductivity measurement circuit, designed to characterize mixing within the high-pressure flow loop.

From the circuit, we find $= I(R_0 + R_{water})$, U is the sine AC signal voltage with a peak value of 5V. We measured the peak-to-peak value of $U_0 = IR_0 = \frac{UR_0}{R_0+R_{water}}$, where the resistance of the water solution $R_{water} = \frac{f_g}{C_{water}}$, further we have $U_0 = \frac{UR_0}{R_0+f_g/C_{water}}$.

There were three factors affecting U_0. First was the resistor we added in the circuit, i.e., R_0. We set $R_0 = 475\Omega$ for all eight channels. Second was the geometric factor f_g. We needed to calibrate the geometric factor f_g of the eight channels, individually. Third was the flow condition at the point where the measurement took place. The flow condition included the velocity profile and ionic concentration profile, which would be a good indicator of the turbulence flow condition and homogenous mixing performance in the high-pressure flow loop.

In order to calibrate the geometric factor f_g of the eight channels, we performed electrical conductivity measurement of ionic solutions in water in a beaker (Figure 25).

At a certain solution concentration, using the U_0, which we measured, we could calculate $R_{water} = \frac{U-U_0}{U_0} R_0$. The theoretical electrical conductivity C_{water}, at a certain concentration is $C_{water} = \frac{f_g}{R_{water}}$. Thus, we can measure $f_g = C_{water} \frac{U-U_0}{U_0} R_0$ (cm^{-1}) for each of the eight channels.

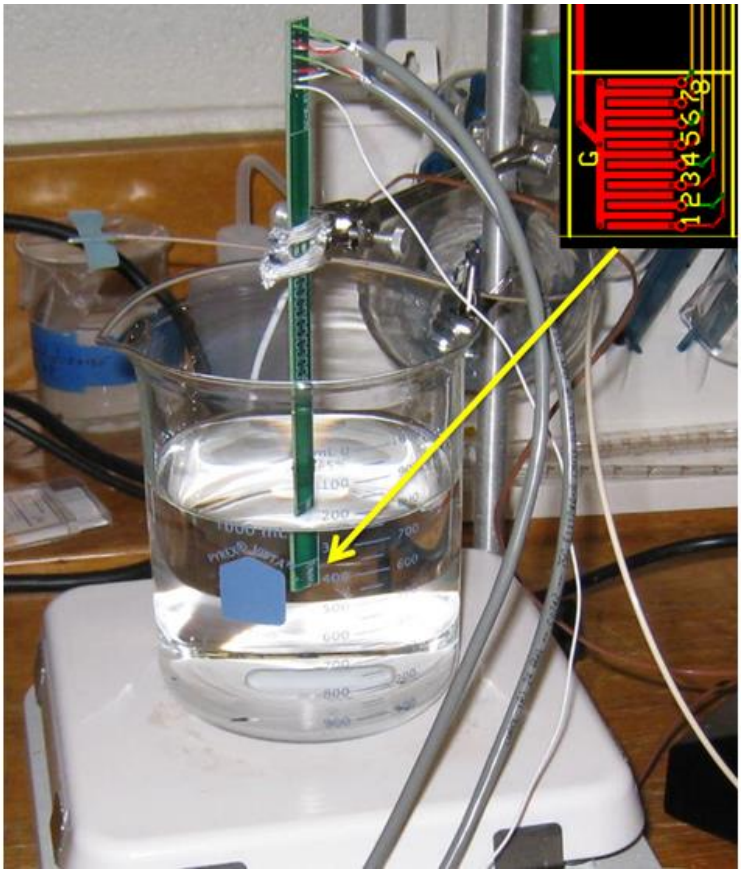

Figure 25: Setup of electrical conductivity measurement in a beaker.

According to the measurement principle, we injected 5 mol/L NaCl water solution at 0.5 mL/min into 750 mL water in a beaker placed on a magnetic stirrer. We assumed that the solution in the beaker is well mixed instantly; therefore all eight channels should measure the same electrical conductivity corresponding to a uniform salt concentration. Since the solution in

the high-pressure flow loop would be highly diluted, we performed the calibration at a low concentration – the weight percentage of the salt in the solution was 0.3%, which had a theoretical electrical conductivity of 5.69 mS/cm (Wolf, 1966, Weast and Astle, 1989). Then we calculated the geometric factors of the eight channels, shown in Table 4 below.

Table 4: Geometric factors of eight channels calculated from the injection of NaCl solution into water in a beaker.

f_1	f_2	f_3	f_4	f_5	f_6	f_7	f_8
6.290	5.525	5.552	5.467	5.423	5.448	6.103	5.453

Once we calibrated the geometric factor, we could convert our U_0 data into electrical conductivity data, $C_{water} = \frac{U_0 f_g}{(U-U_0)R_0}$. Thus, in this manner we could obtain measurements of the electrical conductivity of the solution in the flow loop as a function of time or alternatively, the electrical conductivity as a function of concentration.

The electrical conductivity curves of eight channels from the beaker injection test are plotted as a function of weight percentage of the salt in the solution (Figure 26). The eight channels measured the same electrical conductivity level at any moment, which met our expectation of the uniform salt solution resulted from the instant mixing in the beaker.

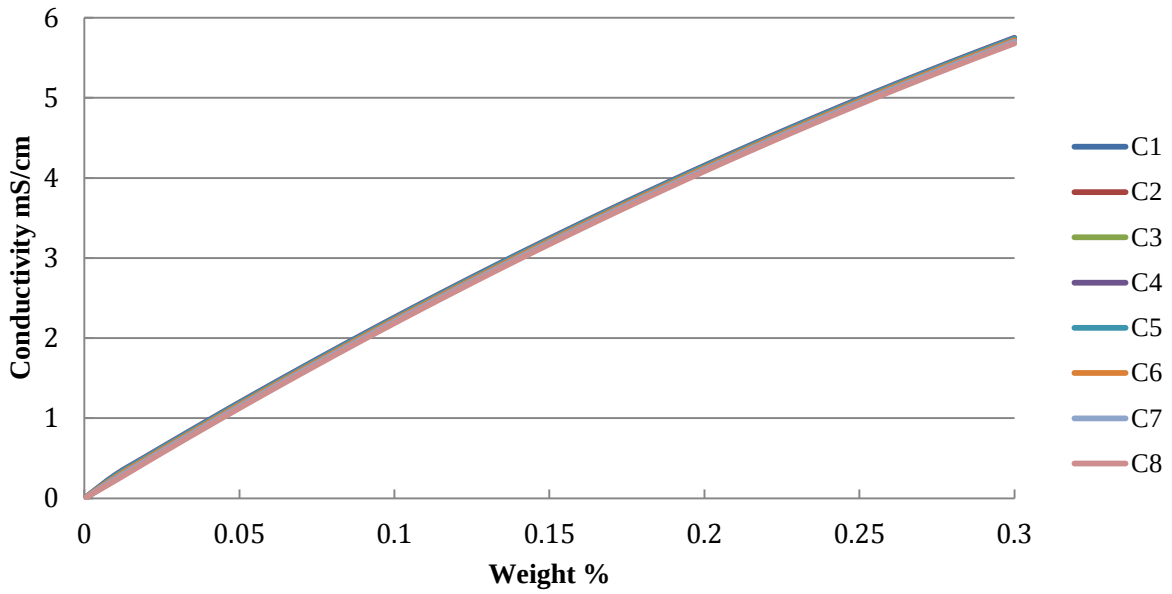

Figure 26: The data logging of electrical conductivity measurement from eight channels placed in a well-mixed solution with an increasing ionic concentration.

In order to check the effect of the velocity profile inside the flow loop, we needed to circulate aqueous solution of acids/bases/salts in the flow loop and measure the electrical conductivity. Since the internal volume of the flow loop is 2-3 times that of the water volume in the beaker, we decided to use a NaOH solution, with an electrical conductivity that is 3 times that of a NaCl solution with the same mass concentration (Wolf, 1966, Weast and Astle, 1989).

We measured the electrical conductivity of 0.05 mol/L NaOH solution at varying flow rate in the flow loop. The result indicated that at flow rates between 0 to 12 L/min, the voltage we measured didn't change with the velocity. When the flow rate went above 15 L/min, the signal became noisier. Thus, we decided to pick up 8 L/min as our flow rate for the electrical

conductivity measurement experiments. At this flow rate, the Reynolds number of water flow in the high-pressure flow loop was around 12,000, well in the turbulence regime.

On the top-left corner of the high-pressure flow loop, there was a four-way junction port connecting to a horizontal straight section, which was about 60” long, until the connection with the next four-way junction port (Figure 23). We put an axial injection inlet through the horizontal opening of the four-way junction port at the top-left corner, and extended the thin saline solution tube to the outlet of the port 20” along the centerline of horizontal pipe. The electrodes were inserted through the next four-way junction port vertically from above so they aligned inside the flow tube in the radical direction for measurements of the radial electrical conductivity profile.

The distance between the mixing start point and the measuring point was about 40”, which was long enough for the turbulent flow to be fully developed and mixed. Theoretically, the radial velocity profile shouldn’t affect the electrical conductivity measurement, and the concentration detected by the eight channels should be identical at our measuring point.

The curves of electrical conductivity vs. time when we injected a 5 mol/L NaOH solution at 0.5 mL/min into the flow loop preloaded with water are plotted. When we did this measurement, the electrodes were put in a bottom-up position in the four-way junction port. Thus, the eight channels from 1 to 8 were laid from top to bottom in the section view (Figure 27).

As shown by the curves, channels 2 to 6 were always measuring the same electrical conductivity value. After about 15 minutes, we stopped the NaOH solution injection and kept the water running at 8 L/min inside the flow loop, and the curves turned to be flat subsequently. That indicated that the internal flow was already well mixed at the measuring point, as expected.

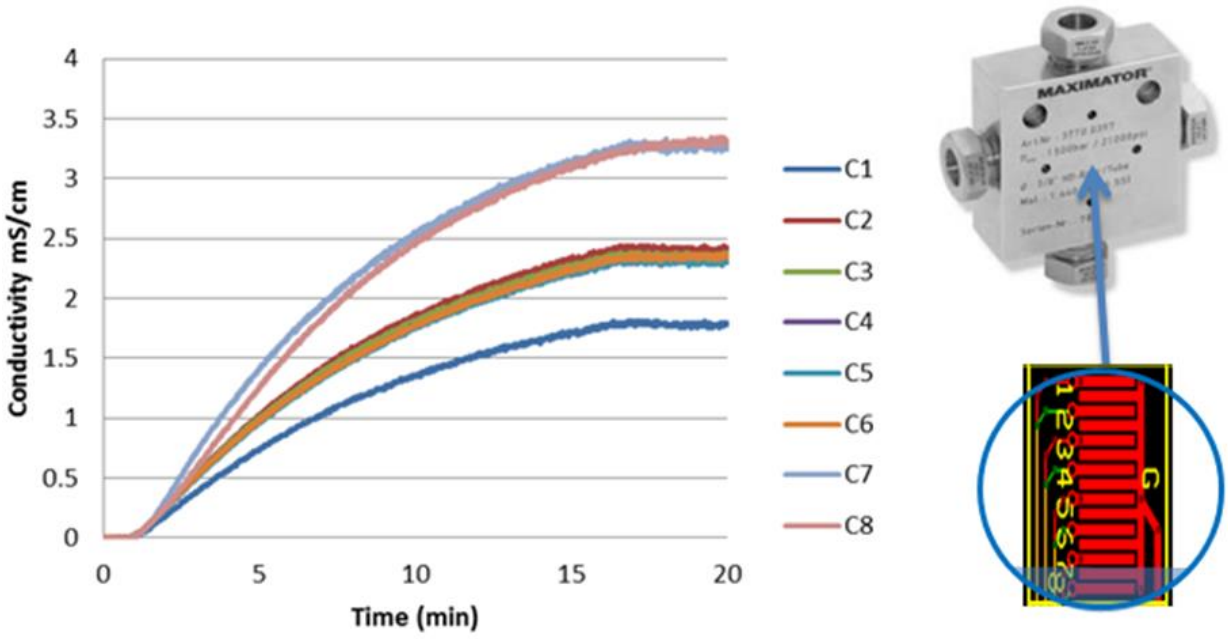

Figure 27: Electrical conductivity vs. time curves of 5 mol/L NaOH solution injected into the flow loop at 0.5 mL/min.

However, the electrical conductivity levels measured by channels 1, 7 and 8 were separated from the rest of curves. One possible explanation is that the flow loop was made of conductive metal, and therefore introduced electromagnetic interference to the electrical conductivity measurements. Especially for the electrodes close to the wall of the flow loop, the geometric factors could be affected and no longer equal to the numbers we calibrated from the beaker test.

We suspected that the way we put the electrodes into the flow loop cross section, i.e., the bottom-up direction, also made an impact. The setup might leave some extra space at the bottom of the cross, where a high-concentration reservoir could accumulate, and resulted in higher electrical conductivity measurements on channels 7 and 8 than the others. Meanwhile, in all the electrical conductivity measurement experiments, we simply filled the flow loop with water at ambient pressure, and some spare space with air bubbles was inevitable in the flow loop. Since

water flow didn't fill up the entire cross section, channel 1 was not fully covered by the mixed solution, and resulted in lower electrical conductivity measurements than the others.

The issues of high-concentration reservoir at the bottom and the air bubbles at the top of the cross were observed more obviously during the draining and refilling processes (Figure 28).

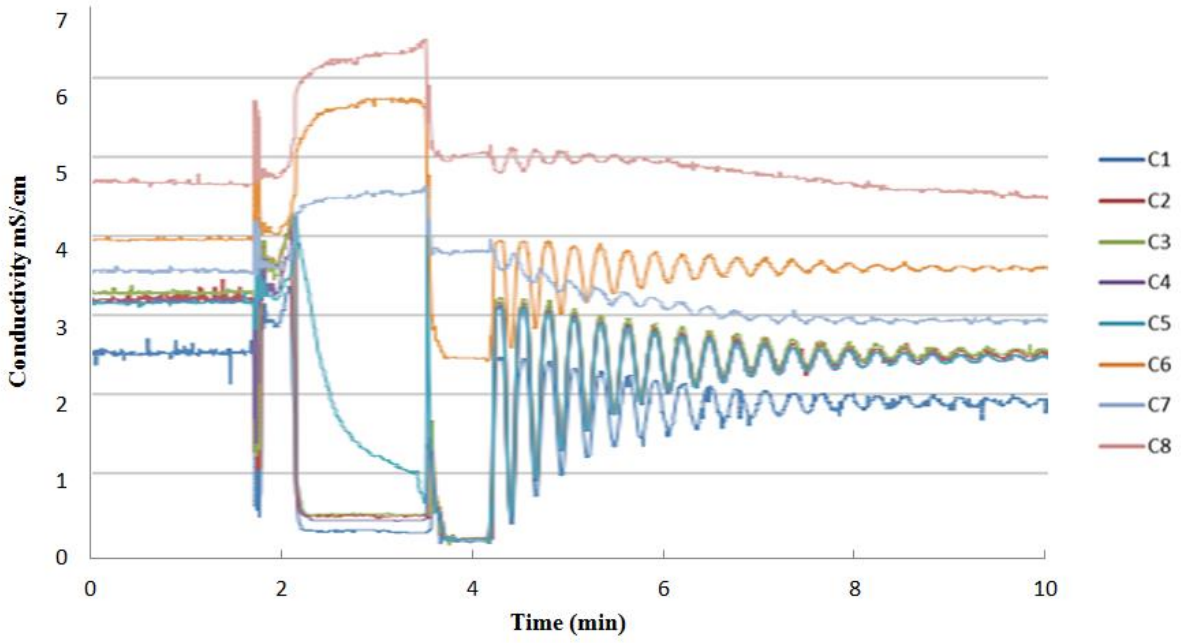

Figure 28: Electrical conductivity vs. time curves of draining and refilling processes.

The curves started with the well-mixed solution running at 8 L/min after the previous injection of NaOH solution. Shortly after the 2nd minute, we stopped the circulation pump and started to drain the solution in the flow loop. The electrical conductivity measurements from the upper channels (1-5) decreased immediately, while the electrical conductivity measurements of the lower channels (6-8) increased because of the high-concentration reservoir at the bottom. Shortly before the 4th minute, we started to refill the flow loop with deionized (DI) water. Since the NaOH solution in the flow loop was not completely drained, the remaining solution served as

a plug and demonstrated the axial diffusion performance when we turn on the circulation pump again shortly after the 4th minute. The result indicated that if we do a plug injection into an 8 L/min water flow, it would take less than 10 minutes to get well diffused in the axial direction of the entire flow loop.

Learning the lessons from the experiments above, we changed the direction of our electrodes, into a top-down position in the cross. Thus, the eight channels from 1 to 8 were laid from bottom to top in the section view. This modification would avoid the high-concentration reservoir issue at the bottom of the cross. Also, we add a water outlet line to the top of the next cross in the downstream of the measuring cross, in order to push out air bubbles when we load the flow loop with water at ambient pressure, and get the cross section filled up with as much water as possible.

Further, we conducted another injection with 5 mol/L NaCl solution into the flow loop (Figure 29). It's worth noting that the x-axis, weight% of NaCl in the entire flow loop, was calculated based on a rough estimation of the internal volume of the high-pressure flow loop as 1.5 L. The calibration of the accurate internal volume is discussed in the next section.

As shown by the curves, all channels gave the same electrical conductivity measurements except for channels 1 and 7. However, channel 8, which was on the top in this case, no longer got lower electrical conductivity measurements. Nor did channel 2, which was near to the bottom, get higher electrical conductivity measurements. Because we deliberately modified the setup to avoid air bubbles at the top and high-concentration reservoir at the bottom, these results, to some extent, helped to verify our hypotheses of those issues in the previous electrical conductivity measurement experiments.

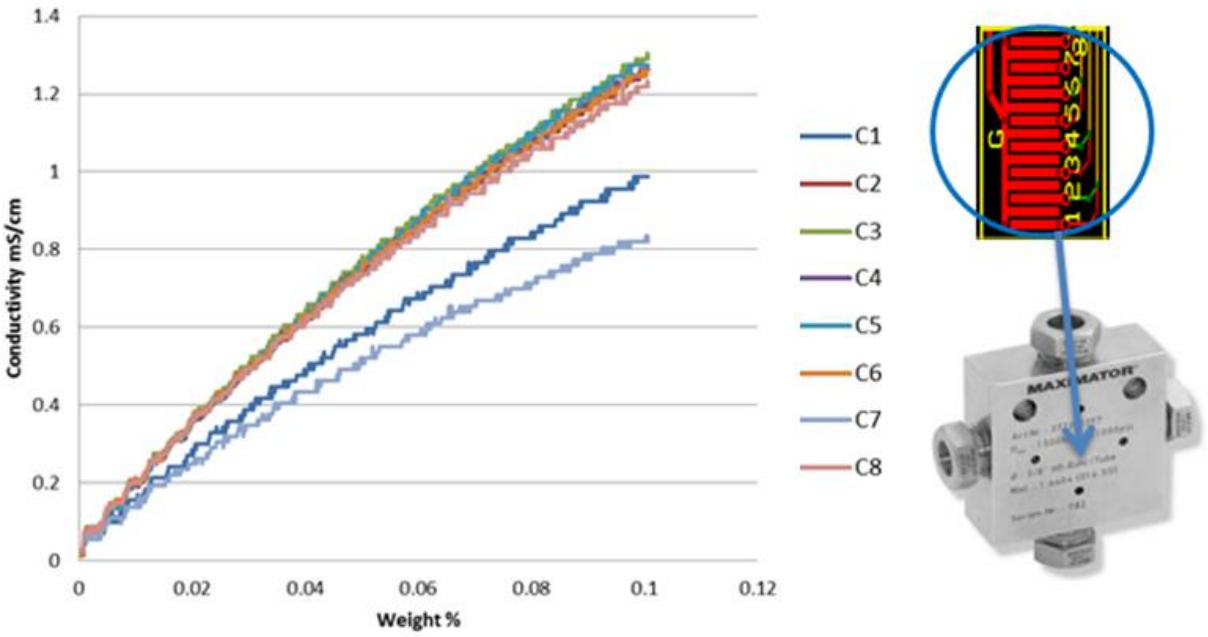

Figure 29: Electrical conductivity vs. concentration curves of NaCl solution injection into the flow loop.

Since NaCl solution is quite corrosive to the electrodes, we suspected that channels 1 and 7 were already corroded during this experiment, and the geometric factors of two channels didn't hold any more. The comparison of new and used electrodes showed clear corrosion, and confirmed our suspicion (Figure 30). That also explained why channels 1 and 7 still gave odd electrical conductivity measurements in this experiment where the setup had already been modified. Were the electrodes well functioned; we should be able to demonstrate uniform electrical conductivity profile in the flow cross-section.

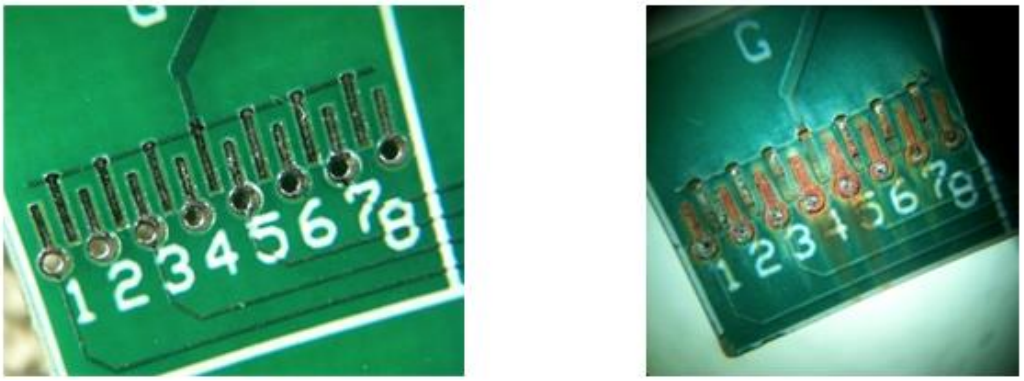

Figure 30: Comparison between new and corroded electrodes.

Due to time and budget constraints, we did not pursue more electrical conductivity measurement experiments. The results above were adequate to verify that the flow inside the high-pressure flow loop was turbulent, and homogenous mixing was achieved in the fully developed flow.

4.3 Internal Volume Calibration

The electrical conductivity measurement was a qualitative approach to understand the mixing performance in the high-pressure loop. However, laboratory evaluation of the SF_6-water and $^{14}CO_2$-water tracer injection called for highly accurate quantitative experiments. Therefore, we needed to calibrate the internal volume of high-pressure flow loop with adequate precision. Because of many small and odd shaped cavities in the system a simple calculation of all the open volumes was considered too crude.

We designed our approach by converting the volume measurement to a weight measurement to get best accuracy. We first filled the flow loop with CO_2 gas at ambient pressure, and then used a liquid nitrogen cooled cold finger structure, which was connected with the flow loop on

one of the four-way junction ports, to trap the CO_2 out of the flow loop. The mass of the CO_2 in the cold finger could then be determined by measuring the weight difference of the cold finger before and after trapping the CO_2. A vacuum gauge was connected in the line between the flow loop and the cold finger to measure the internal pressure at the end of the CO_2 trapping process (Figure 31).

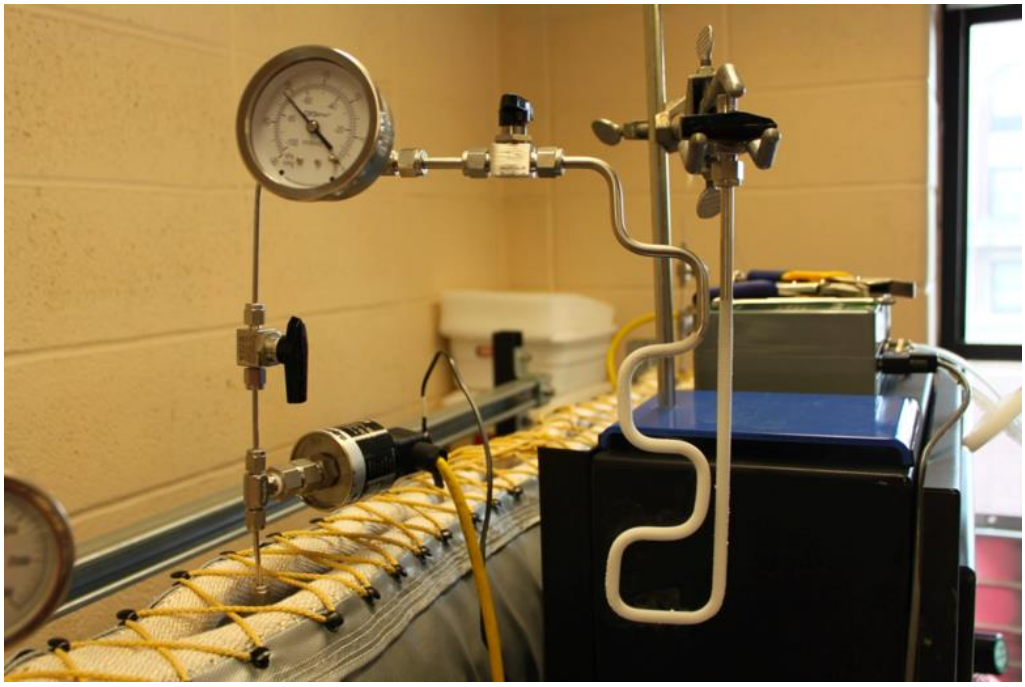

Figure 31: Liquid nitrogen cold finger setup in the high-pressure flow loop for CO_2 weight measurements.

We recorded the temperature and pressure inside the flow loop before and after applying the cold finger trap and then calculated the CO_2 density according to the equation of state developed by Span and Wagner (1996). Once the densities were determined, the internal volume could be calculated (Eq. 5).

$$V = \frac{\Delta m}{\rho_1 - \rho_2} \tag{5}$$

The results of six measurements are listed in Table 5, subscripts 1 and 2 indicate the before and after values, respectively. The average flow loop internal volume was 1.872 L, with a standard deviation of 0.0082 L (0.44% uncertainty).

Table 5: Test results from CO_2 weight measurement experiments conducted in the high pressure flow loop to define internal volume of the system.

T_1 (^oC)	P_1 (kPa)	ρ_1 (g/L)	T_2 (^oC)	P_2 (kPa)	ρ_2 (g/L)	Weight of CO_2 (g)	Flow loop internal volume (L)
23.70	101.1	1.8120	23.60	22.6	0.4036	2.623	1.862
23.70	101.1	1.8120	23.60	23.6	0.4214	2.591	1.863
24.40	101.3	1.8112	24.20	30.8	0.5491	2.368	1.876
23.60	101.6	1.8216	23.40	32.1	0.5739	2.345	1.880
24.30	101.3	1.8119	24.10	38.3	0.6833	2.109	1.869
23.70	101.1	1.8120	23.60	40.1	0.7167	2.059	1.880

An error analysis was also performed for this experimental approach. As listed in Table 6, there were two major categories of errors, random and systematic errors. The random errors, which included both instrument and operator errors, were represented by the standard deviation. The systematic errors were caused by, on one hand, adding the volume of the liquid N_2 cold

finger structure to the flow loop; on the other hand, the accuracy levels of the instruments involved in those measurements. All together, the total error was about 2%.

Table 6: Error analysis of CO_2 weight measurement experiments.

Random Errors		**Systematic Errors**		
Instrument Errors	Standard Deviation 0.44%	Volume Added	About 5 mL, compared to 1.872 L	0.27%
		Thermocouple	About 1~2 K, compared to 298.15 K	0.67%
Operator Errors		Vacuum Gauge	Full scale value accuracy	1.5%
		Ambient Pressure	Read from IRGA	< 1%
		Digital Scale	± 0.001 g, compared to 2.5 g	0.04%

Since the internal volume would be so critical to the estimation of expected tracer concentrations in all laboratory evaluation of the SF_6-water and $^{14}CO_2$-water tracer performance, we also performed a manual calculation to double check the internal volume. We measured the length of the flow loop piece by piece (Figure 32).

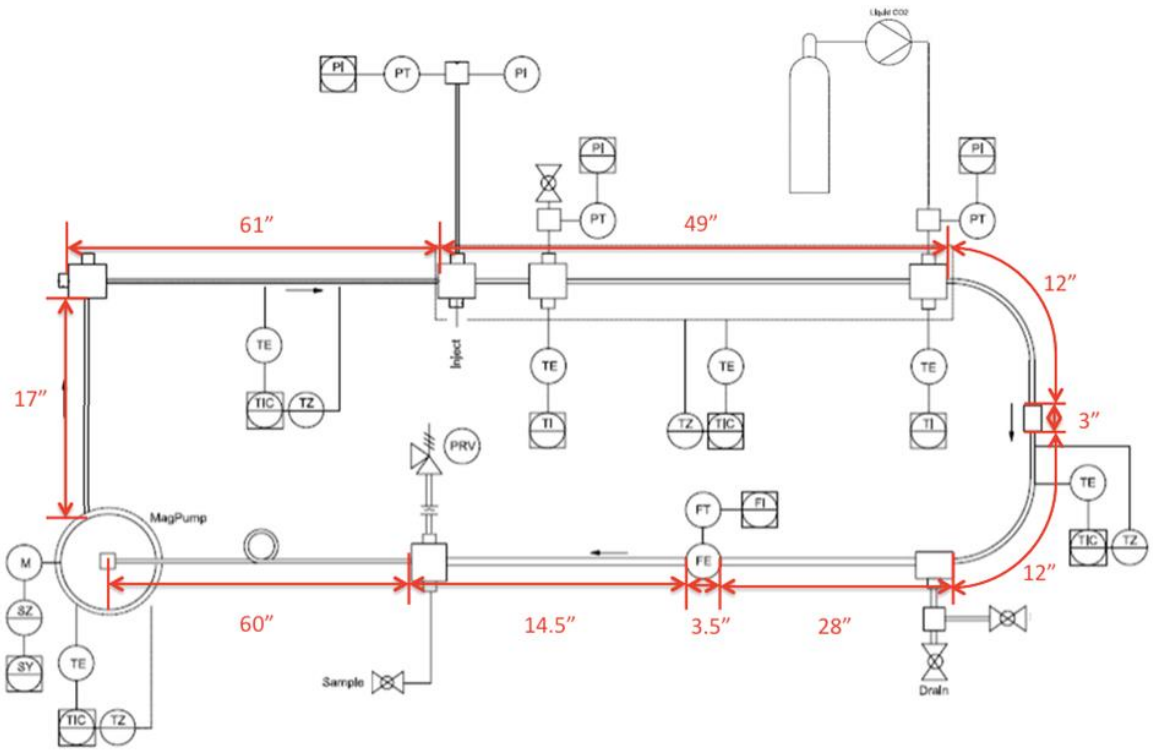

Figure 32: Length measurements of the high-pressure flow loop for the manual calculation of the system internal volume.

The inner diameter of the hose was 19 mm. The inner diameter of all the stainless steel tubing was 0.688” = 17.47 mm. The inner diameter of the flow meter equaled with the outer diameter of the stainless steel tubing, 1” = 25.4 mm. Thus, we get:

$$\begin{aligned}\text{Main section volume} &= \text{stainless steel pipe} + \text{hose} + \text{flow meter} + \text{circulation pump} \\ &\approx \frac{\pi}{4}\times\left(500.38\times 1.74752^2+152.4\times 1.9^2+7.62\times 2.54^2\right)+130 \\ &\approx 1800.9\ \text{mL}\end{aligned}$$

The extra volume introduced by other separate components (pressure gauge, three pressure sensors, drain valve, pressure relief valve, and the joints), was estimated to be between 60 and 70 mL. The resulting total internal volume should be very close to our experimental result: 1.872 L.

Therefore, we decided to proceed with 1.872 L as the internal volume of the high-pressure flow loop for all further experiments.

4.4 SF_6-Water Tracer Evaluation Experiment

After we gained a comprehensive understanding of flow characteristics and a proper measurement of the internal volume, the next step was to evaluate the performance of the tracer loops generated by the membrane system, when injected into supercritical $^{12}CO_2$ in the high-pressure flow loop.

The details of the SF_6-water tracer injection experiment are as follows.

1) Tracer making conditions in membrane system

We planned to use a GC (gas chromatograph) to detect the SF_6 concentration in the CO_2 samples taken from the high-pressure flow loop. In order to make sure that the SF_6 concentrations in the samples were within the detectable range of the GC, we used 5% SF_6 and 95% N_2 (by volume) as the gas supply for the membrane system to make SF_6-water tracer loops.

As mentioned in Chapter 3, the SF_6-water tracer loops were made with the same procedures as the $^{12}CO_2$-water tracer loops. We just replaced the Mylar bag filled with pure $^{12}CO_2$ with a Mylar bag filled with SF_6 and N_2 mixture on the gas supply side, and adjusted the water flow rate from 0.15 mL/min to 0.05 mL/min to ensure full saturation. The set temperature of the SF_6-water tracer making process was 30 °C. Based on the results of the previous investigation, our expectation of the SF_6-water tracer concentration should be the solubility of SF_6 in water at 30 °C,

with a 4% standard deviation, which was converted to 0.004664 cc STP/mL, with a 3% standard deviation.

The tracer loop we used to collect the SF_6-water tracer solution had an internal volume of 0.5 mL, with a 5% standard deviation. The tracer loop weighed 13.9840 g and 14.4580 g respectively, before and after filling with the SF_6-water solution. Thus, the actual volume of SF_6-water solution in the tracer loop was calculated to be 0.4749 mL. The total amount of SF_6 in the tracer loop was 4.941×10^{-9} mol; the specific concentration was 1.040×10^{-8} mol SF_6 per mL of solution, both with a 3% standard deviation.

2) Tracer injection conditions in high-pressure flow loop

Inside the high-pressure flow loop, $^{12}CO_2$ was maintained in the supercritical region. The initial temperature and pressure were 34.2 °C and 10,112.5 kPa (1,452 psig). After the injection and sampling process, the final temperature and pressure were 34.3 °C and 10,036.7 kPa (1,441 psig). According to the equation of state developed by Span and Wagner (1996), we calculated the initial and final $^{12}CO_2$ density to be 727.60 kg/m^3 and 724.59 kg/m^3, respectively. Therefore, the total molar amount of $^{12}CO_2$ in the flow loop started at 30.95 mol and ended at 30.84 mol. The difference was quite compatible with the amount of samples we taken out during the test, more details on the sampling method will follow.

A Teledyne ISCO pump, which is a high-precision, high-pressure syringe pump, was used for tracer injection. Water was used as the working fluid in the ISCO pump to push the SF_6-water tracer solution into the high-pressure flow loop. The dead volume of the injection port was

estimated to be 0.05 mL. The injection rate was 0.01 mL/min; and the injection period lasted for 90 minutes.

3) Sampling method in high-pressure flow loop

Both before and after the injection process, we took three data points at every 5 minutes, which was the same sampling interval during the 90-minute injection period. Therefore we collected 24 data points in total. At each sampling data point, we duplicated the samples for accuracy concerns. Before we took each sample, we discarded about 25 mL of CO_2 gas (at room temperature and pressure) to flush the sampling line first, and then withdrew a 20 mL syringe of CO_2 (at room temperature and pressure) from the high-pressure flow loop. So we would lose a certain amount of CO_2 at the end of the whole experiment. Assuming that we withdrew the same amount of CO_2 gas at each sampling point, then that amount should be the difference between the initial and final amount divided by 24, i.e., 0.00451 mol, which is about 101 mL at STP. The number was quite reasonable (at each of the 24 data points, we discarded about 25 mL twice and collected two samples, each was of slightly more than 20 mL; thus the sum of lost gas at each data point was above 90 mL at ambient condition), and would be used in the calculation of expected SF_6 concentration in the high-pressure flow loop.

4) Results and discussion

The experimental and expected SF_6-water tracer injection curves are plotted together. The grey lines indicate the lower and upper ranges of the expected concentrations (Figure 33). The expected values were calculated based on the assumption that the SF_6 concentration in the tracer solution was the theoretical solubility of SF_6 in water at 30 °C (King and Saltzman, 1995,

Mroczek, 1997). The concentration of SF_6 in supercritical CO_2 flow was reported as the average concentration of those two samples at the same sampling point. The error bars of the experimental data take the standard deviation of the two samples taken at one data point and the error of GC measurement. The error bars of the expected data only considered the 3% standard deviation from the SF_6 solubility during tracer making process as mentioned before. There were indeed other factors that would introduce errors, which are discussed subsequently.

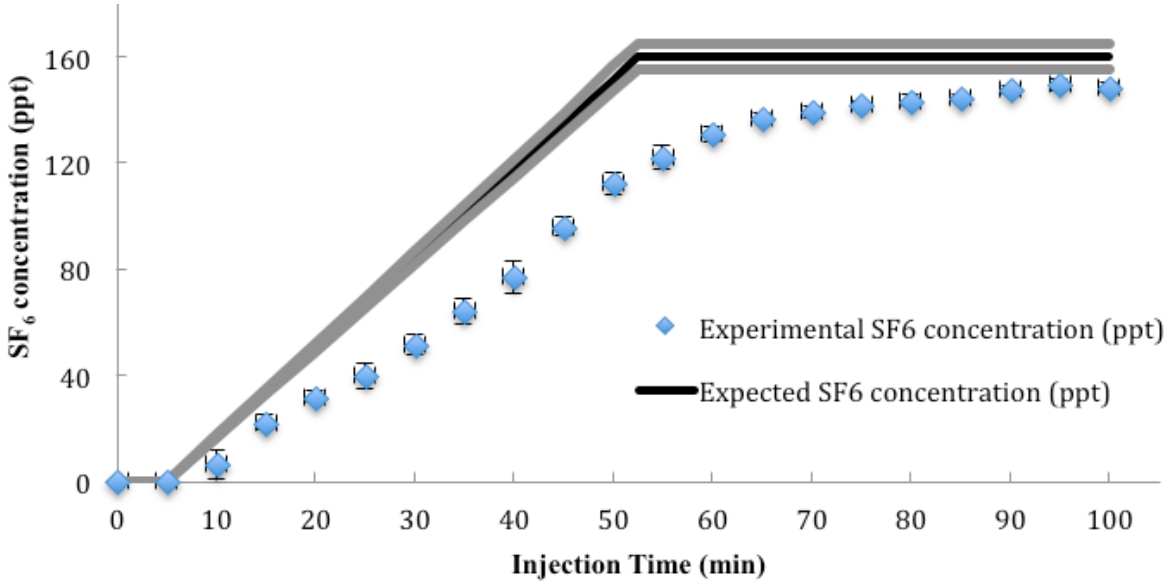

Figure 33: SF_6 concentration vs. injection time of SF_6-water tracer loop injection test; expected SF_6 concentration is represented by the black line whereas measured concentrations are represented as blue diamond symbols.

As seen in the plot, the slope of the experimental curve is not quite as steep as the expected one. In other words, there was a slight delay of tracer concentration increase during the injection process, compared with the theoretical curve. Several issues related to injecting, mixing, sampling, and measuring processes might have caused that.

First, in the pure CO_2 or $^{12}CO_2$-water tracer injection experiments in the IRGA flow loop we conducted previously, the injection rate of the tracer into the IRGA loop was 0.15 mL/min, and the IRGA data collection rate was 0.2 Hz (5 second sampling interval). So we had enough data points and were able to calculate the slope of CO_2 concentration increase quite accurately. However, in the case of our SF_6-water tracer injection experiment in the high-pressure flow loop, the injection rate of the tracer was only 0.01 mL/min and the total volume of the tracer was less than 0.5 mL. The much slower injection rate would cause some axial diffusion effects.

Second, we sampled every 5 minutes manually, rather than the continuous recording done by the IRGA automatically. Collecting only 20 mL of gas sample from such high-pressure supercritical flow was extremely challenging. Even though we did flush the sampling line before taking every sample, it was extremely difficult to control the volume we discarded. Thus, it's possible that we ended up with a small portion of lower $SF_6/^{12}C$ ratio gas mixture from the last sample point into the following sample, and diluted it subsequently. After the complete injection of the SF_6-water solution into the high-pressure flow loop, the experimental results stabilized and therefore indicated the final $SF_6/^{12}C$ ratio in the high-pressure flow loop.

As a result, the slope of the experimental values didn't accurately represent the slope of SF_6 concentration increase. The only way to check the amount of SF_6 in the tracer loop was through comparing the difference of the SF_6 concentration in the supercritical CO_2 flow, before and after the entire injection period.

The expected final SF_6 concentration after the injection of the tracer was 159.86 ppt, and the average of the last three experimental points was 148.25 ppt. The deviation between experimental result and theoretical expectation was 7.3%, which might look high, since it fell out

of the 3% error bars of our expected curve (the random error of the tracer concentrations, based on the performance of the filling station discussed in Chapter 3). However, the real tolerance of the results should be much larger, since there were a number of steps involved in the entire experiment that could have introduced errors.

The main processes in the experiment that might introduce errors are as follows.

a) When preparing the SF_6-N_2 gas mixture, we used 60 mL syringe repeatedly to inject 570 mL N_2 and 30 mL SF_6 into a 1L gasbag, which would then be the used as the gas supply for the membrane system. There would be random errors in the handling and reading of the gas volume in the syringes.
b) At the sample port, in front of each 20 mL sample syringe, there was a plastic valve. Though we did flush the sample line and the valve, there was still approximately 1mL air remained in the dead space between the syringe and valve connection. This extra volume always entered the syringe and diluted our sample as a result. It would cause about 5% systematic error, which could not be avoided.
c) The temperature and pressure of the high-pressure flow loop might also have some slight offsets, which would affect our calculation of the total amount of CO_2. This issue was considered as another systematic error.

Taking all the above into consideration, our SF_6-water tracer injection experiment demonstrated a good performance of the tracer tagging system we developed.

4.5 $^{14}CO_2$-Water Tracer Evaluation Experiment

The $^{14}CO_2$-water tracer injection into supercritical CO_2 was the final test for our laboratory scale evaluation of the complete $^{14}CO_2$ tagging system. We used similar experimental conditions for the $^{14}CO_2$-water tracer injection experiment as we did for the SF_6-water one. Some modifications were made to deal with the radioactive material safely during the process.

The details of the $^{14}CO_2$-water tracer injection experiment are as follows.

1) Tracer making conditions in membrane system

In order to make the radioactive $^{14}CO_2$-water tracer loops in a well-controlled manner, we developed a safety protocol, including detailed operating procedures and a waste management plan. Since the carbon-14 tracer loops for the HPFL and Iceland field test were made in the same set of tracer making experiments, the procedures are stated together in Chapter 5.

The $^{14}CO_2$-water tracer making conditions were at 0.15 mL/min water flow rate and 30 °C temperature. And our $^{14}CO_2$-water tracer concentration expectation was the solubility of CO_2 in water at 30 °C (4% uncertainty), which equals to 0.655 cc STP/mL (4% uncertainty).

The tracer loop we used to collect the $^{14}CO_2$-water tracer solution had an internal volume of 0.5 mL, with a 5% standard deviation. The tracer loop weighed 13.9746 g and 14.4616 g respectively, before and after filling with $^{14}CO_2$-water solution. Thus, the actual volume of $^{14}CO_2$-water solution in the tracer is calculated to be 0.4879 mL. The total radioactivity of one tracer loop is 0.0084 μCi; the specific concentration is 2.931×10^{-10} mol ^{14}C per mL of solution, both with a 4 % standard deviation.

2) Tracer injection conditions in high-pressure flow loop

Inside the high-pressure flow loop, $^{12}CO_2$ is maintained in the supercritical region. The initial temperature and pressure were 34.0 °C and 10,167.7 kPa (1,460 psig). After the injection and sampling process, the final temperature and pressure were 33.9 °C and 9,905.7 kPa (1,422 psig). According to the equation of state developed by Span and Wagner (1996), we calculated the initial and final $^{12}CO_2$ density to be 731.87 kg/m^3 and 724.44 kg/m^3, respectively. Therefore, the total molar amount of $^{12}CO_2$ in the flow loop started at 31.13 mol and ended at 30.81 mol. Water was used as the working fluid in the ISCO pump to push the $^{14}CO_2$-water tracer solution into the high-pressure flow loop through the injection port (Figure 23). The injection rate was 0.01 mL/min; and the injection period lasted for 90 minutes.

3) Sampling method in high-pressure flow loop

Because of the radioactive nature of $^{14}CO_2$, we could no longer use the plastic syringes to take samples from the high-pressure flow loop. Instead, we used glass serum bottles for the sampling purpose. The 100 mL sample bottles were sealed with butyl rubber stoppers and had aluminum caps crimped onto them. In the setup for evacuating the bottles, a needle was inserted through the butyl rubber stopper into the sample bottle, and connecting it to a vacuum pump (Figure 34). The sample bottles were evacuated to below 2.8m Torr before taking samples from the high-pressure flow loop.

Figure 34: Setup of C14 sample bottle evacuation before CO_2 sampling.

At the sample port in the high-pressure flow loop, in order to control the amount of CO_2 we transferred into the sample bottles, we added a relief valve bypass to the sample port (Figure 35). A three-way valve was used for flushing the lines every time before we took a sample. The set pressure of the relief valve is 135.8 kPa (5 psig). Any bubbles in the water trap would indicate that the set pressure had been reached in the sample bottle. There was a chamber of Sodasorb CO_2 absorbents to trap all the radioactive waste gas at the end of the pipelines.

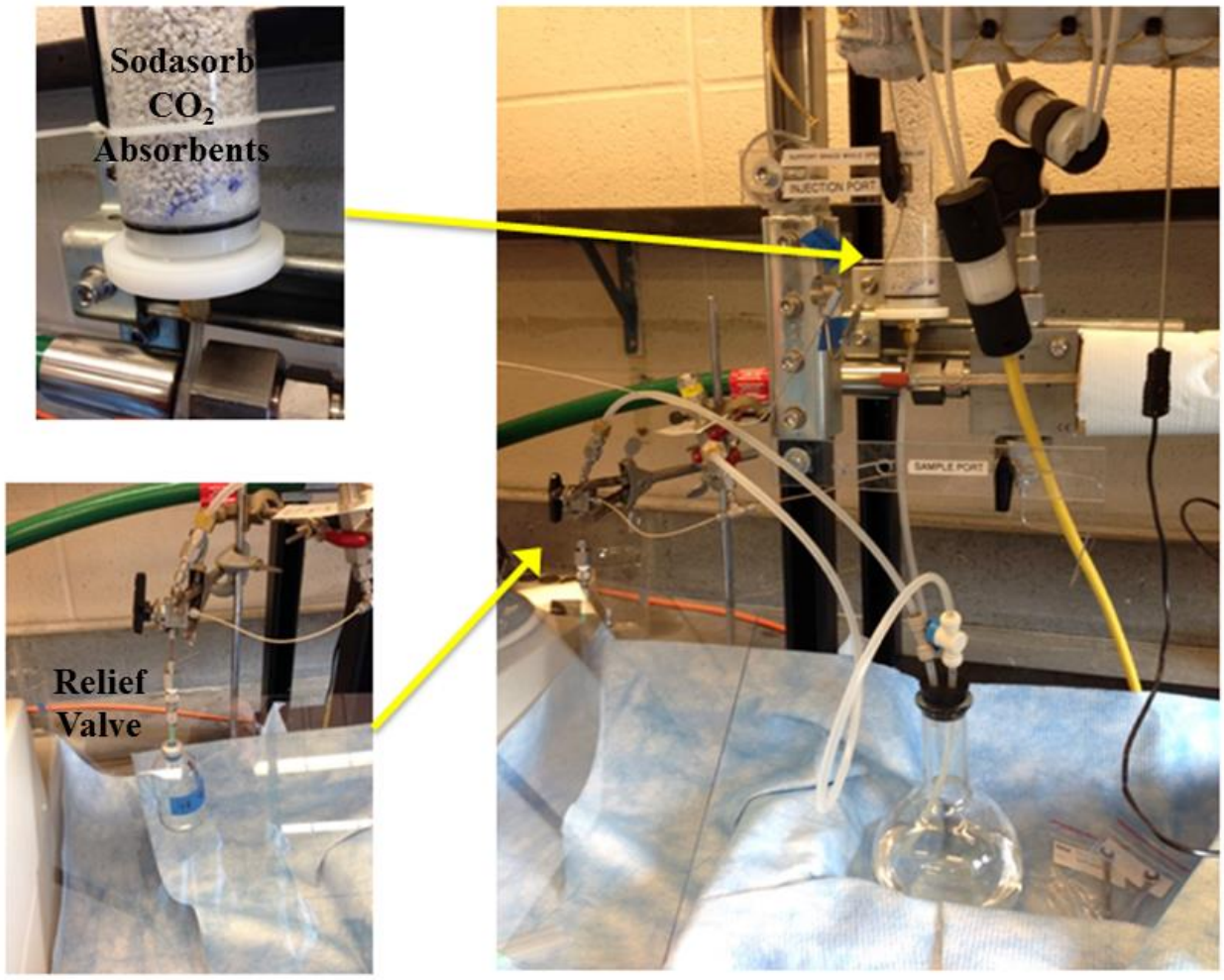

Figure 35: Sample port setup in high-pressure flow loop for C14 samples, showing the Sodasorb CO_2 absorbents and relief valve.

We took one CO_2 sample before the injection as background, and then took CO_2 samples every 5 minutes throughout the entire injection process. Each sample bottle contained about 124 mL CO_2 gas at STP (converted from CO_2 sample gas at 135.8 kPa pressure and room temperature inside each 100 mL sample bottle). Every time before we collected one sample bottle of CO_2 gas from the high-pressure flow loop, we discarded some gas by flushing the sampling line first. The discarded gas was collected in the chamber of Sodasorb CO_2 absorbents.

Thus, we would lose a significant amount of CO_2 in the high-pressure flow loop at the end of the whole experiment. Assuming that we withdrew the same amount of CO_2 gas at each sampling point, then that amount should be the difference between the initial and final amount divided by 20, i.e., 0.0158 mol, which is about 354 mL at STP. The number was quite reasonable and would be used in the calculation of expected $^{14}C/^{12}C$ ratio in the high-pressure flow loop. We also conducted wipe tests in the lab before and after the $^{14}CO_2$-water tracer injection experiment. The results both showed 0 DPM ($< 10^{-7}$ μCi activity) of C14 residues, which were below detection.

4) Results and discussion

At the end of the injection experiment, we obtained 20 sample bottles; each contains about 124 mL CO_2 gas at STP. They were packed and shipped to Lawrence Livermore National Laboratory for analysis using Accelerator Mass Spectrometry.

The experimental and expected $^{14}CO_2$-water tracer injection curves are plotted together. The grey lines indicate the lower and upper ranges of the expected concentrations (Figure 36). The dead volume of the injection port was still 0.05 mL as shown at the beginning. Recall that the premixing $^{14}CO_2$ cartridge we purchased as the gas source for making the $^{14}CO_2$-water tracer loops itself had a 10% tolerance of its radioactive specific activity. We combine that 10% together with the 4% standard deviation from the CO_2 solubility during tracer making process to get the error bars ($10.77\% = \sqrt{10\%^2 + 4\%^2}$) for the expected curve. As for the experimental data, we simply used the measurement tolerance as individual error bars for each sample point.

The expected values were calculated based on the assumption that the total CO_2 concentration in the tracer solution was the theoretical solubility of CO_2 in water at 30 °C (Span

and Wagner, 1996). The expected $^{14}C/^{12}C$ ratio after the injection of the tracer was 3.92 Modern, and the average of the last three experimental points was 4.16 Modern, where 1 Modern = 1.176 ppt $^{14}C/^{12}C$ ratio (Karlen et al., 1965). The deviation between experimental result and theoretical expectation was 6.1%. So the experimental result of the stabilized $^{14}C/^{12}C$ ratio fell well within the range of the 10.77% tolerance.

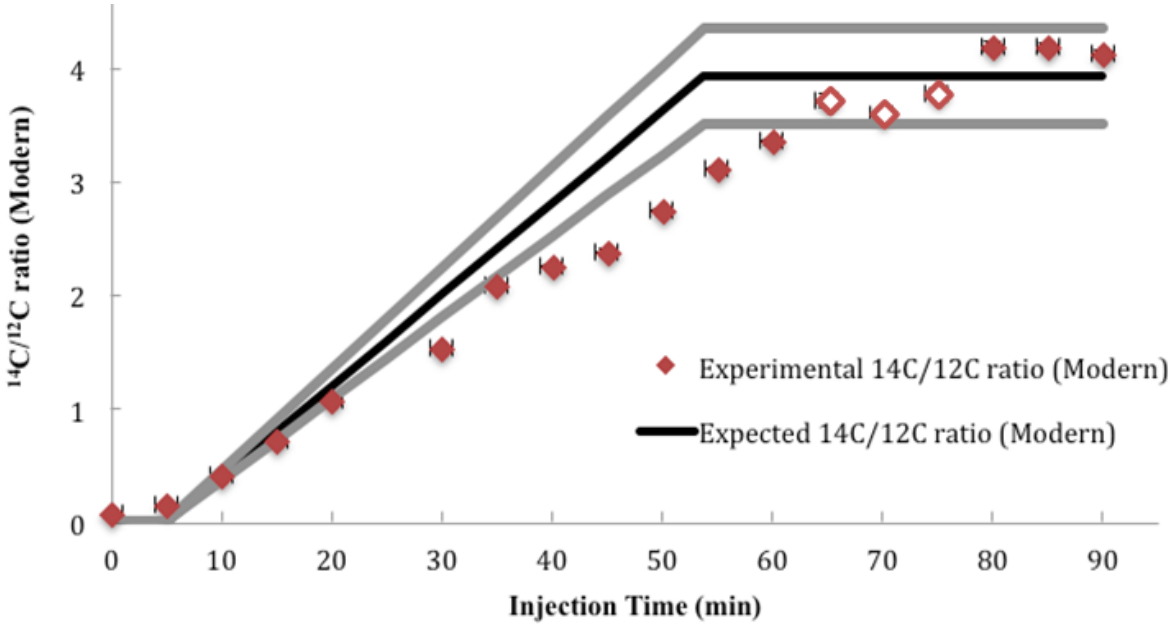

Figure 36: $^{14}C/^{12}C$ ratio vs. injection time of $^{14}CO_2$-water tracer loop injection test; expected $^{14}C/^{12}C$ ratio is represented by the black line whereas measured concentrations are represented as red diamond symbols; three questionable data points are marked with open dots.

It's also worth noting that, the last six experimental points should all indicate the stable $^{14}C/^{12}C$ ratio, because the injection of $^{14}CO_2$-water tracer solution was already completed in the first 60 minutes. However, Lawrence Livermore National Laboratory noted that the three samples (65 min, 70 min and 75 min) had low ion current in Accelerator Mass Spectrometry.

Therefore those three values were less trustworthy than the last three ones. We only considered the last three points when calculating the experimental value of the final $^{14}C/^{12}C$ ratio.

A similar effect of a slight delay in the tracer concentration increase during the injection process (as seen in the SF_6-water tracer injection experiment) also occurred in the $^{14}CO_2$-water tracer injection experiment. The biggest challenge was to collect the gas sample into 100 mL glass bottles from such high-pressure supercritical flow. Even though we did flush the sampling line before taking every sample, it's extremely difficult to control the volume we discarded. Thus, it's possible that we ended up with a small portion of lower $^{14}C/^{12}C$ ratio gas mixture from the last sample point into the following sample, and diluted it subsequently. After 60 minutes of injection, the $^{14}CO_2$-water solution should be all injected into the high-pressure flow loop. And once we had the sampling line completely flushed after a few more samples (65 min, 70 min and 75 min), we finally got samples with the same composition as the internal flow. The relatively constant level of the last three samples indicates that the flow got well mixed in the high-pressure flow loop and reached the final $^{14}C/^{12}C$ ratio.

More importantly, the sampling issue discussed above would not affect our field test in Iceland, since we were going to perform the injection of our $^{14}CO_2$-water tracer loop into continuous CO_2/water flow, rather than a fixed volume. We should be able to achieve proper $^{14}C/^{12}C$ ratio in the downstream as long as the $^{14}CO_2$ concentration in our tracer was as expected, which had been verified by the $^{14}CO_2$-water tracer injection experiment.

In summary, our laboratory scale evaluation demonstrated the accuracy and effectiveness of our tracer loops and injection system. We would then proceed to the field test in Iceland.

Chapter 5: Iceland Field Test of the $^{14}CO_2$ Tagging System

The objective of the field test was to demonstrate how well the $^{14}CO_2$ tagging system would perform in real-world geological carbon sequestration, and determine the accuracy of the proposed technology. The CarbFix project in Iceland offered an excellent opportunity to test the developed devices although the CarbFix applications did not require the level of sophistication achieved in this tagging system. The tagged CO_2 stream was monitored immediately in the downstream of the tracer addition point, both before and after underground injection. The measurements were verified by conventional ^{14}C detection methods.

5.1 CarbFix Carbon Sequestration Site

Reykjavik Energy, in collaboration with the University of Iceland, CNRS in Toulouse, France and Columbia University in the United States launched the CO_2 storage project in 2007. In nature, CO_2 is released from solidifying magma, some of which reaches the surface through geothermal vents, while some is stored, for example in the form of calcium carbonate ($CaCO_3$). The Hengill area, near the Hellisheidi plant, was chosen partly because its rock is made of basalt, one of the most reactive rock types in the world (Oelkers et al., 2008). Mineral carbonation can be enhanced by injecting CO_2 in silicate rocks rich in divalent cations (Ca^{2+}, Mg^{2+}, Fe^{2+}) and by injecting CO_2 fully dissolved in water (Gislason et al., 2014).

The overall aim of the project is to mineralize CO_2 in the form of solid carbonates by interaction of CO_2 charged water with basaltic rocks (Gislason et al., 2010). The CO_2 was injected through boreholes down to 400-800 meters. In theory, it would react with calcium from the basaltic rock and form calcium-carbonate minerals, similar to the Icelandic spar, a stable mineral known to persist in the Earth for tens of millions of years. If the CarbFix project turns out to be a success, the technology can be applied to other basaltic terrains around the world.

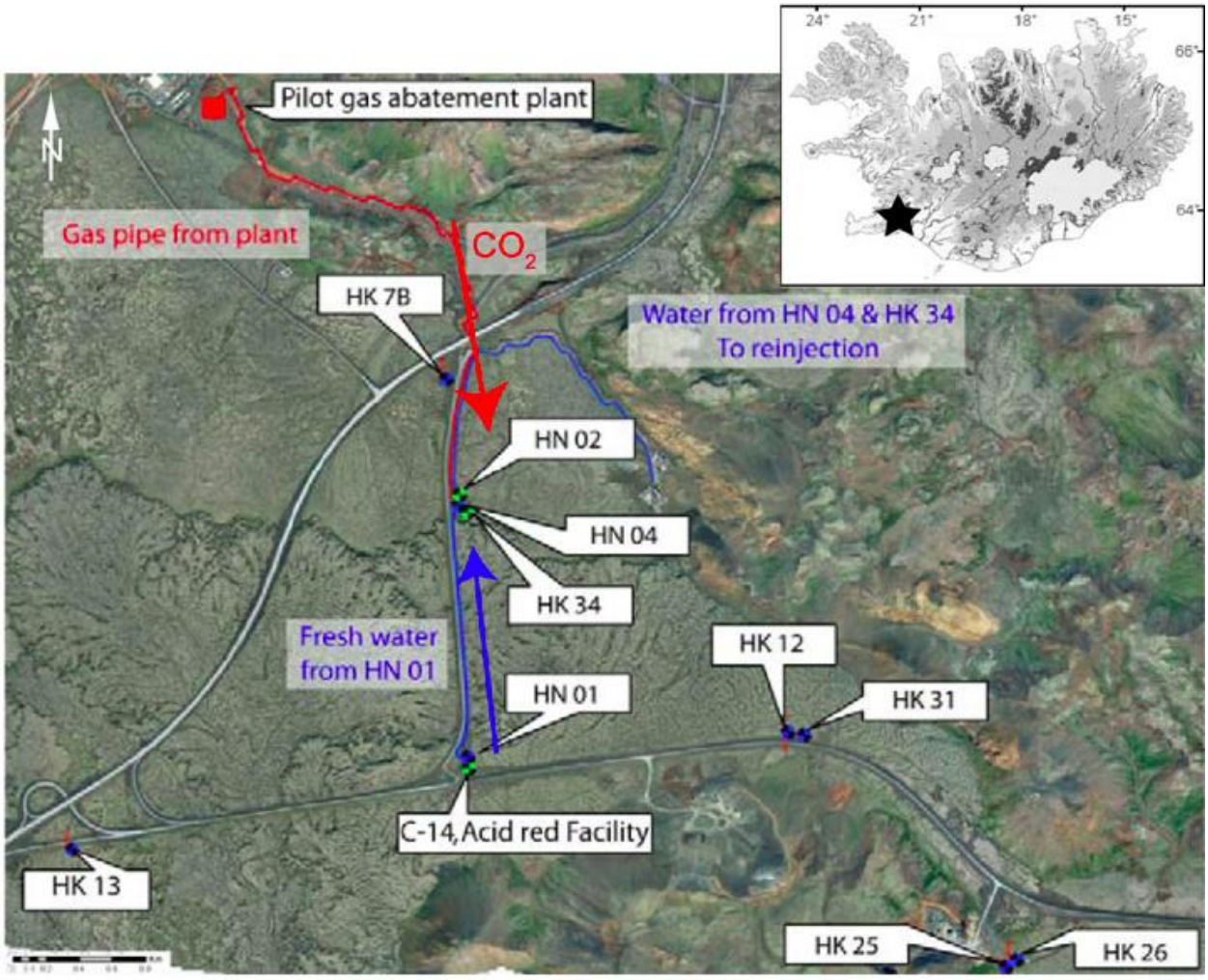

Figure 37: Map of pipelines and wells at the CarbFix Carbon Sequestration Site (Source: Reykjavik Energy).

The distributions of pipelines and wells at the field are illustrated in the map above (Figure 37). The injection borehole, HN-2, is approximately 2,000 m deep and cased down to 400m. The plan is to inject gaseous CO_2 together with groundwater provided from an adjacent deep groundwater well into the borehole where it has been demonstrated that gaseous CO_2 will be fully dissolved into the water before entering the aquifer at ~500 m depth (Alfredsson and Gislason, 2009). In order to evaluate the hydro-geochemical patterns and proportions of CO_2 mineralization in the aquifer, a full-scale monitoring program is required. It includes monitoring of conservative, gas and isotope tracers injected with the waters, amidorhodamine G (acid red dye) and trifluormethylsulphur pentafluoride (SF_5CF_3) as well as measurements of the water composition (Alfredsson et al., 2011).

5.2 Carbon-14 Tracer Making Experiments

The design parameter of the carbon-14 tracer for Iceland field test assumed the flow of CO_2 in the pipeline on site was 3 kg/min. In order to achieve a $^{14}C/^{12}C$ ratio around 5 Modern (1 Modern=1.176 ppt), the radioactivity of one Iceland tracer loop for daily supply was close to 32.7 μCi. Since that was only about 0.55 μmol $^{14}CO_2$ in one tracer loop, we needed to use $^{12}CO_2$ to dilute $^{14}CO_2$ and use the diluted gas mixture as the gas supply for the membrane system. We also planned to make $^{14}CO_2$-water tracer loops to conduct the demonstration experiments on the high-pressure flow loop (see section 4.5 in chapter 4). The amount of $^{14}CO_2$ needed in one HPFL tracer loop is about 1/3,200 of that in one daily supply Iceland tracer loop to achieve a comparable $^{14}C/^{12}C$ ratio, i.e., around 5 Modern, in the high-pressure flow loop.

Our initial idea to accomplish these goals was using a cartridge filled with pure $^{14}CO_2$ and diluting it with $^{12}CO_2$ with some structure on the membrane system. However, given the large dilution factor, it's very likely to cause inaccuracy in establishing the concentration ratio; a system like this is also prone to contamination and safety issues. Therefore, we then developed an alternative idea of using a cartridge pre-mixed by the supplier with $^{14}CO_2$ and $^{12}CO_2$ as the gas supply. We ordered the premixing cartridge from ViTrax, which consisted of $^{12}CO_2$ and $^{14}CO_2$ gas mixture, with a total radioactivity of 850 μCi, and the specific activity of 21.25 μCi/mL (± 10%). The specific activity was calculated to allow us to use the gas mixture directly as the gas supply for the tracer making experiments to generate the 2 mL daily supply Iceland tracer loops.

Compared to the Iceland tracer loops, the $^{14}CO_2$ content in HPFL tracer loops was 3,200 times smaller. As discussed before, the internal volume of the Iceland tracer loop is 2 mL, while that of the HPFL tracer loop is 0.5 mL. Together with this 4 times internal volume difference, we only needed to further dilute the $^{14}CO_2$ and $^{12}CO_2$ gas mixture by 800 times for it to serve as the gas supply for the high-pressure flow loop tracer loop making experiments. To achieve this dilution factor, we decided to split a small volume of the $^{14}CO_2$ and $^{12}CO_2$ gas mixture from the premixing cartridge, and perform a one-time dilution to achieve the best accuracy. After the dilution, the operating procedures were identical for both Iceland and HPFL tracer loops.

Due to contamination concerns in the membrane system, we had to produce the low carbon-14 content tracer loops, i.e., HPFL tracer loops, before we proceeded to make the high carbon-14 content ones, i.e., Iceland tracer loops. So we started with splitting a small volume of the gas

mixture from the premixing cartridge, and diluting it with $^{12}CO_2$ in a Mylar bag on the membrane system. The detailed calculations and operations are described in the following.

First, we had to figure out the internal volume of the ViTrax cartridge. The cylinder itself was custom manufactured and the company didn't have precise numbers for the internal volume and pressure. Thus, we conducted an Archimedes' principle experiment to estimate the internal volume (Figure 38). We measured the weight of the whole cartridge, which was made mainly by 316 stainless steel with a density of 7.99 g/mL. The total volume of the solid parts in the cartridge was calculated accordingly. We then measured the weight of water that the cartridge displaced when it was fully submerged. The corresponding water volume was the external volume of the cartridge. The difference between the external volume and the solid volume, 26.54 mL, should be a good estimation of the internal volume of the cartridge.

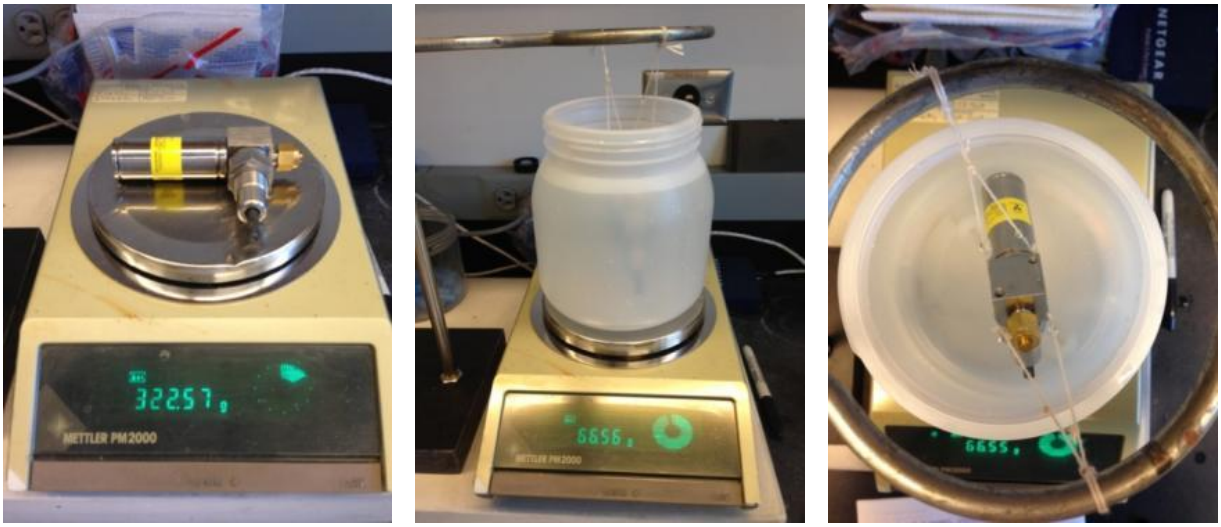

Figure 38: Archimedes' principle experiment to determine the internal volume of the cartridge.

Based on the internal volume of the cartridge, we then built the structure to split volume and calculate the amount of $^{12}CO_2$ needed for further dilution (Figure 39). The red frame indicates

the cartridge side and the green one indicates the split volume. The space of the split volume was made of a piece of 1/4” tubing connecting to a SS-42GS4 two-way ball valve on each end. On the cartridge side, the internal volume of SS-4BG bellows valve was 1.6 mL, the bellows part would add about 1 mL when it’s fully opened during the volume splitting. Together with the 1/4” tubing and SS-42GS4 ball valve part, the cartridge side volume was estimated to be 28.22 mL, and the split volume was calculated to be 0.687 mL. Therefore, the split volume would have 20.17 μCi radioactivity from the total 850 μCi, with the same specific activity of 21.25 μCi/mL. The desired specific activity at 1 atm for HPFL tracer loop making experiments was 0.025 μCi/mL. Hence, 20.17/0.025 – 20.17/21.25 = 806 mL of $^{12}CO_2$ was needed in a Mylar bag on the membrane system to further dilute the split volume of the gas mixture.

Figure 39: Schematic diagram of splitting volume structure.

After splitting the volume, we first closed the two-way ball valve connected to the carbon-14 cartridge (V13 in Figure 16), and then opened the two-way ball valve connected to the membrane system (V12 in Figure 16). Once the split gas mixture entered the membrane system, we cooled down and warmed up the liquid nitrogen cold finger in the membrane system three

times to mix the split off gas well with the 806 mL $^{12}CO_2$ in the Mylar bag, before the diluted gas mixture was finally transferred into the membrane contactor.

This well-mixed gas mixture, ideally, with a specific activity of 0.025 μCi/mL, would serve as the gas supply for the HPFL tracer making experiments. We carefully followed the procedures we developed to make three HPFL tracer loops (0.5 mL, 0.009316 μCi each), two Intra-Cavity Opto-Galvanic Spectrometer (ICOGS) tracer loops (2 mL, 0.037265 μCi each), and three direct detection tracer loops (0.01 mL, 0.000186 μCi each) in series. The ICOGS tracer loops were made for my colleague to test the ^{14}C laser detector, while the direct detection tracer loops were made just in case we would like to perform some other analysis with even lower carbon-14 content in the future. Each tracer was capped individually and stored for future experiments.

Radioactive waste was also well managed at the end of this tracer making experiment. Any 0.025 μCi/mL gas mixture left in the system had been trapped in the CO_2 absorber in the chamber by evacuating the whole system. The premixing cartridge was isolated from V13 and still contained the 21.25 μCi/mL gas mixture for the second tracer making experiment that generated the Iceland tracer loops. Also, we broke the connections from 1L Mylar bag to V11, and from the CO_2 absorber chamber to the vacuum pump to take wipes for Environmental Health and Safety (EH&S) staff to run radioactivity analysis , which verified that there was no residue left in the system after making the HPFL tracer.

The membrane system was put inside a fume hood during the tracer making experiments (Figure 40). The blue/white part was the membrane exchanger wrapped with exterior insulation foam to better maintain the set temperature of its outlet.

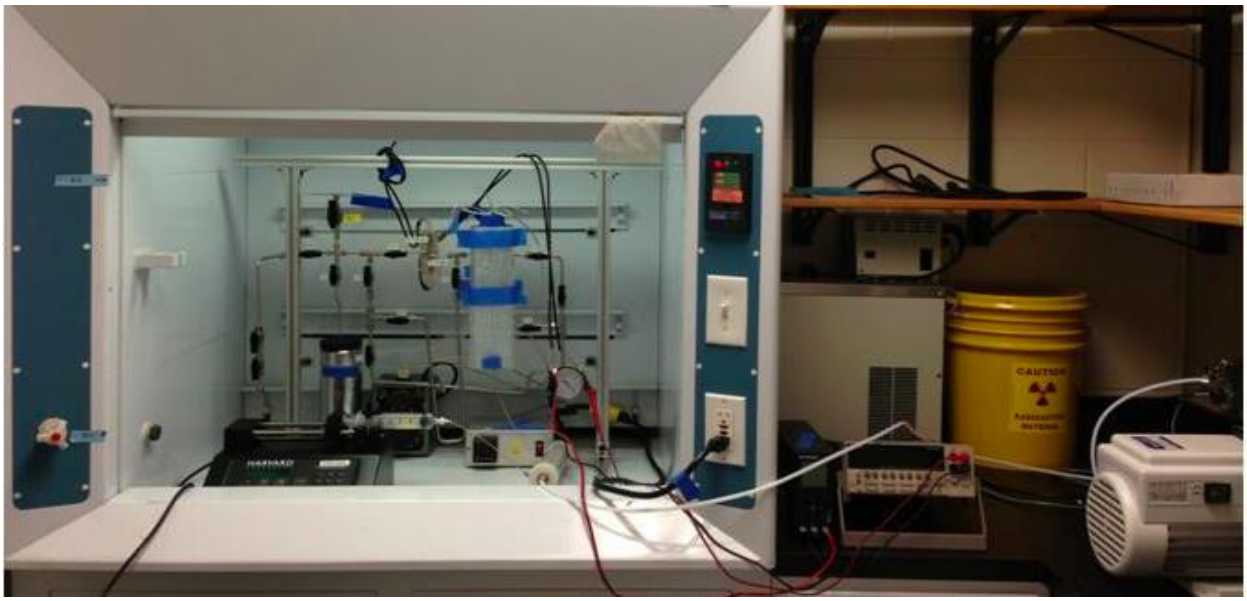

Figure 40: A picture of the whole membrane system inside a fume hood in the radiocarbon laboratory at the Lamont-Doherty Earth Observatory.

Then for the Iceland tracer making experiment, we reconnected the vacuum pump to the CO_2 absorber chamber, and attached a new 100 mL Mylar bag to V11. A liquid nitrogen cold finger was used again to trap all premixed radioactive gas mixture out of the cartridge. And this time, we made three Iceland tracers (2 mL, 31.71 μCi each) in series and capped each one individually.

At the end of the Iceland tracer making experiment, we recycled the radioactive gas mixture in the upstream of the membrane system by placing the cartridge into liquid nitrogen for 40 minutes (Figure 41). The shape change of the Mylar bag and the pressure transducer both indicated that almost all upstream radioactive residues were recycled, which was about half the amount of the initial 850 μCi radioactivity. The downstream radioactive residues were trapped in the CO_2 absorber in the chamber safely as well by evacuating the whole system for another 30 minutes.

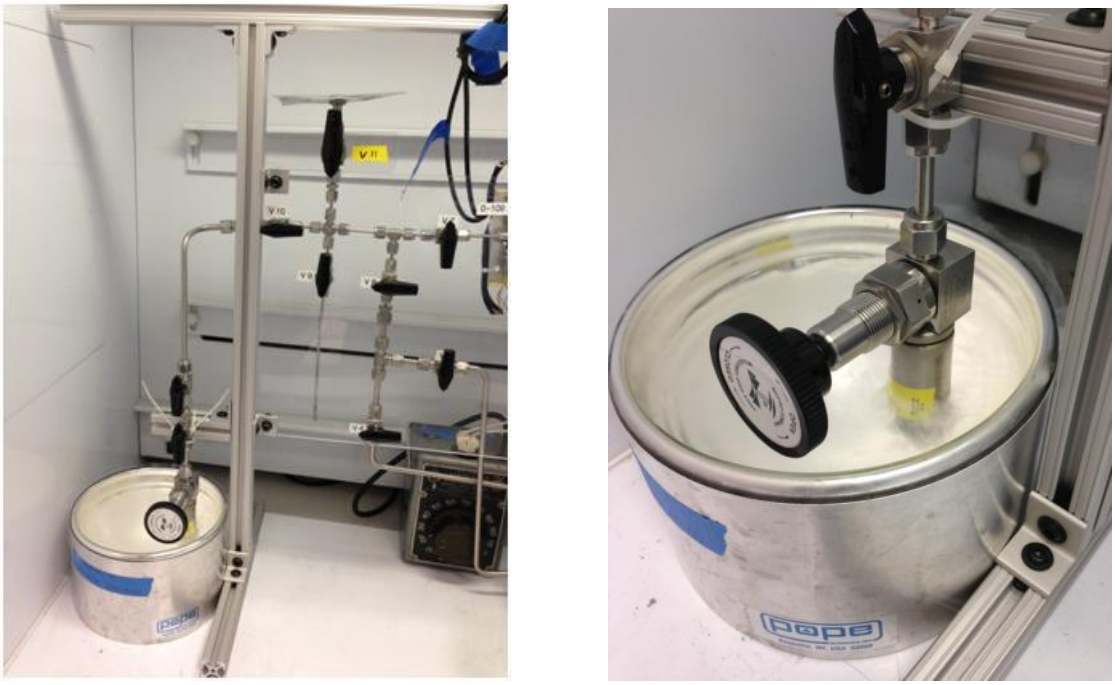

Figure 41: Photo of recycling the upstream $^{14}CO_2$ residues back into the cartridge.

We conducted wipe tests of the main connections and major components in membrane system before, between, and after the two tracer making experiments. The results of the wipe tests are listed in Table 7.

Before the experiment, the membrane system was free of carbon-14. After the HPFL tracer making experiment, there was also no detectable radioactive residue in the system. The Iceland tracer making experiment exposed the system to the radioactive gas mixture with a relative higher carbon-14 concentration, and therefore showed a slightly higher radioactivity level. However, all numbers are low compared to the radioactive safety standard (200 DPM). Wipe tests were conducted on the membrane system again before it was packed and stored in February 2015. The membrane system was shown to be free of ^{14}C and reusable.

Table 7: Wipe test results before, between and after the LDEO C14 tracer making experiments.

	Sample	C-14 [DPM]	Activity [μCi]
Wipe tests before the first experiment	Background	0	0
	Cartridge	5	2.25×10^{-6}
	V11	0	0
	Vacuum Connection	2	9.01×10^{-7}
	Vacuum pump	0	0
	Syringe	0	0
	Power Supplies	0	0
Wipe tests in the middle of the two experiments	Background	6	2.70×10^{-6}
	V11	0	0
	Vacuum Connection	0	0
Wipe tests at the end of the second experiment	Background	6	2.70×10^{-6}
	V11	17	7.65×10^{-6}
	Vacuum Connection	0	0
	Vacuum pump	17	7.65×10^{-6}
	Syringe	18	8.11×10^{-6}
	Power Supplies	0	0

With detailed safety protocol, well-planned operating procedures and waste management plan, our tracer making experiments turned out to be a success. The tracer loops were capped at both ends for storage and transportation purpose (Figure 42). We also kept a record of all the temperature, pressure, weight and volume information throughout the entire experiments for future experiments and analysis.

Figure 42: Photos of tracer loops. From left to right: three Iceland tracer loops, three HPFL tracer loops, three direct detection tracer loops, and two ICOGS tracer loops.

5.3 Experimental Setup and Sample Collection

The completed $^{14}CO_2$ tagging system was tested at the CarbFix Carbon Sequestration Site, and samples were collected for $^{14}C/^{12}C$ ratio measurement done by the Lawrence Livermore National Laboratory using Accelerator Mass Spectrometry.

Continuous injection of the developed ^{14}C tracer loops into ground water flow was conducted at HN-1. The injection well HN-2 is at about 1 km distance downstream. When the water flow rate was 2 kg/s, it took 17 minutes to arrive at the surface sampling port near HN-2, and 46

minutes to flush the entire volume in the injection well. Surface samples were taken before the underground injection with half an hour intervals for six hours. A bailer sample was also collected from the injection well HN-2 (500 m underground) four hours after the ^{14}C tracer injection started at HN-1.

The tracer loops used in the field test were made at the Lamont-Doherty Earth Observatory as described in Chapter 3, and shipped to Iceland. One tracer used was the ICOGS 2 loop, which had a ^{14}C content of 0.034 μCi. We injected it at 5.5556 μl/min (this flow rate was supposed to inject 2 mL in a time period of 6 hours) for 6 hours, and collected both surface and bailer samples. The other tracer used was the Iceland 2 loop, which had a higher ^{14}C content of 29.10 μCi. We injected it at 1.3889 μl/min (this flow rate was supposed to inject 2 mL in a time period of 24 hours) for 2 hours, and collected surface samples only. The detailed specifications for these tracer loops are shown in Table 8.

Table 8: Specifications of tracer loops used in field test at the CarbFix injection test site.

Tracer	Weight of Tracer Solution (g)	Tracer Solution Volume (mL) at 25 °C	Deviation from Expected Volume (2 mL)	Specific Radioactivity (μCi/mL)	Total Radioactivity (μCi)
ICOGS 2	1.9840	1.9899	0.505%	0.017	0.034
Iceland 2	1.9815	1.9874	0.630%	14.64	29.10

A high force/high pressure programmable syringe pump (PHD 4400 Hpsi Model, manufactured by Harvard Apparatus, Holliston, MA) with an accuracy of ± 0.35% and a reproducibility of ± 0.05% was used to conduct the precise injection of tracer loops. Using DI water as working fluid, a BD 3 mL syringe with a diameter of 8.66 mm was connected to the 2 mL tracer loop. In front of the tracer loop, there was a check valve to make sure that only flow in the injection direction was allowed. Finally, the injection line went into the center of the water pipeline (Figure 43).

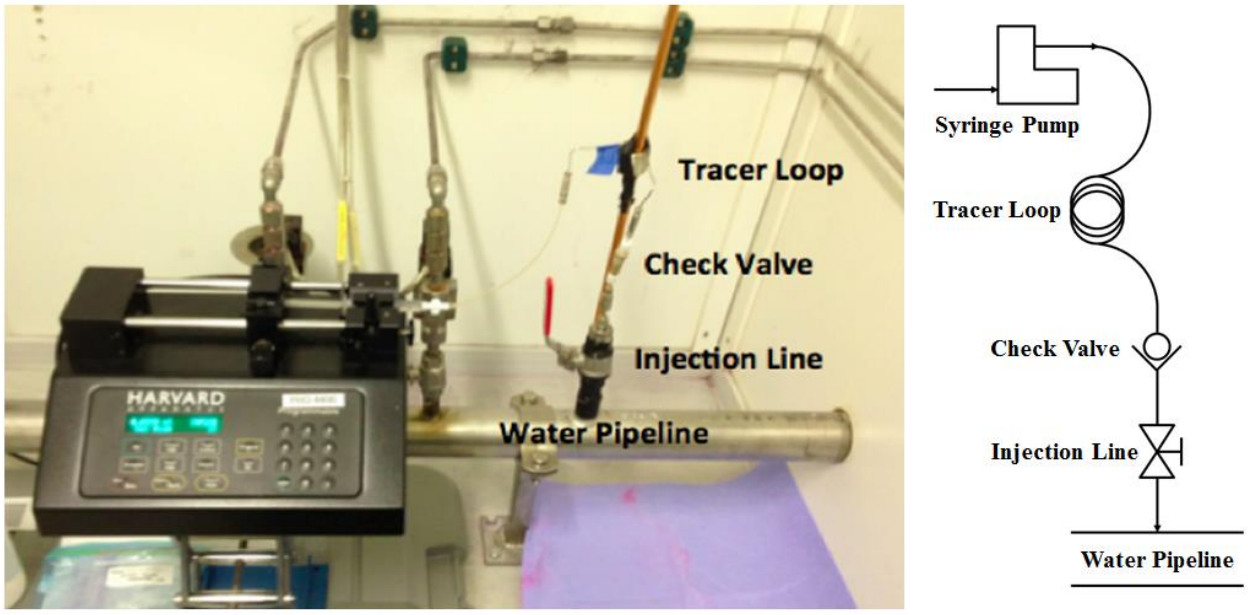

Figure 43: Injection setup at HN-1 in field test, showing the syringe pump, tracer loop, check valve, injection line and water pipeline.

The dead volume of the injection line was 0.1 mL, which we would take into consideration during our field test. Wipe tests were performed before and after our field test. The results verified that there was no radioactive residue at HN-1.

The ports to take surface water samples were located in a hut at the injection site before HN-2. The port we used was the one in the middle for injection well water sampling (Figure 44). We first took background water samples before our ^{14}C tracer injection at HN-1. Once we started our ^{14}C tracer injection, surface water samples were taken every half an hour. On the same day of our field test, alkalinity samples were also taken from the same port every hour.

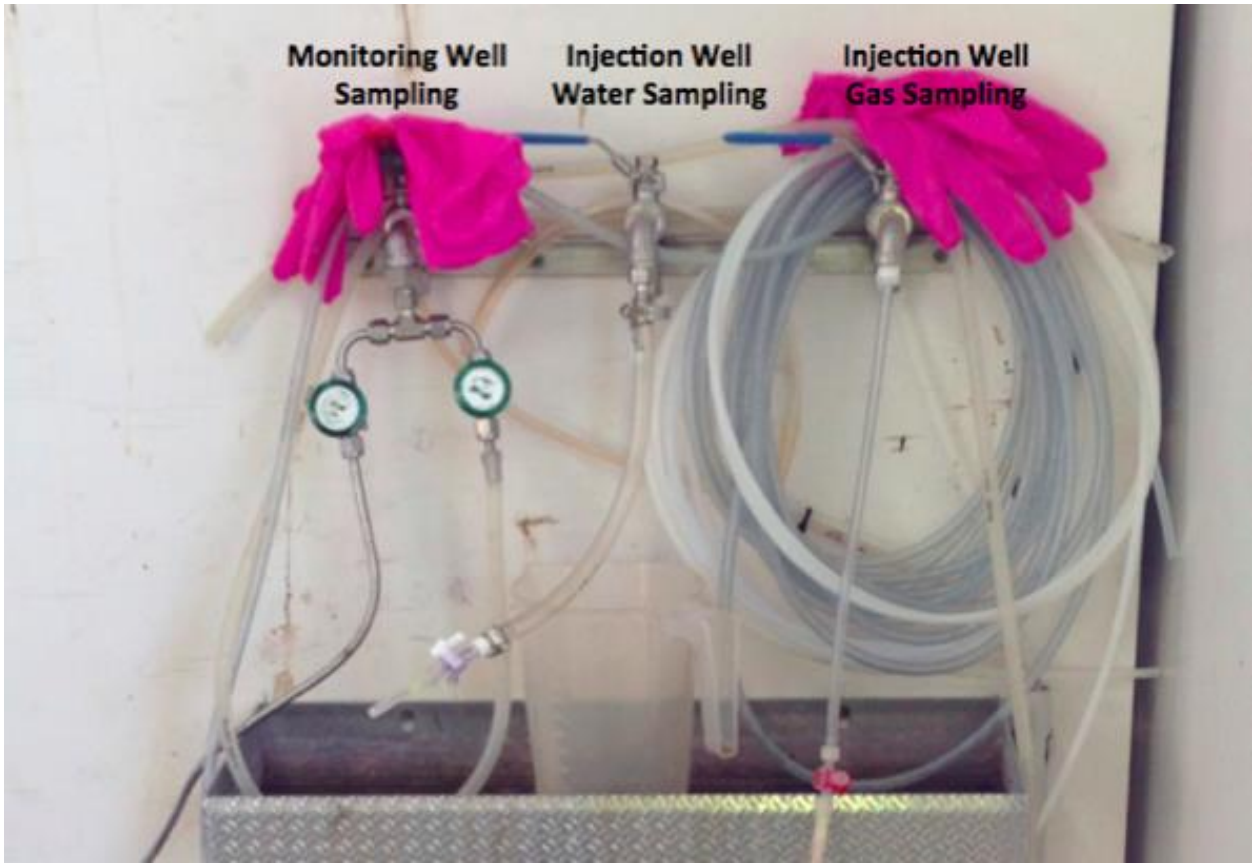

Figure 44: Surface water sampling ports in a hut before HN-2 in field test.

Each time before we collected the sample, we opened the injection well water sampling line and flushed 2 L out of the line. Then the sample was taken in a 120 mL glass bottle, which had been evacuated to below 2.8 mTorr before. During the filling process, a needle was inserted

through the butyl rubber stopper into the sample bottle, and connecting it the water sampling line, until it filled up with the water sample (Figure 45). It took about 5 minutes to flush the line and fill up the bottle.

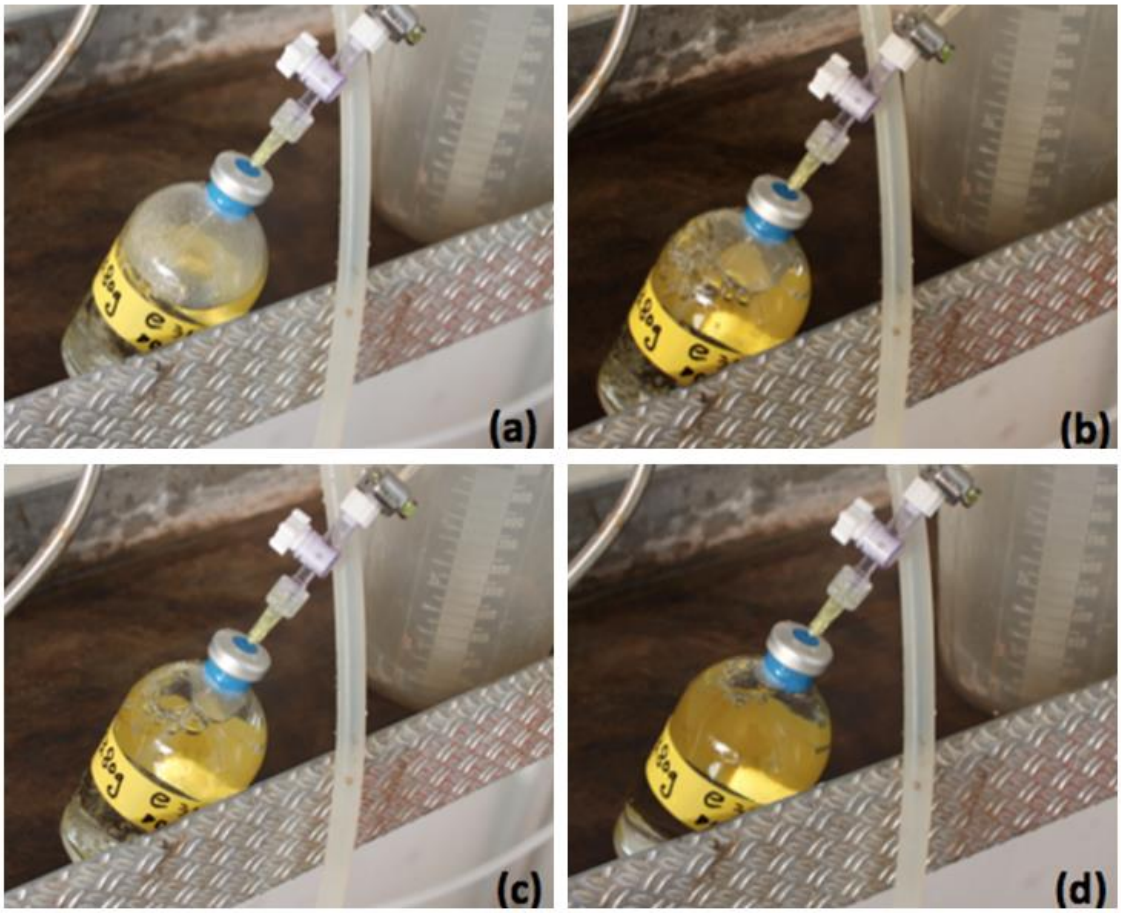

Figure 45: Injection well water sampling process, showing water sample filling up the sample bottle from a to d.

In addition to the surface water samples, water samples were collected in the injection well at 500 m depth with a bailer (Figure 46). It took 20 minutes to load the bailer into the injection well (about 500 m underground). We started to take the bailer sample at 4 hours after we started the

injection of ICOGS 2 $^{14}CO_2$-water tracer loop. The internal volume of the bailer was 1L, and needed 2 hours to get filled.

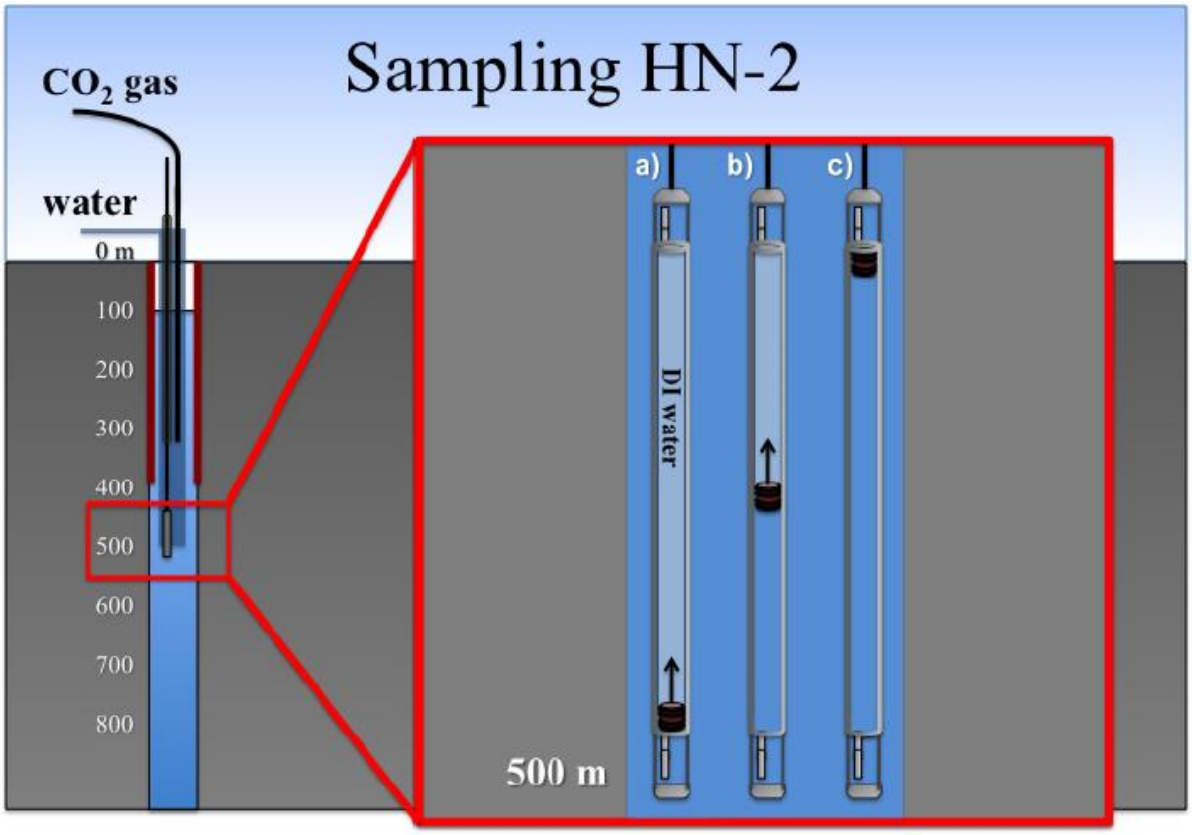

Figure 46: Schematic diagram of bailer sampling at HN-2 (Alfredsson et al., 2011).

Once the bailer was filled with water from the injection well, we unloaded the bailer and took three 120 ml glass bottles of the water samples from the bailer. A detailed list of all the carbon-14 samples collected in the ICOGS 2 tracer injection field test is shown in Table 9.

Table 9: Carbon-14 samples collected in the ICOGS 2 tracer injection field test.

Sample	Description	Notes
DOE 14C-1.1 11.02.14	Background water flow	
DOE 14C-1.2 11.02.14		
DOE 14C-2 11.02.14	0.5 h after tracer injection started	
DOE 14C-3 11.02.14	1 h after tracer injection started	
DOE 14C-4 11.02.14	1.5 h after tracer injection started	
DOE 14C-5 11.02.14	2 h after tracer injection started	
DOE 14C-6 11.02.14	3 h after tracer injection started	
DOE 14C-7 11.02.14	3.5 h after tracer injection started	
DOE 14C-8 11.02.14	4 h after tracer injection started	
DOE 14C-9 11.02.14	4.5 h after tracer injection started	
DOE 14C-10 11.02.14	5 h after tracer injection started	
DOE 14C-11.1 11.02.14	Bailer sample from 500m underground (loaded from 3.5 h to 5.5 h after tracer injection started, consider the middle, i.e., 4.5 h as the time point)	Internal pressure of the bottle was a little high
DOE 14C-11.2 11.02.14		Needle broke and may have resulted in some air being sucked in the bottle
DOE 14C-11.3 11.02.14		Best among the three bailer samples

5.4 Extraction of Iceland Carbon-14 Samples

We brought back all the samples from Iceland field test and performed the extraction of the CO_2 gas from the water samples, in order to make the samples suitable for the $^{14}C/^{12}C$ ratio measurement using Accelerator Mass Spectrometry. The setup for extracting CO_2 gas from water was developed by researchers at the Lamont-Doherty Earth Observatory (Figure 47). The main components are marked as well. The basic idea of the extraction process is to transfer the water sample into the system from the left, extract the CO_2 gas out of water by acidification with hydrochloric acid, go through H_2O trap in ethanol-dry ice bath and CO_2 trap in liquid N_2 bath, and transfer the CO_2 gas sample into a glass rod on the right side. The extraction was done in a series of stages as follows:

Stage 1: Evacuating the mixing bowl and getting rid of air bubbles in acid;

Stage 2: Injecting the sample and beginning capture the CO_2 released;

Stage 3: Capturing the remaining CO_2 reacting with the hydrochloric acid;

Stage 4: Separating the desired CO_2 from any water vapor through the H_2O trap, and freezing the CO_2 in the liquid nitrogen-temperature CO_2 trap;

Stage 5: Thawing the frozen CO_2 and determining the amount captured with pressure measurement of the calibrated volume;

Stage 6: Evacuating the glass tube and transferring the CO_2 to the glass tube.

The final product would be a flame sealed glass tube containing the CO_2 gas extracted from the water sample. All Iceland carbon-14 samples were extracted in this system.

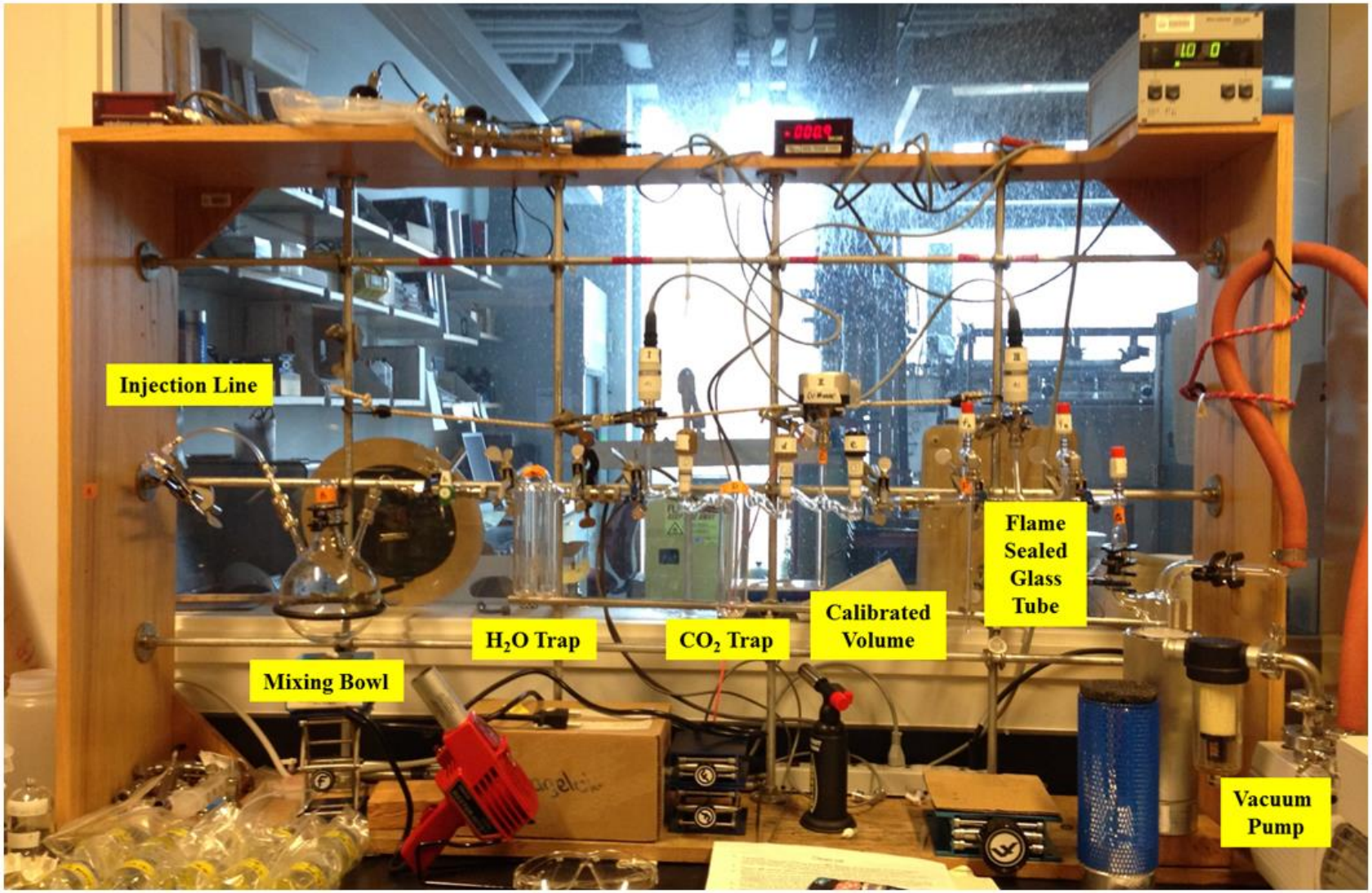

Figure 47: CO_2 gas extraction setup at the Lamont-Doherty Earth Observatory.

5.5 Results and Discussions

We picked and extracted the most essential gas samples, and sent them to Lawrence Livermore National Laboratory for Accelerator Mass Spectrometry $^{14}C/^{12}C$ ratio measurement. The results of $^{14}C/^{12}C$ ratio measurement are listed in Table 10.

Table 10: $^{14}C/^{12}C$ ratio measurement results of extracted carbon-14 samples.

Sample	Description	$^{14}C/^{12}C$ ratio (Modern)
DOE 14C-1.1 11.02.14	Background water flow	0.1720
DOE 14C-2 11.02.14	0.5 h after ICOGS 2 tracer injection started	6.0873
DOE 14C-3 11.02.14	1 h after ICOGS 2 tracer injection started	7.3326
DOE 14C-5 11.02.14	2 h after ICOGS 2 tracer injection started	7.3381
DOE 14C-6 11.02.14	3 h after ICOGS 2 tracer injection started	7.2275
DOE 14C-8 11.02.14	4 h after ICOGS 2 tracer injection started	6.9359
DOE 14C-10 11.02.14	5 h after ICOGS 2 tracer injection started	7.3659
DOE 14C-11.1 11.02.14	Bailer sample from 500m underground, loaded from 3.5 h to 5.5 h after ICOGS 2 tracer injection started	6.3512
DOE 14C-11.3 11.02.14		6.5628

We calculated the expected level of $^{14}C/^{12}C$ in our samples based on the assumptions that the pipeline water flow rate was 2 kg/s, dissolved CO_2 concentration and $^{14}C/^{12}C$ ratio in background water flow were 0.002 mole/L and 0.1720 Modern, respectively. For the samples from the ICOGS 2 tracer loop injection, each sample bottle contained 120 mL water sample, which should contain 2.4×10^{-5} mole CO_2 amount, with a $^{14}C/^{12}C$ ratio of 6.44 Modern.

As shown in the table, the average of our field test samples from 0.5 hour, 1 hour, 2 hours, 3 hours, 4 hours, and 5 hours after we started the ICOGS 2 tracer injection, together with two bailer samples from 500m underground, was 6.90 Modern, with a standard deviation of 0.50 Modern. Thus, the difference between the expected and measured results was 0.46 Modern, 7.1% of the expected value.

The error level of the ICOGS 2 tracer injection field test was well within the 10% tolerance of the radioactive specific activity of our $^{14}CO_2$ gas source during our tracer making process. The precision of our carbon-14 tagging can be further improved, e.g., by using $^{14}CO_2$ gas source with a higher accuracy during the tracer making process and adding more sophisticated control mechanism for tracer injection.

As mentioned at the beginning of section 5.3, we also performed an Iceland 2 tracer injection field test. However we had very limited time, no more than 2 hours, to conduct this experiment. Only surface samples were collected at 1.5 hours and 2 hours after the Iceland 2 tracer injection started. Due to the higher ^{14}C content expected, further dilution was needed for the water samples collected to make the samples suitable for the $^{14}C/^{12}C$ ratio measurement using Accelerator Mass Spectrometry. Multiple problems occurred during both tracer injection and sample dilution processes. So the results from the Iceland 2 tracer injection field test were not

trustworthy. The average $^{14}C/^{12}C$ ratio of the two samples we analyzed was 10.45 Modern, about 50% of the expected value, i.e., 21.01 Modern.

If we recall the ^{14}C tracer making process, the ^{14}C used for making the Iceland 2 tracer was directed from the ^{14}C cartridge, while the ^{14}C used for making the ICOGS 2 tracer was further diluted with $^{12}CO_2$ to achieve a lower ^{14}C content. The ICOGS 2 tracer making process obviously involved more calculations, steps which would only introduced more random errors. Therefore, error analysis of the ICOGS 2 tracer injection results is a conservative evaluation of the carbon-14 tagging performance in the field test.

There were many sources of error in this complex field test. Other than the tolerance level of the ^{14}C content in the tracer, the injection of the tracer involved the syringe pump, with an accuracy of ± 0.35% and the BD 3 ml Syringe used, with an inside diameter of 8.66 mm also introduced a ± 3.5% random error. For the expected concentration calculation, we assumed constant flow rate, CO_2 concentration and $^{14}C/^{12}C$ ratio in the background water flow. However, these parameters did fluctuate throughout our field test. If we were given enough time and resources to perform the field test in a more comprehensive manner, our tracer performance could be further improved.

Ultimately, a ^{14}C detection technology with the online $^{14}C/^{12}C$ measurement capability will help to reduce the complexity of sample handling. Online measurement of the ^{14}C content in the tracer fluid can cut back on the uncertainty of what is being injected, and further enable real-time adjustment of the tracer injection rate to accommodate the background flow condition. Our findings on the ^{14}C detection system were stated briefly in the next chapter.

In summary, the Iceland field test successfully demonstrated a system design whereby $^{14}CO_2$ could be successfully injected into CO_2 flow at the part per trillion levels over extended periods of time in a cost-conscious and straightforward manner. The uncertainty level of the field test is within 10%, which can be further reduced as the technology matures.

Comparing with the DOE's 2030 goal for CCS technology development, i.e., developing and validating technologies to measure and account for 99% of injected CO_2 in the injection zones, and supporting industry's ability to predict CO_2 storage capacity in geological formations to within ± 30%, carbon-14 tagging technology, per se, at this stage is not sufficient to meet these goals. However, together with other geochemical, geophysical and modeling techniques, carbon-14 tagging will serve as an important monitoring, verification, and accounting tool to help achieve the quantitative precision needed in carbon capture, utilization, and storage.

Chapter 6: Future Work

6.1 ^{14}C Detection System and Optimization Study

The objective of this task was to develop an improved ^{14}C detection system. Current monitoring equipment for ^{14}C activity was designed for rather different applications and should be streamlined and improved for CO_2 tagging systems. There are two major applications for ^{14}C detection within the tagging infrastructure explored in this research. The first is the real-time confirmation that the tagging operation delivered the appropriate ^{14}C level, the second is the need to sample reservoir rocks and fluids in the subsurface and establish the amount of ^{14}C present while monitoring carbon flows underground or in establishing an accurate inventory of stored anthropogenic carbon. A third need might arise if the CO_2 delivered to the CO_2 storage site is not all from fossil sources. For example, a power plant may co-fire biomass and thus deliver CO_2 that has some ^{14}C in it. In this case it becomes necessary to monitor the input stream of CO_2 so as to adjust the tracer addition rate accordingly. ^{14}C detection and quantification are therefore necessary both during the tagging operation and for inventory assessment.

We started out with the concept of a scintillation-based counting system that adds a fluorescent dye to the sampled CO_2 stream and directly measures ^{14}C decays. As an alternative, the CO_2 stream can be used to fill either a bubble chamber or a cloud chamber to measure autogenous decays of ^{14}C in the fill gas or liquid in the chamber.

However, these options were set aside because a new method for detecting $^{14}CO_2$ studied at Rutgers University by measuring the impedance change in a plasma that is subjected to intense

light from a $^{14}CO_2$ laser line (Murnick et al., 2010). The concept for the laser detector came from a series of reports (Murnick et al., 2005, 2007, 2008) on the use of Intra-Cavity Opto-Galvanic Spectroscopy (ICOGS). Unfortunately, neither this team, nor several other teams around the world were able to reproduce the high sensitivity claimed by the Rutgers team (Paul and Meijer, 2015). It appears doubtful that the original results are reproducible and it is therefore the conclusion of this research team that the accuracy required for tracing ambient levels of ^{14}C in a CO_2 stream is not achievable in the foreseeable future by this method. The team's experimental results suggest the minimum measureable ^{14}C concentration is at least 4 to 5 orders of magnitude higher than in ambient samples. Therefore the recommendation is to return to scintillation-based systems. Another alternative is to explore whether recent advances in laser technologies, e.g., ring-down spectroscopy, warrant another look at a different laser based technology.

Another current limitation of ^{14}C tagging in geological carbon storage is about the issues related to get sufficient access to the storage reservoir by drilling boreholes. In general, wells present a challenge to integrity and monitoring on geological carbon storage sites. Managing and maintaining well integrity is important to avoiding failure. Risk minimization is addressed through technology application & regulation. For our ^{14}C tagging technology in particular, we also need to perform an optimization study to figure out the boreholes needed to get enough samples for mass balance analyses and accurately monitor the CO_2 inventory in a typical storage reservoir. This effort will be pursued with more complex 3D models representing larger volumes of subsurface and combined with other geophysical approaches to further investigate the CO_2 plume properties (Gouveia and Friedmann, 2006; Lewicki et al., 2007). The optimization study should result in the number of boreholes and location choices which are representative, cost-effective and sufficient.

6.2 Risk Management

In analyzing potential hazards of this new technology, we are not considering the general hazards of carbon sequestration but the additional (incremental) hazards introduced to carbon sequestration by ^{14}C tagging at a level that makes the injected CO_2 look like carbon on the surface of the Earth. In other words, the ^{14}C level in the tagged CO_2 is "1-Modern," or approximately one part per trillion of the carbon present.

Any incremental concern that arises from tagging vast amounts of CO_2 with ^{14}C has to be due to the fact that ^{14}C decays through a weak beta decay with a half-life time of 5,730 years. In any other respect the carbon-14 behaves like every other carbon atom and since the addition is only one part per trillion, there are no discernable incremental impacts apart from the decay. Therefore the focus of this analysis is entirely on the instability of the ^{14}C.

There are two distinct classes of concerns over environmental impacts and safety issues. The first is environmental hazards and risks posed by introducing successfully tagged material into the environment. The question here is whether the disposal of large quantities of tagged CO_2 has any additional environmental or safety concerns above and beyond those arising from storing CO_2. The second question addresses the risks and hazards to people and the environment that are posed by the actual tagging operation either in normal operation or in situations where the tagging operation ended abnormally.

6.2.1 Incremental Risks of storing tagged CO_2

The incremental risks in carbon storage that stem from the fact that the carbon to be stored has been tagged with at a level of ^{14}C that is commensurate with the ^{14}C level in typical bio-carbon or for that matter carbon dioxide in the atmosphere makes the risk of storing such materials virtually negligible.

There are several lines of argument that will reach this conclusion. The first is a simple comparison to natural materials humans and other organisms are constantly exposed to. The second looks directly at the radiation dose that an organism might be exposed to due to the proximity of a large storage of tagged CO_2.

Clearly, exposure to natural carbon that originated at the planet surface with a "1-Modern" content of ^{14}C is not considered a hazard. All organisms on land and in the sea are made from such carbon and therefore the exposure is truly autogenous and entirely unavoidable. The fact that ^{14}C at the natural level is not considered dangerous is visible in everyday life. In handling carbon the question whether products like baking soda are produced from fossil carbon with low ^{14}C content, or modern carbon with a ^{14}C level of approximately one part per trillion relative to other carbon atoms present in a material is not even asked. Nobody is concerned that biofuels contain ^{14}C at the 1-Modern level, whereas petroleum based fuels do not. Furthermore, on the surface of the planet all living organisms have a significant "auto-exposure" because biological materials are made from modern organic carbon. The exception may be organisms that live deep underground. Organisms that live deep underground may not be exposed to radiation from ^{14}C, but they tend to be exposed to various radionuclides that can be found in typical mineral rock, which would far overwhelm a 1-Modern exposure to ^{14}C.

As a second line of argument, it can be shown that the actual radiation exposure from carbon with natural "1-Modern" ^{14}C content leads to radiation exposures that are extremely small. While the half-life of ^{14}C is short, the concentration of ^{14}C in the environment is exceedingly small. Decay rates within the human body are comparable to those of potassium ions decaying, another exposure that is entirely natural and utterly unavoidable. In addition, pure CO_2, or pure graphite creates exposure levels that are miniscule as only a small surface layer in direct contact with an organism can cause exposure. For carbon that is not firmly embedded in the organism's cell tissue, the exposure is very small as the weak beta-decay by which ^{14}C decays has an extremely short penetration depth in water or cell tissue. ^{14}C, unless it is inside the human body does not create any exposure to radiation.

As a result, the exposure to large volumes of carbon is no more harmful than the exposure to a surface layer of the same material. All the material that is not in direct contact with cell tissue simply cannot create an exposure because radiation will not travel through the material. The large size of a reservoir cannot amplify potential hazards because the impact of ^{14}C decays in their very nature is local. However, the most powerful argument for the safety of these materials is that the ^{14}C exposure of any modern organism is essentially driven by the carbon embedded in the organism itself. Carbon sequestration will try to keep the excess carbon from the atmosphere, and from the biosphere. Therefore exposure of humans is not increased by the storage of CO_2 and the exposure of organisms living near the surface is also not increased.

Organisms that are living in the reservoir will be exposed to a higher number of ^{14}C decays then they would be in the absence of such technologies. Indeed they will likely incorporate this carbon into their tissues and thus look like organisms living on the surface. This is unlikely to

create a hazard for these organisms, because living in a mineral formation exposes organisms to far harder radiation from far more abundant sources. Any organism living near or in such reservoirs is exposed to natural background from potassium, uranium, radon and other naturally radioactive constituents of such mineral rock. The exposure to potassium and uranium is far higher as these gamma sources have a significant penetration depth.

Finally, the decay product of ^{14}C is nitrogen, which in itself is non-toxic and harmless and additions of nitrogen atoms at the part per trillion level does not cause any long term hazards in addition to the energy release of the decay event. As a result, we conclude that the incremental risk from having to store vast quantities of CO_2 to which ^{14}C has been added at the 1-Modern level is *de minimis* and can be safely ignored. The same chain of argument also suggest that there are no intrinsic incremental risks that develop because CO_2 samples are taking from the underground.

6.2.2 Hazards of incidental or accidental exposure during operations

While the disposal of tagged CO_2 does not add incremental risks, the actual tagging operation and processing steps taken before this point is reached involve the production, transport and handling of ^{14}C. During these operations, ^{14}C is available in far higher concentrations than in the final waste stream and incidental or accidental exposure to these materials or precursors could result in significant exposures. Therefore, it is necessary to analyze these risks.

On a small scale our research encountered these issues, as we had to handle ^{14}C when we prepared these tagging operations. In discussions with lab-safety groups it became clear that our hazard level was exceedingly small, because the amounts of ^{14}C involved were below normal

thresholds. For example, the activity of one Iceland tracer cartridge is about 30 μCi, while the permissible exposure limits established by the Occupational Safety and Health Administration (OSHA) set 200 mCi as the annual limit on intake via inhalation of carbon dioxide.

However, in designing our experimental design we built in precautions against accidental ^{14}C release, which would only be necessary, if we greatly enlarged our operations. This was undertaken in part in order to assure that the technology is designed to absolutely minimize any losses from the tagging system to the outside. For example, the tagging system has been designed with the goal of minimizing any losses of enriched ^{14}C from the ^{14}C that is being moved through the system. This means that there should be no accumulation of leftover CO_2 in the system.

In analyzing the sources of risks, we need to follow the production chain, which begins with the production of ^{14}C at a nuclear reactor, the transport and shipping of such ^{14}C, the distribution into small cartridges and the use of such cartridges at the tagging facility.

As long as tagging is a small enterprise on the research level, the ^{14}C is simply taken from an existing supply chain that delivers ^{14}C for example for biomarkers in medical studies, or medical diagnostics. However, we have found that the total ^{14}C production of 3 kg is insufficient to supply the demand, which would come from tagging on the order of 30 Gigatons of CO_2 per year. It would take approximately 30 kg of $^{14}CO_2$ to tag 30 Gt of CO_2 at a 1-Modern level. The scale of operations required to produce this much ^{14}C would be sufficiently small to be performed by exposing nitrates to high neutron fluxes inside a single nuclear reactor. Therefore the supply chain for producing the world demand of ^{14}C for tagging purposes of fossil CO_2 would not require substantial changes to the existing nuclear infrastructures. Hazards and risks of such a

production process would not significantly alter the risks associated with operating nuclear reactors.

The ^{14}C could be delivered as dissolved carbonate, and as such would be easily transportable. Compared to shipments of radioactive waste materials, the hazards involved in this effort are quite small and have not been studied further. There are no new or novel risks and the total amount of radionuclides is quite small.

The remaining issue is the potential for exposure at the filling station. This risk can be dramatically attenuated by working in a fume hood, as we did for this project. The large volume of air moving through the fume hood is more than sufficient to dilute minor losses of ^{14}C down to background levels. If a greater degree of containment is deemed necessary, the work can always be carried out in a sealed glove box that is purged through a bed of calcium hydroxide or other aggressive CO_2 scrubber. The resulting carbonate would then be disposed of as waste.

For a large CO_2 sequestration site, which injects million tons of CO_2 annually, the implementation of our tagging approach would involve many small cartridges. About 1.3 Ci activity is needed to tag 1 million tons of CO_2, which breaks down to 3.5 mCi in a daily dose. Therefore, even though a mishap with a single cartridge would not pose a significant hazard, it is necessary to consider the impact on a particular location if such events happen not once but with certain regularity. As an analogous example, radiation safety analysis has generally considered that the indirect exposure of people who get in contact with patients after they have received radiation treatment or e.g. iodine treatment for thyroid problems is sufficiently small that members of the public are not at risk. By contrast, hospital staff needs to be monitored, as they are not exposed to a single patient for a short time, but they meet with a continuous stream of

patients. An exposure of a few seconds or minutes with a single person is quite different than multiple such exposures every day for many decades. Recently it has been noted that some members of the public also could have more frequent exposure. For example, in many locations, iodine treatment for thyroid has become an outpatient treatment, and patients coming from afar tend to stay in a single hotel near the hospital, which in turn gives personnel working at the front desk or in cleaning rooms a far higher level of exposure than typical members of the public. Similarly, here one needs to consider frequent use of these cartridges, or frequent filling of such cartridges, which will leave a residual exposure level.

The ultimate advantage of gaseous CO_2 is that it rapidly disperses and thus high concentrations are not retained. Contaminations with CO_2 are not likely to be cumulative, but just sequential, as long as one follows the simple precaution of keeping CO_2 sorbents away from the operation. Indeed, the only useful sorbents are those that are used to trap the ^{14}C in a well-designed trap, which aims to keep it out of the atmosphere. However, even in the most extreme scenarios the amount of radioactivity that would be handled within a safety plan of an operation is far smaller than radioactivity that is routinely managed in many different locations.

In short, while the hazards are undoubtedly real, they are very small and can be managed with far less effort than is routine in nuclear waste management.

6.3 ^{14}C in Carbon Management

We can use ^{14}C not only for underground detection, but also as a good indicator of the fossil nature of a fuel. Namely, if a ^{14}C detector is installed at the end of a power plant, one will be able to tell the fuel of the power plant to be either pure fossil ($^{14}C/^{12}C \approx 0$) or pure biomass ($^{14}C/^{12}C \approx$

1 Modern), or the composition of the mixture of them by analyzing the $^{14}C/^{12}C$ ratio. However, when the plants also burn peat, it's unfair to compare peat with biomass/fossil fuel by its $^{14}C/^{12}C$ ratio. The formation of peat takes hundreds to thousands of years, which, over time, is often the first step in the geological formation of other fossil fuels such as coal. While the $^{14}C/^{12}C$ ratio of peat can be somewhere between 0 to 1 Modern, which is similar to that of a biomass/fossil fuel mixture, burning peat will have more environmental impact in terms of increasing the CO_2 level in the atmosphere.

We define the "Fossilness" of different fuels using a general formula: $1\text{-}T_1/T_2$, where we introduce a correction factor T_1/T_2. T_1 is the lifetime of operation, while T_2 is the time scale for the fuel to regenerate. Let f represent the fossilness of fuel, then we get $0 \leq f \leq 1$. To be specific, $f_{fossil} = 1,\ f_{biomass} = 0, 0 < f_{peat} < 1$. The plants burning different fuels are discussed as follows.

1) Fossil fuel

We may use the lifetime of a coal plant, usually 30 to 50 years as T_1, and T_2 is millions of years, $T_1 << T_2$. Therefore, the fossilness ≈ 1.

2) Biomass

For those plants that burn merely biomass, T_2 is around tens of years. And people usually burn the amount they planted, therefore $T_1 \approx T_2$ and the fossilness ≈ 0. That's the reason why people usually consider biomass as carbon neutral.

If people consume biomass slower than its growth ($T_1 > T_2$), we even get negative fossilness there and it actually helps store CO_2 (at least temporally from the atmosphere). But on the contrary, if people burn biomass too fast ($T_1 < T_2$), the fossilness > 0, and they are still adding CO_2 into the atmosphere. To analyze this impact, we should also take the time scale of natural equilibrium of carbon dioxide among the surface pool into consideration.

3) Peat

The regeneration time of peat is normally thousands of years. There are several different views to set T_1 and consider the fossilness of peat.

First, we may still use the lifetime of a peat plant, usually 30 to 50 years as T_1, and we date the average age of peat layers that are going to be produced/used during that lifetime as T_2 (since different layers of a peat land will have different ages). Basically, we get $T_1 < T_2$. Therefore, the fossilness < 1, and only that portion of peat production should be considered as fossil fuel.

Second, if policy makers set emission regulation goals phase by phase, then we can use the time period of one carbon tax charging cycle as T_1, and the average age of peat layers that are going to be produced/used during that cycle as T_2. For example, when there is an annual regulation, then T_1 is 1; the annual fossilness of a peat production land is $1-1/T_2$. Since the shallower layers of a peat land has smaller T_2, the annual fossilness will increase year by year, which makes sense because the deeper people dig, the older the peat are, and therefore make it more like fossil fuel.

Third, we may use the time of a whole peat land to be used up as T_1, which is closer to the definition of it in the case of biomass. If one uses a peat land slow enough to make T_1 equivalent

to the time scale of peat regeneration and therefore achieves zero fossilness of the whole process, then peat can be consumed in a carbon neutral way with no carbon penalty.

Based on the definition of fossilness stated above, $^{14}C/^{12}C$ ratio can be easily derived from fossilness. For fossil fuels, $f_{fossil} = 1$, $^{14}C/^{12}C$ = (1- f) Modern = 0 Modern. For biomass, $f_{biomass} = 0$, $^{14}C/^{12}C$ = (1- f) Modern = 1 Modern. For a mixture of f fossil fuels and (1- f) biomass, $0 < f < 1$, $^{14}C/^{12}C$ = (1- f) Modern.

The proposed carbon-14 isotope tagging technology frames a concept of online CO_2 monitoring. It not only can be used as an inventory tool for geological carbon storage, but also can play an important role in carbon management more broadly. Similar to the idea of smart meters in the electricity grid, we can use the ^{14}C tagging technology to enable real time carbon monitoring and accounting, which therefore will make the carbon market (through either cap-and-trade mechanism or carbon tax mechanism) more efficient. The structure of an online $^{14}CO_2$ monitoring meter working on a CO_2 pipeline is shown in a schematic diagram (Figure 48).

The $^{14}CO_2$ monitoring meter collects real-time fossilness data of the gas stream in the CO_2 pipeline. The data are sent back to an online control system, which controls the addition of ^{14}C tag into the gas stream to achieve a 1 Modern Carbon-14 level. That means, for pure biomass based fuel, there is no need to add any ^{14}C.

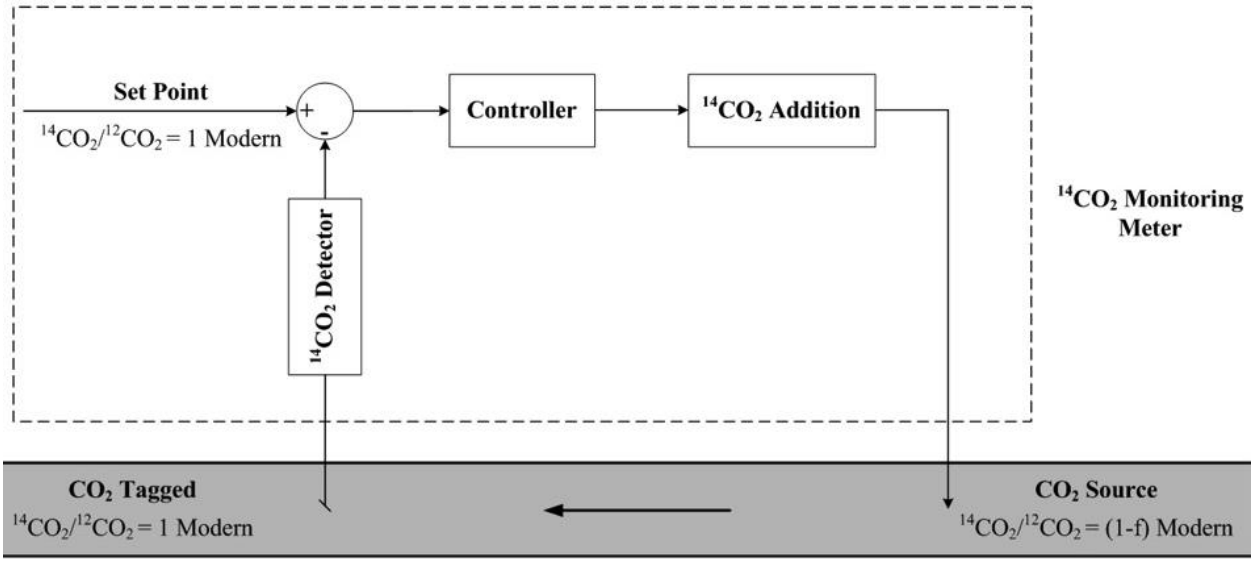

Figure 48: Schematic diagram of $^{14}CO_2$ monitoring meter.

At the upstream side of a CO_2 transportation pipeline, online $^{14}CO_2$ monitoring can provide carbon emission auditing data for either carbon tax or cap-and-trade mechanism to charge power plants according to the fossilness of their fuels. At the downstream of a CO_2 transportation pipeline, online $^{14}CO_2$ monitoring can contribute to the control of flow conditions before injection for permanent storage. Once the CO_2 gets injected underground, $^{14}CO_2$ also serves the purposes of mineral carbonation study and leakage detection, etc.

Chapter 7: Conclusion

The focus of the work discussed in this dissertation is on the challenge of developing a tagging system that makes it possible to accurately, reliably and reproducibly increase the ^{14}C concentration in a large CO_2 stream (e.g., 3 kg/min) with a tracer amount of one part per trillion which is equivalent to ambient levels of ^{14}C in carbon near the Earth's surface.

In this dissertation, I presented the ^{14}C tagging technology in great detail through describing the tasks that I made major contributions, i.e., the filling station for making the tracer loops (Chapter 3), the high-pressure flow loop system for laboratory-scale evaluation (Chapter 4), and the field test in Iceland (Chapter 5). I summarized my colleague's work on the $^{14}CO_2$ Detection System, provided the risk management analyses and future work recommendations (Chapter 6). This dissertation therefore served as a comprehensive story of developing carbon-14 isotope tagging for monitoring, verification and accounting in geological carbon storage.

The research showed that the original claim – that accurate tagging at the part per trillion level while operating with only miniscule quantities of tagging material, and minimizing the production of ^{14}C contaminated waste streams – is a challenging but, indeed, solvable task. Safety concerns over handling highly enriched $^{14}CO_2$ cartridges resulted in the demand for very small aliquots or cartridge volumes, which makes it difficult to accurately fill the cartridges and discharge the content in a well-controlled, steady manner.

The research effort explored two options for storing small amounts of tagging material in a small cartridge whose content could then be injected in a controlled manner into the CO_2 flow. Both approaches involve a syringe-style injection of a fluid. The first uses gaseous CO_2 highly enriched with $^{14}CO_2$; the second uses a thousand times larger fluid sample with the tagging $^{14}CO_2$ dissolved in an incompressible fluid, in this case water.

While the former option has the advantage of conceptual simplicity the second proved far more practical. The difficulties with the former method to a large extent arise due to the compressibility of carbon dioxide gas. As a result, with this method it is necessary to carefully control the pressure during charging the system, and equally importantly, it is necessary to control the pressure difference between the large flow to be tagged and the pressure in the tagging fluid. In order to minimize the impact of fluctuations in the pipeline pressure, the cartridge pressure would have to be set extremely high, which further complicates the design.

The development settled on the design of a water-filled micro cartridge (i.e., tracer loop). This method was chosen because it allowed for exquisite control of the tag concentration, and by injecting an incompressible fluid the metering of the injection rate was greatly simplified. Filling such a micro cartridge presented its own set of challenges, which were overcome by exposing the water in hollow fiber bundle to the gas to be dissolved. The project successfully demonstrated the ability to dissolve accurately determined quantities of $^{14}CO_2$ into tracer loops, which act as micro cartridges. The additional water in the tracer loop has been shown not to be a concern. As a result of the injection, the water vapor concentration in the CO_2 stream is changed by about one part per billion, which is well below the drying specifications for large industrial flows of carbon dioxide.

The work resulted in a complete and successful design of the filling station to make tracer loops with minimal ^{14}C waste production. It showed the safe and reliable handling of such tracer loops, and demonstrated the injection of the tracer content into a simulated carbon dioxide flow in a pressurized flow loop system. During filling of the tracer loops, water was exposed to $^{14}CO_2$ through a gas exchange membrane. By carefully controlling temperature and pressure, it was proved possible to have the water achieve equilibrium conditions with the surrounding gas. The water was then pushed forward into a series of tracer loops. The individual tracer loop could be used for injecting the tag into a carbon dioxide flow. The entire process from filling the tracer loop, to discharging it evenly into the sequestration stream has been developed, demonstrated and quantified in the laboratory, and demonstrated in a field test in Iceland.

Not only was the injection of $^{14}CO_2$ demonstrated into a high-pressure flow loop system simulating a pipeline, but the work also showed that a similar controlled injection of SF_6 is also feasible. Here again SF_6 was allowed to equilibrate with water and the SF_6 enriched water was added to the flow in the high-pressure flow loop. SF_6, which does not naturally occur in the environment and which can be detected at the part per trillion level has proven to be an excellent tracer for fluid flows (Ritchey and Rumbaugh, 1996). However, unlike $^{14}CO_2$, it will not partake in the chemical reactions the geo-sequestered carbon dioxide might encounter. Hence a comparison between a SF_6 tracer and a $^{14}CO_2$ tracer can shed light on chemical reactions that may proceed in the storage area (Matter et al., 2014).

Now that CO_2 tagging technology has been developed, it becomes useful to consider sampling technologies that can detect the ^{14}C underground. Rather than adding up all the carbon found underground, not all of which will be anthropogenic in its source, we propose in effect to

count ^{14}C atoms and from that calculate the total amount of anthropogenic carbon in a particular location. Since the fractionation of the ^{14}C in chemical and physical transport processes is very small, it is possible not only to track the gaseous or liquid CO_2 in the pore space but also CO_2 that has been dissolved into pore waters or CO_2 that has been converted into solid carbonates. This work enables a whole suite of new technologies, many of which still need to be developed.

In summary, the project has defined the foundation of carbon-14 tagging for the monitoring, verification, and accounting of geo-sequestration. The positive results represent a first step toward a larger technology set that will include accurate accounting methods for the upstream tagging process, and inventory techniques which can convert sampling results into estimates of the amount of anthropogenic carbon that has been stored that does not rely on an injection history and the apparent absence of leaks. Finally, leak detection is greatly enhanced, because any indication of modern carbon above the injection point but still well below the surface is a clear indication of a leak. This value of ^{14}C tagging has been demonstrated in the Iceland experiments, where the availability of ^{14}C and SF_6 data allowed an unambiguous conclusion that a significant fraction of the injected CO_2 had been chemically converted. The technologies developed during this project have made possible the routine addition of ^{14}C to CO_2 during sequestration in large volumes.

References

Agence internationale de l'énergie. (2012). Energy technology perspectives 2012: Pathways to a clean energy system. OECD/IEA.

Alfredsson, H. A., & Gislason, S. R. (2009). CarbFix-CO_2 sequestration in basaltic rock: Chemistry of the rocks and waters at the injection site, Hellisheidi, SW-Iceland. Geochimica et Cosmochimica Acta Supplement, 73, 26.

Alfredsson, H. A., Wolff-Boenisch, D., & Stefánsson, A. (2011). CO_2 sequestration in basaltic rocks in Iceland: Development of a piston-type downhole sampler for CO_2 rich fluids and tracers. Energy Procedia, 4, 3510-3517.

Allis, R., Chidsey, T., Gwynn, W., Morgan, C., White, S., Adams, M., & Moore, J. (2001, May). Natural CO_2 reservoirs on the Colorado Plateau and southern Rocky Mountains: Candidates for CO_2 sequestration. In Proceedings of the First National Conference on Carbon Sequestration (pp. 14-17).

Aradóttir, E. S., Sigurdardóttir, H., Sigfússon, B., & Gunnlaugsson, E. (2011). CarbFix: a CCS pilot project imitating and accelerating natural CO_2 sequestration. Greenhouse Gases: Science and Technology, 1(2), 105-118.

Bachu, S., W.D. Gunter and E.H. Perkins (1994): Aquifer disposal of CO_2: hydrodynamic and mineral trapping, Energy Conversion and Management, 35(4), 269–279.

Benson, S. M. (2006). Monitoring carbon dioxide sequestration in deep geological formations for inventory verification and carbon credits. 2006 SPE Annual Technical Conference and Exhibition, San Antonio, Texas, 24-27 September 2006, SPE 102833.

Benson, S. M., E. Gasperikova, and G. M. Hoversten (2004). Overview of monitoring techniques an protocols for geologic storage projects, IEA Greenhouse Gas R&D Program Report.

Busenberg, E. and L. N. Plummer L. N. (2000). Dating young groundwater with sulfur hexafluoride: Natural and anthropogenic sources of sulfur hexafluoride. Water Resources Research 36(10), 3011-3030.

Chazan, G. (2009). Shell's plan to lead in storage of carbon dioxide hits a snag. The Wall Street Journal.

Clark, I. D., & Fritz, P. (1997). Environmental isotopes in hydrogeology. CRC press.

De Figueiredo, M. A. (2007). Regulating carbon dioxide capture and storage.

Figueroa, J. D., Fout, T., Plasynski, S., McIlvried, H., & Srivastava, R. D. (2008). Advances in CO_2 capture technology—the US Department of Energy's Carbon Sequestration Program. International journal of greenhouse gas control, 2(1), 9-20.

Fontes, J. C., & Garnier, J. M. (1979). Determination of the initial ^{14}C activity of the total dissolved carbon: A review of the existing models and a new approach. Water resources research, 15(2), 399-413.

Gabelman, A., & Hwang, S. T. (1999). Hollow fiber membrane contactors. Journal of Membrane

Science, 159(1), 61-106.

Gasperikova, E., & Hoversten, G. M. (2006). A feasibility study of nonseismic geophysical methods for monitoring geologic CO_2 sequestration. The Leading Edge, 25(10), 1282-1288.

Gielen, D. (2008). Energy technology perspectives. Paris: International Energy Agency.

Gislason, S. R., Wolff-Boenisch, D., Stefansson, A., Oelkers, E. H., Gunnlaugsson, E., Sigurdardottir, H. & Fridriksson, T. (2010). Mineral sequestration of carbon dioxide in basalt: A pre-injection overview of the CarbFix project. International Journal of Greenhouse Gas Control, 4(3), 537-545.

Gislason, S. R., Broecker, W. S., Gunnlaugsson, E., Snæbjörnsdóttir, S., Mesfin, K. G., Alfredsson, H. A., & Oelkers, E. H. (2014). Rapid solubility and mineral storage of CO_2 in basalt. Energy Procedia, 63, 4561-4574.

Grigsby P. W., MD; Barry A. Siegel, MD; Susan Baker, MBA; John O. Eichling, PhD, JAMA. 2000; 283: 2272-2274.

Godwin, H. (1962). Half-life of radiocarbon. Nature, 195.

Gouveia, F. J., & Friedmann, S. J. (2006). Timing and prediction of CO_2 eruptions from Crystal Geyser, UT (pp. 1-14). United States. Department of Energy.

Gunter, W.D., E.H. Perkins and T.J. McCann (1993): Aquifer disposal of CO_2-rich gases: reaction design for added capacity. Energy Conversion and Management, 34, 941–948.

Gunter, W.D., B. Wiwchar and E.H. Perkins (1997): Aquifer disposal of CO_2-rich greenhouse gases: Extension of the time scale of experiment for CO_2-sequestering reactions by geochemical modelling. Mineralogy and Petrology, 59, 121–140.

Ho, D. T. and P. Schlosser (2000). Atmospheric SF_6 near a large urban area. Geophysical Research Letters 27(11), 1679-1682.

Hoversten, M., et al. (2006). Theoretical limits for seismic detection of small accumulations of carbon dioxide in the subsurface. Proceedings of the 8th International Workshop on Greenhouse Gas Technology, Trondheim, Norway, June 19-22.

Hovorka, S. D., S. M. Benson, C. Doughty, B. M. Freifeld, S. Sakurai, T. M. Daley, Y. K. Kharaka, M. H. Holtz, R. C. Trautz, H. Seay Nance, L. R. Myer, and K. G. Knauss (2006). Measuring permanence of CO_2 storage in saline formations – the Frio Experiment. Environmental Geosciences 13: 105-121.

Karlen, I., Olsson, I. U., Kallberg, P., & Kilicci, S. (1965). Absolute determination of the activity of two C-14 dating standards. Arkiv Geofysik., 4.

King, D. B., & Saltzman, E. S. (1995). Measurement of the diffusion coefficient of sulfur hexafluoride in water. Journal of geophysical research, 100(C4)

Lewicki, J. L., Oldenburg, C. M., Dobeck, L., & Spangler, L. (2007). Surface CO_2 leakage during two shallow subsurface CO_2 releases. Geophysical Research Letters, 34(24).

Matter, J. M., Broecker, W. S., Gislason, S. R., Gunnlaugsson, E., Oelkers, E. H., Stute, M., & Wolff-Boenisch, D. (2011). The CarbFix Pilot Project–storing carbon dioxide in basalt. Energy

Procedia, 4, 5579-5585.

Matter, J. M., Stute, M., Hall, J., Mesfin, K., Snæbjörnsdóttir, S. Ó., Gislason, S. R., & Broecker, W. S. (2014). Monitoring permanent CO_2 storage by in situ mineral carbonation using a reactive tracer technique. Energy Procedia, 63, 4180-4185.

Matter, J. M., Takahashi, T., & Goldberg, D. (2007). Experimental evaluation of in situ CO_2 ‐ water ‐ rock reactions during CO_2 injection in basaltic rocks: Implications for geological CO_2 sequestration. Geochemistry, Geophysics, Geosystems, 8(2).

Matter, J. M., W.S. Broecker, M. Stute, S.R. Gislason, E.H. Oelkers, A. Stefansson, E. Gunnlaugsson, G. Axelsson, and G. Björnsson (2008). Permanent Carbon Dioxide Storage into Basalt: The CarbFix Pilot Project, Iceland. Energy Procedia 1(2009), p. 3641-3646.

Metz, B., Davidson, O., De Coninck, H. C., Loos, M., & Meyer, L. A. (2005). IPCC special report on carbon dioxide capture and storage: Prepared by working group III of the intergovernmental panel on climate change. IPCC, Cambridge University Press: Cambridge, United Kingdom and New York, USA, 4.

Mook, W., & Rozanski, K. (2000). Environmental isotopes in the hydrological cycle. IAEA Publish.

Mroczek, E. K. (1997). Henry's Law constants and distribution coefficients of sulfur hexafluoride in water from 25 °C to 230 °C. Journal of Chemical & Engineering Data, 42(1), 116-119.

Murnick, D. E., Dogru, O., & Ilkmen, E. (2007). Laser based ^{14}C counting, an alternative to AMS in biological studies. Nuclear Instruments and Methods in Physics Research Section B: Beam Interactions with Materials and Atoms, 259(1), 786-789.

Murnick, D. E., Dogru, O., & Ilkmen, E. (2008). Intracavity optogalvanic spectroscopy. An analytical technique for ^{14}C analysis with subattomole sensitivity. Analytical chemistry, 80(13), 4820-4824.

Murnick, D., Dogru, O., & Ilkmen, E. (2010). ^{14}C analysis via intracavity optogalvanic spectroscopy. Nuclear Instruments and Methods in Physics Research Section B: Beam Interactions with Materials and Atoms, 268(7), 708-711.

Murnick, D. E., & Okil, J. O. (2005). Use of the optogalvanic effect (OGE) for isotope ratio spectrometry of $^{13}CO_2$ and $^{14}CO_2$. Isotopes in Environ Health Studies, 41(4), 363-371.

Oelkers, E.H., S.R. Gislason, and J. Matter (2008). Mineral carbonation of CO_2. Elements, Vol. 4, 331-335.

Pacala, S., & Socolow, R. (2004). Stabilization wedges: solving the climate problem for the next 50 years with current technologies. science, 305(5686), 968-972.

Paul, D., & Meijer, H. A. (2015). Intracavity OptoGalvanic Spectroscopy Not Suitable for Ambient Level Radiocarbon Detection. Analytical Chemistry, 87(17), 9025-9032.

Pearce, J. M., Holloway, S., Wacker, H., Nelis, M. K., Rochelle, C., & Bateman, K. (1996). Natural occurrences as analogues for the geological disposal of carbon dioxide. Energy Conversion and Management, 37(6), 1123-1128.

Peterson, J., M. MacDonell, L. Haroun, nad F. Monette (2007). Radiological and chemical fact sheets to support health risk analyses for contaminated areas. Argonne National Laboratory.

Rangwala, H. A. (1996). Absorption of carbon dioxide into aqueous solutions using hollow fiber membrane contactors. Journal of Membrane Science, 112(2), 229-240.

Ritchey, J. D., & Rumbaugh, J. O. (1996). Subsurface fluid flow (ground-water and vadose zone) modeling (Vol. 1288). ASTM International.

Salvi, S., F. Quattrocchi, M. Angelone, C.A. Brunori, A. Billi, F. Buongiorno, F. Doumaz, R. Funiciello, M. Guerra, S. Lombardi, G. Mele, L. Pizzino and F. Salvini (2000): A multidisciplinary approach to earthquake research: implementation of a Geochemical Geographic Information System for the Gargano site, Southern Italy. Natural Hazard, 20(1), 255–278.

Slavin, T., & Alok, J. (2009). Not under our backyard, say Germans, in blow to CO_2 plans. The Guardian.

Span, R., & Wagner, W. (1996). A new equation of state for carbon dioxide covering the fluid region from the triple-point temperature to 1100 K at pressures up to 800 MPa. Journal of physical and chemical reference data, 25(6), 1509-1596.

Stevens, S. H., Fox, C., White, T., Melzer, S., & Byrer, C. (2002, October). Production operations at natural CO_2 Fields: Technologies for geologic sequestration. In Proceedings of the 6th International Conference on Greenhouse Gas Control Technologies (GHGT-6), J. Gale and Y. Kaya (eds.) (pp. 1-4).

Stocker, T. F., Qin, D., Plattner, G. K., Tignor, M., Allen, S. K., Boschung, J., & Midgley, B. M. (2013). IPCC, 2013: climate change 2013: the physical science basis. Contribution of working group I to the fifth assessment report of the intergovernmental panel on climate change.

Streit, J., A. Siggins and B. Evans (2005): Predicting and monitoring geomechanical effects of CO_2 injection, Carbon Dioxide Capture for Storage in Deep Geologic Formations—Results from the CO_2 Capture Project, v. 2: Geologic Storage of Carbon Dioxide with Monitoring and Verification, S.M. Benson (ed.), Elsevier Science, London, pp. 751–766.

Stute, M., & Deák, J. (1989). Environmental isotope study (^{14}C, ^{13}C, ^{18}O, D, noble gases) on deep groundwater circulation systems in Hungary with reference to paleoclimate. Radiocarbon, 31(3), 902-918.

Treybal, R. E. (1968). Mass-transfer operations (Vol. 3). New York: McGraw-Hill.

Van der Hoeven, M. (2013). World Energy Outlook 2013.

Watson, M. N., Boreham, C. J., & Tingate, P. R. (2004). Carbon dioxide and carbonate cements in the Otway Basin: implications for geological storage of carbon dioxide. The APPEA Journal, 44(1), 703–720.

Weast, R. C., & Astle, M. J. (1989). CRC handbook of chemical and physics. CRC Press, Boca Raton, FL, 1989, p. D-221.

Wigley, T. M., & Schimel, D. S. (2005). The carbon cycle (Vol. 6). Cambridge University Press.

Wolf, A. V. (1966). Aqueous solutions and body fluids; their concentrative properties and conversion tables. Harper and Row, New York.

Zhang, H. Y., Wang, R., Liang, D. T., & Tay, J. H. (2006). Modeling and experimental study of CO_2 absorption in a hollow fiber membrane contactor. Journal of Membrane Science, 279(1), 301-310.